Diverse subtypes of fast-spiking inhibitory neurons in neocortex

by

Arthur Sugden

B.A., Wesleyan University; Middletown, CT, 2008

A dissertation submitted in partial fulfillment of the
requirements for the degree of Doctor of Philosophy
in Molecular Biology, Cellular Biology, and Biochemistry at Brown University

PROVIDENCE, RHODE ISLAND

May 2015

This dissertation by Arthur Sugden is accepted in its present form
by Molecular Biology, Cellular Biology, and Biochemistry as satisfying the
dissertation requirement for the degree of Doctor of Philosophy.

Date________________ ____________________________________

Barry Connors, Ph.D., Advisor

Date________________ ____________________________________

Scott Cruikshank, Ph.D., Co-advisor

Recommended to the Graduate Council

Date________________ ____________________________________

Gilad Barnea, Ph.D., Reader

Date________________ ____________________________________

David Berson, Ph.D., Reader

Date________________ ____________________________________

Alex Jaworski, Ph.D., Reader

Date________________ ____________________________________

Corey Harwell, Ph.D., Outside Reader

Approved by the Graduate Council

Date________________ ____________________________________

Peter Weber, Dean of the Graduate School

Vitae

Arthur Ulrich Sugden

Molecular Biology, Cellular Biology, and Biochemistry

Brown University

arthur_sugden@brown.edu

608-772-3888

Education

Ph.D *May 2015*

Molecular Biology, Cellular Biology, and Biochemistry, Brown University

- Advisor: Barry Connors
- Dissertation: ``Diverse subtypes of fast-spiking inhibitory neurons in neocortex"

B.A. *May 2008*

Astronomy & Physics, Wesleyan University

- Advisor: John Salzer
- Senior Thesis: ``Alfalfa Hα: The Star-Formation-Rate Density of the Local Universe"

Conference Posters

- Sugden AU, Patrick SL, Burwell, RD Connors BW. "Robust inhibition and gamma oscillations in a cortical area that lacks parvalbumin-expressing inhibitory interneurons." *Society for Neuroscience* 2014
- Connors BW, Neske GT, Sugden AU, Crandall SR, Cruikshank SJ. "Roles of electrical synapses in gamma-band activity of sensory and association cortex." *Society for Neuroscience* 2014
- Sugden AU, Patrick SL, Anand A, Burwell, RD Connors BW. "Ventral postrhinal cortex: a network adapted to inhibition without parvalbumin-expressing interneurons." *Society for Neuroscience* 2013
- Van Sistine A, Salzer JJ, Janowiecki S, Sugden AU, Haynes MP, Giovanelli R, Wilcots EM. "The ALFALFA Hα Survey." *American Astronomical Society* 2013
- Singh T, Patrick SL, Sugden AU, Burwell, RD Connors BW. "An exceptionally sparse network of parvalbumin-expressing inhibitory interneurons in the ventral postrhinal cortex." *Society for Neuroscience* 2012
- Haynes K, Most H, Cannon JM, Haugland K, Salzer JJ, Scudder J, Sugden A, Weindling J. "The Stellar and Gaseous Contents of the Orion Dwarf Galaxy." *American Astronomical Society* 2009
- Norby K, Sugden AU, Sugden B. "From Stars to Cells: Automated Signal Quantification in Fluorescence Microscopy." *Integration of Mathematical & Biological Sciences* 2008
- Norby K, Sugden AU. "Synthesis and Partitioning of KSHV Genomes." *McArdle Symposium on Cancer* 2008

- Kellar J, Salzer J, Wegner G, Sugden A. "Hα Dots: Finding Isolated Extragalactic Emission-Line Objects in Narrow-Band Images." *American Astronomical Society* 2008
- Sugden A, Salzer J, Kellar J, Cannon J, Moran E, Dieck C, Williams A. "ALFALFA Hα: A Narrow-Band Survey of Star Formation in the Local Universe." *American Astronomical Society* 2008

Publications

- Sugden AU, Patrick SL, Fogerson PM, Burwell RD, Connors BW. "Cortical inhibitory function in the absence of canonical parvalbumin-expressing interneurons." *In Prep*
- Sugden AU, Connors BW. "Network gamma oscillations in neocortex do not require gap junctions." *In Prep*
- Chiu Y, Sugden AU, Hayes M, Norby K, Sugden B. "KSHV Uses an Unprecedented Mode of Partitioning in Genomes." *In Prep*
- Sistine AV, Salzer JJ, Sugden AU, Giovanelli R, Haynes MP, Janowiecki J, Jaskot AE, Wilcots EM. "The ALFALFA H$alpha$ Survey I. Project Description and Methods." *In Review*
- Allen JA, Akkaynak D, Sugden AU, Hanlon RT. "Adaptive camouflage body patterning and dermal flap morphology in the cryptic slender filefish, Monacanthus tuckeri, on a coral reef." *Biological Journal of the Linnean Society, In Press*
- Chiu Y, Sugden AU, Sugden B. "Epstein-Barr Viral Productive Amplification Reprograms Nuclear Architecture, DNA Replication, and Histone Deposition." *Cell Host & Microbe* 14.6 (2013): 607-18.

- Soruco MM, Chery J, Bishop EP, Siggers T, Tolstorukov MY, Leydon AR, Sugden AU, Goebel K, Feng J, Xia P, Vedenko A, Bulyk ML, Park PJ, Larschan E. "The CLAMP protein links the MSL complex to the X chromosome during Drosophila dosage compensation." *Genes Dev* 27 (2013): 1551-6.

- Savva YA, Jepson JE, Sahin A, Sugden AU, Dorsky JS, Alpert L, Lawrence C, Reenan RA. "Auto-regulatory RNA editing fine-tunes mRNA re-coding and complex behaviour in Drosophila." *Nature communications* 3 (2012): 790.

- Jepson JEC, Savva YA, Yokose C, Sugden AU, Sahin A, Reenan RA. "Engineered Alterations in RNA Editing Modulate Complex Behavior in Drosophila." *J Biol Chem* 286.10 (2011): 8325-37.

- Cannon JM, Haynes K, Most H, Salzer JJ, Hauglund K, Scudder J, Sugden A, Weindling J. "The Stellar and Gaseous Contents of the Orion Dwarf Galaxy." *Astronomical Journal* 139 (2010): 2170.

- Sugden A, Salzer J. "Supernova 2009W." *CBET* 1793 (2009): 1.

- Nanbo A, Sugden AU, Sugden B. "The coupling of synthesis and partitioning of EBV's plasmid replicon is revealed in live cells." *EMBO* 26.19 (2007): 4252-62.

Honors

- NIH F31 NRSA (2012-2015)

- Honorable Mention, NSF GRFP (2011)

Teaching Experience

- Instructor and designer: Illustrator for Scientists, 4 lectures, Brown University, *Fall 2014*

- Guest lecturer: Introduction to Cre/Lox, Brown University, *Fall 2014*

- Co-instructor and co-designer: HHMI Summer Course in Molecular Biology, Brown University, *Summer 2011 & 2012*

- Teaching Assistant: Introduction to Genetics, Brown University, *Spring 2010*

Acknowledgements

Dedicated to Mom and Dad

First, I must thank an extraordinary mentor who took a risk accepting a third-year student without any training in neuroscience into his lab. Dr. Barry Connors is a fantastic advisor, calmly sitting through erratic, excited explanations of new data and suggesting a more organized approach to understanding it. Barry is also generous; he invites students to his home, shares his deep understanding of the academic system, and is willing to review dissertation chapters while on vacation. I could not be luckier. Thank you.

I have also depended completely on the expertise of Dr. Scott Cruikshank. I would have floundered in the lab unable to perform any electrophysiology without his patient and extensive teaching. In three and a half years, Scott has taught me enough to write a dissertation based largely on electrophysiological experiments. Scott has an exceptional talent that I admire: he says only what he knows. Thus, I only become completely confident in a statement if he can be convinced of its veracity. For all of your help and your wisdom, thank you.

Saundra Patrick is both our lab manager and a gem. With unwavering positivity, she has done the vast majority of the immunohistochemistry in this dissertation and has guided me through the rest. She has reminded me not only to love science, but to love life. Around her, the world is rosy. For that, thank you.

The lab (including honorary members) is an exceptional group of people. All are astute and well-informed. Like an adventure story, the lab feels like a band of friends, each with a shared goal but set out on individual quests. Lab meetings are thus a struggle and joy. It has been a treat to work with Garrett Neske, Dr. Shane Crandall, Dr. Chris Deister, Michelle Fogerson, Dr. Tanya Stevens, Dr. Nathan Vierling-Claassen, Dr. Tim Zolnik, Rosa Martinez Garcia, and Liz McDonnell.

My thesis committee has always steered me well. When we were convinced that no new cell type existed in vPOR, they presciently pushed me to make sure. The final two months before the due date of this dissertation have been spent reconfirming what I should have finished testing long ago. Dr. Gilad Barnea has been on the committee since the beginning, advising across multiple phyla, and has seen the development from a slide that only partially differentiated between glycinergic and GABAergic neurons to a thesis focused on dissecting a subset of GABAergic interneurons. His insight has been key in mutagenic screens in *Drosophila*, the genetic analysis of Cx36 conditional knockouts, and conveying my data clearly, amongst other things. Dr. David Berson has made essential suggestions with the most gentle hand I have experienced. His push to characterize the cells of the vPOR thoroughly has led both to a mad scramble and better science. Dr. Alex Jaworski is an expert in neuronal development and axon guidance. He has graciously joined the thesis committee and I eagerly anticipate his comments. Dr. Corey Harwell is an expert in the development of cortical circuits from the faculty of Harvard Medical School and has graciously joined the committee has an outside reader. I am excited to get his expert input on the fascinating region of vPOR.

In addition to my formal advisors, two other faculty have acted as informal advisors. Dr. Rebecca Burwell defined postrhinal cortex in the rodent and piqued our lab's and my interest in that region. She has offered continuing guidance in understanding POR, its inputs, and its function. Dr. Stephanie Jones has sat through years of struggling to model gap junctions in somatosensory cortex, gently guiding me through its difficulties.

I am incredibly grateful to all of the former members of my committee, Dr. Eric Morrow, Dr. Mark Zervas, Dr. Anne Hart, and Dr. Mike McKeown, for their patience and advice in an ever-evolving set of projects and interests. I have also had the pleasure of working with three other faculty, Dr. Rob Reenan, Dr. Kim Mowry, and Dr. Erica Larschan. Rob has an exceptional ability to convey joy in science, which he generously shared with me.

Finally, to my undergraduate advisor, Dr. John Salzer, I am forever indebted to you for teaching me what science is and how to approach it rigorously. I have loved all of the science I have been a part of, but the late nights and mornings on Kitt Peak working together were true highlights.

To my advisors and compatriots, thank you.

To my family, Roth, Alpert, Oertel, and Sugden, thank you. Like any good child, I had to rebel against my parents. As happy and successful biologists, they conveyed a love of science and biology in particular. In response, I tried in order the fields of archaeology, psychology, law, astronomy, and physics during college, gradually drifting towards their interests. I thoroughly enjoyed astronomy, but as hard as I tried, the pleasure my parents conveyed in the work dragged me into their fields of molecular biology and neuroscience. I now have the distinct pleasure of having collaborated scientifically with my mother, my father, and my wife. It is your fault that I am writing this dissertation, and for that I thank you.

And to my partner in science and in life, my wife Lauren, thank you. I followed you across the country to get here, and I will follow you wherever else you want to go.

Abstract of " Diverse subtypes of fast-spiking
inhibitory neurons in neocortex " by Arthur Sugden, Ph.D., Brown University, May 2015

Inhibitory interneurons are essential for normal cortical function. They prevent seizures, regulate temporal and spatial coding, and generate oscillations and synchrony in pyramidal cells. The largest subtype of inhibitory interneurons is fast-spiking (FS) cells, which mediate feedforward inhibition and have been implicated in the generation of gamma oscillations, the oscillations that may bind a percept together as it passes through groups of neurons. FS cells are canonically marked by the calcium-binding protein parvalbumin (PV), whose levels have been linked to synaptic plasticity.

Like-types of adult neocortical inhibitory neurons are linked by gap junctions with a probability of greater than 50% within 50 microns. FS cells are linked by gap junctions, and these gap junctions have long been thought to add to the generation of gamma oscillations.

In this dissertation I have asked two questions. First, ventral postrhinal cortex, a subset of the parahippocampal region, lacks canonical PV-expressing FS cells. Within this area, it has been possible to ask how is inhibition altered in a neocortical region lacking canonical FS cells? Second, using a two-pronged approach of in vitro electrophysiology and a computational model, I have asked what roles do gap junctions play in neocortical gamma oscillations?

In examining these problems, I have found three results. First, the commonly-stated overlap between parvalbumin (PV) and FS cells does not apply in ventral postrhinal cortex. The majority of FS cells in this region are PV-negative, and these cells extend into neighboring cortex with canonical FS cells. Second, the absence of canonical FS cells from vPOR and the corresponding decrease in inhibitory cell density does not decrease total inhibition onto excitatory cells, due to decreased inhibition onto inhibitory cells in vPOR. Third, gamma oscillations do not require gap junctions in neocortex, unless compensation in RS cells for the lack of gap junctions in inhibitory cells is masking the effect.

Contents

List of Tables

List of Figures

Chapter One

Introduction

Ten days after a mouse zygote forms, the outer shell of the brain begins to split into six separate layers Kwon et al. (2011). Parental cells are lined up as spokes on a wheel, providing a path along which their daughter cells will travel Lui et al. (2011). First, an outer layer devoid of excitatory neurons is formed, layer 1 Kwon et al. (2011). Daughter cells are formed sequentially, and they build the remainder of the neocortical shell from the bottom up Finlay and Darlington (1995). In the next day or two, excitatory neurons march along their spokes formed of radial glia to take their places in the bottom layer, number 6. In the following days, swarms of cells follow them to fill in layers 5 and 4. Finally, by 16 days after the single cell zygote began replicating, layers 2 and 3 have been filled in with just under 100,000 cells per cubic millimeter Schuz and Palm (1989).

If the process ended here, the brain would be severely limited in its ability to perform computations and would be in a state of perpetual seizures.

As the layers of excitatory neurons are being formed, two clusters of primordial inhibitory neurons are developing. The primary cluster resides near the center of the brain in the medial ganglionic eminence (MGE) Wichterle et al. (2001). These cells will eventually go on to become the neurons that enforce rhythms on the brain, including a rhythmic pulsing that may bind together percepts as they travel through the mind Engel and Singer (2001); Fishell and Rudy (2011b). In a separate cluster distant from the MGE, inhibitory cells of the caudal ganglionic eminence (CGE) will later spread along the outer edge of cortex, taking nonspecific sensory input and relaying it to the excitatory neurons of layers 2 and 3 Cruikshank et al. (2012).

This intricate ballet coordinated in space and time, which occurs during the development of every mammal, had its early antecedents around the time that *Tyrannosaurus Rex* and *Velociraptor mongoliensis* roamed the supercontinent of Pangea Rakic (2009). After 100 million years, the evolutionary branches leading to rodents and humans diverged, and after another

100 million years, we still retain this shared development Rakic (2009).

The majority of the outer shell of the brain is the neocortex and consists of a generalized pattern of circuits organized into 6 layers (though often layers 2 and 3 are linked, Figure 1). The neocortex performs the most advanced mammalian processing. The patterns by which neocortical cells are connected are sufficiently consistent that conclusions about the visual system of humans have been drawn from studies of the whisker sensation of mice Laramée and Boire (2014). This is not far-fetched; for example, ratios of the two major classes of inhibitory cells differ by less than 5% across the vast majority of the neocortex Xu et al. (2010).

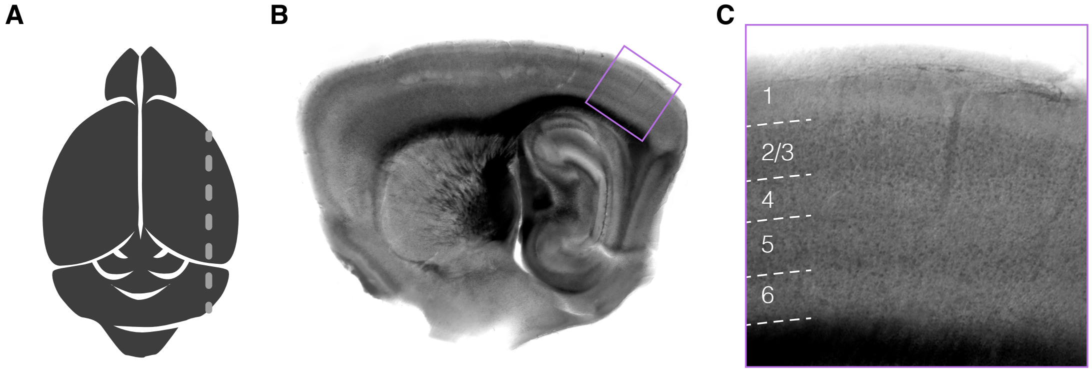

Figure 1.1: Six-layered neocortex (A) Schematic of the brain from above with dotted line showing the orientation of B and C. (B) A slice of the brain taken in the parasagittal plane depicted in A, imaged with differential interference contrast microscopy (DIC). Anterior is to the left, posterior to the right. Purple box is the region in C. (C) Higher magnification of six-layered neocortex with layers 2 and 3 combined.

There are a great number of circuit loops in the neocortex (e.g. Anderson et al. (2010); Cossart (2010); Silberberg and Markram (2007)). This is intuitive; with only roughly 16 billion neurons in the adult human neocortex, we can perform a vast array of computations Alonso-Nanclares et al. (2008); Carne et al. (2006). The computer upon which I write this manuscript has one billion transistors within it, but its binary operations cannot compare to the recurrent computations possible by the human brain.

These loops require inhibitory cells. Imagine the case of two excitatory cells synapsing on each other. When one fires, the other might fire soon after, and vice versa. Stimulating one cell will lead to an endless stimulation between the two cells. Like a poking match between toddlers, it can only end with everyone getting hurt. In the case of runaway excitation, the damage may come in the form of seizures. Inhibitory cells can act as brakes on the system, providing feedback inhibition onto excitatory cells Bromfield et al. (2006). An inhibitory cell can also provide feedforward inhibition Cruikshank et al. (2007); input from the central relay system of the brain, the thalamus, can excite both an inhibitory cell and an excitatory cell, for example. The inhibitory cell then synapses on its excitatory cell partner, providing it with a quick on-off stimulus.

Another fascinating role for inhibition is in modulating the gain of a circuit Kepecs and Fishell (2014). Many of the objects we interact with are limited by gain, for example the scales we use to measure ingredients for our solutions. Each is accurate only within a small range of weights–three orders of magnitude. Without inhibitory cells, the brain could experience just such a problem. With inhibitory cells, inhibitory and excitatory cells can be driven in parallel. Their combined output would be independent of the amplitude of the stimulus onto the system.

The goal of this dissertation is to better understand the connections and characteristics of a subset of these inhibitory neurons. To do so, I will review the current understanding of inhibitory cell types, the gap junctions that connect them, the cortical rhythms they entrain in the brain, and the special role of the postrhinal cortex.

1.0.1 Inhibitory cell types

All neocortical inhibitory interneurons are linked by their primary release of the inhibitory neurotransmitter γ-aminobutyric acid (GABA) Celio (1986). GABA activates two types of

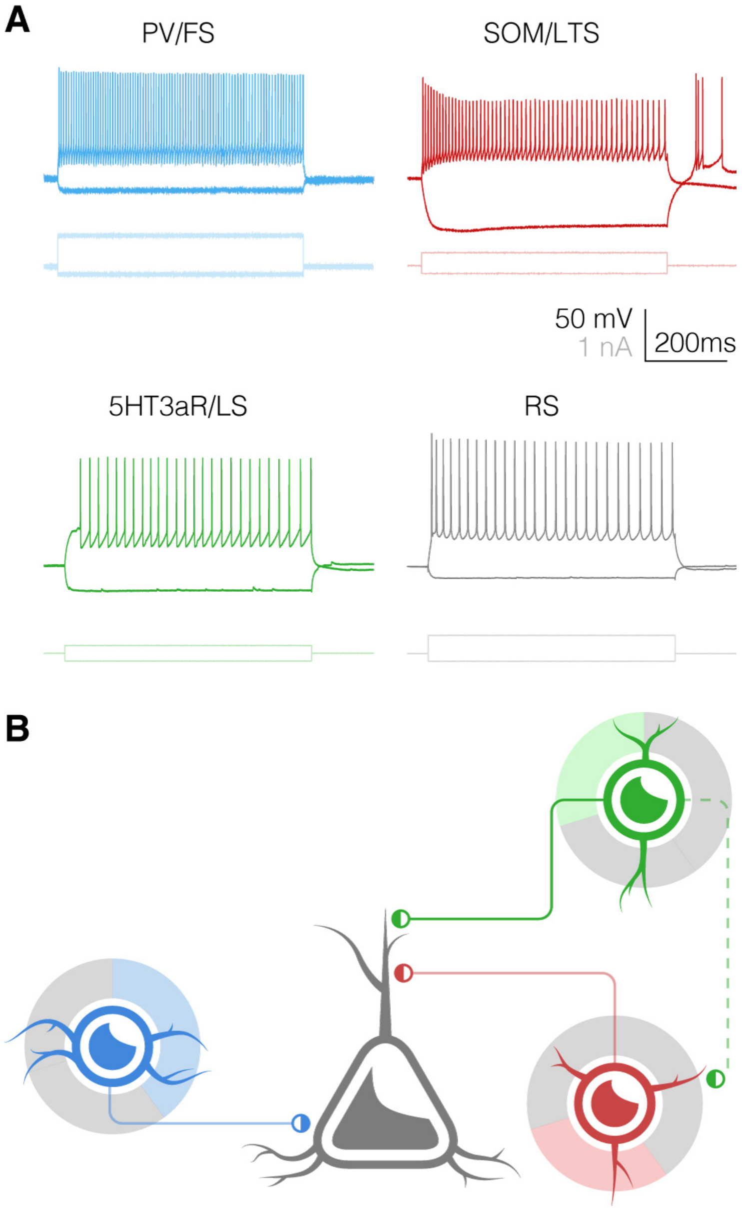

Figure 1.2: (A) Cells of the neocortex at -150 pA and rheobase+200 pA, except 5HT3aR/neurogliaform/LS cell which is at rheobase+50 pA to show late spike. (B) Connection schematic for the cells. Example Martinotti SOM cell, basket FS cell, and neurogliaform 5HT3aR cell (solid) or VIP 5HT3aR cell (dashed) synapsing on an excitatory cell. Pie charts show that PV cells make up 40% of inhibitory cells, SOM cells make up 30%, and 5HT3aR make up the remaining 30% Rudy et al. (2010).

receptors on postsynaptic neurons, $\mathrm{GABA_A}$ and $\mathrm{GABA_B}$. $\mathrm{GABA_A}$ receptors are ligand-gated ion channels selective for chloride Barnard et al. (1998). Chloride has a reversal potential of approximately -90 mV in the mature cortex Kaila et al. (2014), so the opening of these channels generally inhibits cells by driving their membrane potentials towards more negative voltages away from spike threshold. GABA_B receptors, on the other hand, are slow-acting G protein-coupled receptors that can inhibit by opening potassium channels in postsynaptic membranes Barnard et al. (1998).

Three proteins are important for production of and signaling with GABA. The first, vesicular GABA transporter (VGAT), loads vesicles with GABA Gasnier (2000). VGAT is essential for, but not exclusive to, GABAergic neurons as it also loads glycine into vesicles Gasnier (2000). The vast majority of neocortical inhibition is GABAergic, so VGAT can be considered a GABAergic marker in the neocortex Fishell and Rudy (2011a). One of two proteins of the glutamic acid decarboxylase (GAD) family convert the excitatory neurotransmitter glutamate into GABA. Cells can express one or both variants, but in an animal in which GFP has been inserted into the GAD67 locus, GFP and thus GAD67 appears to be expressed in all neocortical interneurons Tamamaki et al. (2003). Furthermore, the disruption of GAD67 leads to the upregulation of its partner, GAD65 Tamamaki et al. (2003). A second animal in which Cre has been inserted into the GAD65 locus shows extensive labeling of inhibitory cells Taniguchi et al. (2011). In total, these observations suggest that both GAD proteins are expressed in nearly all or all inhibitory cells of the neocortex.

The majority of inhibitory cells have their origins in the MGE Wichterle et al. (2001). There, they reside within a gradient of the developmental protein Wnt, which is secreted from the developing thalamus Chang (2014). At the rear or caudal end, the MGE is bathed in Wnt and produces mostly cells expressing the neuropeptide somatostatin (SOM). At the front or rostral end, little of the Wnt reaches the developing inhibitory cells and they develop primarily into cells that express the calcium-binding protein parvalbumin (PV).

Historically, cells were recorded in vitro and in vivo and classified by consistent properties in their responses to depolarizing current. The synaptic effects of these cells could be determined by stimulating pairs of recorded cells; this identified regular-spiking (RS) cells as excitatory, while cells with fast-spiking (FS) phenotypes were classified as inhibitory, as eventually were a variety with non-FS phenotypes Markram et al. (2004); McCormick et al. (1985) (Figure 2A). Since then, the non-FS group has been further subdivided into SOM-positive and SOM-negative cells (Figure 2A). These electrophysiological phenotypes are easy to distinguish. RS cells have much broader spikes than do inhibitory cells. Of the inhibitory cells, FS cells have fast, narrow spikes and SOM cells have high resistance and strong spike-height adaptation.

PV was first used as a selective neuronal marker in rat brains in 1981 Celio and Heizmann (1981). This work was followed five years later by elegant efforts from the same lab to prove that PV marked inhibitory cells Celio (1986). There, alternating slices of tissue one twentieth the diameter of a cell were bathed in antibodies to PV and the inhibitory signaling molecule GABA. Cells positive for PV were also positive for GABA. Soon after, it was determined that PV marked cell types with two distinct shapes: chandelier cells and basket cells DeFelipe et al. (1989). Chandelier cells are a rare type of PV-positive interneuron that form presynaptic terminals along the axonal initial segment of excitatory cells Karube et al. (2004); Somogyi (1977); Taniguchi et al. (2013). The vast majority of PV cells are basket cells, which selectively target the cell bodies and proximal dendrites of excitatory cells, forming a shell of synapses that looks basket-like Karube et al. (2004); Rudy et al. (2010) (Figure 2B). It is worth noting that much of the recent characterization of PV basket cells has been performed with the PV-IRES-Cre mouse line (e.g. Helm et al. (2013); Pfeffer et al. (2013)), which has limitations to be described in Chapter 2.

Early on, it was suggested that PV marked cells that fired rapidly with narrow spikes DeFelipe et al. (1989). Since then, it has been demonstrated that nearly all PV-positive cells are fast spiking and it has become canon that FS cells have a nearly one-to-one overlap with PV expression Gelman and Marín (2010); Gentet et al. (2010); Helm et al. (2013); Lee et al. (2010); Pfeffer et al. (2013); Rudy et al. (2010); Uhlhaas and Singer (2010); Xu et al. (2010); Yang et al.

(2012). PV cells are essential for feedforward inhibition Cruikshank et al. (2007), are the most abundant type of cortical inhibitory interneuron Rudy et al. (2010), and may generate cortical gamma oscillations Cardin et al. (2009). Now we know that in at least two models of autism, maternal exposure to depakote during pregnancy and the Neurologin-1 mutant, patches of neocortex lack PV cells Gogolla et al. (2009). Clearly, these cells play an important role in the normal function of the neocortex.

SOM was discovered as a marker of GABAergic neurons around the same time that the localization of PV was being determined Hendry et al. (1984). A decade later, SOM and PV were being used to differentiate subpopulations of inhibitory interneurons Gonchar and Burkhalter (1997); Kawaguchi and Kubota (1997). SOM cells are a more diverse group of inhibitory cells, although nearly all share spike-height and spike-frequency adaptation upon depolarization (Rudy et al. (2010), Figure 2A, and Chapter 2). One of the primary types of SOM cells is termed the Martinotti cell and sends axonal arbors up from the layer in which its soma resides towards the pia Rudy et al. (2010) (Figure 2B). In stark contrast to the basket cells that target cell bodies, these SOM cells target distal parts of apical dendrites of pyramidal cells.

Random transgenic insertions of DNA containing GFP driven by the GAD67 promoter show just how variable SOM-expressing cells can be Ma et al. (2006); Oliva et al. (2000). One random insertion termed GIN marks a subset of canonical primarily layer 2/3 Martinotti-like SOM cells Oliva et al. (2000). Another insertion, X94, marks SOM cells that synapse most commonly in layer 4 that are claimed to have a more FS-like phenotype (Ma et al. (2006) and Chapter 2).

In a region distinct from the MGE, the CGE, a heterogeneous group of cells begins to develop. These cells are marked by the serotonin receptor 5HT3aR, and they settle primarily in the upper layers of neocortex Lee et al. (2010). The serotonin receptor 5HT3aR was first demonstrated to mark a subset of inhibitory interneurons in neocortex by Morales et al. (1996), but identification of these cells as a group was slow. In contrast to PV and SOM, there are not selective antibodies for 5HT3aR because it is part of a family of similar molecules Rudy et al. (2010). Eventually, a mouse was created that selectively expressed GFP from the 5HT3aR locus, making it finally possible to mark cells without the arduous process of in situ hybridization.

5HT3aR marks the most heterogenous class of cortical interneurons, one with subsets labeled by vasoactive intestinal peptide (VIP), neuropeptide-Y (NPY), Reelin, and others Rudy et al. (2010) (Figure 2A). One subset of 5HT3aR cells called neurogliaform cells inhibit pyramidal cells with slow $GABA_B$ inhibition that is strong enough to modulate the excitability of small regions of cortex Tamás et al. (2003) (Figure 2B). Recent work suggests that input to these cells comes from non-specific parts of the central sensation relay system, the thalamus Cruikshank et al. (2012).

It was discovered in 2010 that the markers PV, SOM, and 5HT3aR identify the entirety of inhibitory cells of the somatosensory region of the adult neocortex Lee et al. (2010). Moreover, the ratios of SOM- and PV-positive inhibitory cells differ by no more than 5% across large swaths of the neocortex Xu et al. (2010). Until it is shown otherwise (Chapter 2), we can think of PV-, SOM-, and 5HT3aR-expressing cells as the three canonical classes of inhibitory interneurons.

I have listed classes of neurons already, but I have in large part passed over the issue of what defines a neuronal cell class. Experiments in the nineteenth century defined neurons based on their shapes or morphologies, due to the ease with which neurons in tissue could be stained y Cajal (1890). Upon improvement of electrophysiological recording techniques, cells were independently sorted by their spiking patterns. These techniques have been united by immunohistochemistry and genetic expression of reporter proteins Masland (2004). We will define a class of cells by the intersection of these four characteristics–immunohistochemistry, genetic expression, electrophysiology, and morphology.

Until recently, the primary method of identifying protein localization was by immunohistochemistry (e.g. Celio and Heizmann (1981); Hendry et al. (1984)). Immunohistochemistry is the only method described by which we can actually define cells by their expression of endogenous proteins. However, it has some fundamental drawbacks. Antibodies are commonly made by injection into animals, which develop an immune response that can be isolated. This makes consistency between batches of antibodies variable. In addition, it is often difficult to generate antibodies to a single member of a family of similar proteins Lee et al. (2010). Finally, cells may actively vary levels of a protein, making the entire population difficult to identify Donato et al. (2013). This difficulty leads immunohistochemistry to have false negatives, but few false positives for the best antibodies.

Another more demanding method is to target the precursor to the protein, its mRNA, by in situ hybridization (ISH). Except in rare cases, to have protein in a cell one must have recently had mRNA. ISH carries the distinct advantage that we can synthesize nucleotide sequences with ease, making it possible to target the mRNA of any protein. However, mRNA can be generated, but modified or destroyed prior to becoming a protein. With the development of riboSeq, sequencing those mRNAs to which ribosomes are attached, it has been determined that some mRNAs are present in large quantities in the nucleus, but are never translated Bazzini et al. (2012); Ingolia (2014). Therefore, a high-quality ISH will have few false negatives, but may have many false positives Lee et al. (2010).

Two genetic techniques have made the identification of cell classes dramatically easier, but carry similar caveats to those above. One method relies on chance to obtain the desired target. A large region of DNA in the form of a bacterial artificial chromosome (BAC) is modified to contain a promoter of interest upstream of a reporter gene Yang et al. (1997). The BAC inserts randomly into the DNA, where a variety of DNA signals and methylation lead to activation of the gene in a subset of the cells in which the promoter would be activated. This has been used to great effect to study SOM cells as described above Ma et al. (2006); Oliva et al. (2000).

In 1994, the DNA of a mouse was manipulated such that it had only alterations to its sequence within a targeted gene Gu et al. (1994). From this process called knock-in, one can express a reporter gene activated by the gene promoter of interest Taniguchi et al. (2011). Labs have now generated a wide variety of mouse lines with expression from different promoters that signal distinct cell types Taniguchi et al. (2011). As an added benefit, a system has been devised to split the reporter from the promoter via the Cre recombinase. Depending on the poorly-understood vagaries of motifs in the DNA, a reporter may perfectly reflect the production of protein, mRNA, or may have many false negatives.

We have particular interest in three mouse lines: SOM-Cre Taniguchi et al. (2011), PV-IRES-Cre Hippenmeyer et al. (2005), and PV-2A-Cre Madisen et al. (2009). All of these animals were generated in a C57 black 6 (C57BL/6) background. The SOM-Cre mouse was created by inserting the Cre recombinase downstream of the intact somatostatin gene, separated by an internal ribosome entry site (IRES). The normal SOM mRNA transcript is lengthened, but retains signals in the downstream 3' end of the gene. The IRES has a much lower affinity for ribosomes than the start site upstream of the primary gene of the transcript, and therefore marks only cells that have had high expression levels, transient or constitutive Madisen et al. (2009). Because the activation of a reporter by Cre is binary, when a cell has expressed the SOM transcript for any part of its life, any reporter in the cell will be activated indefinitely. The expression pattern of this animal labels all SOM immuno-positive cells in addition to a subset of PV-positive cells Hu et al. (2013).

PV-IRES-Cre was generated similarly. It, too, marks cells expressing PV protein well, but it may miss cells expressing low levels of PV Hippenmeyer et al. (2005); Madisen et al. (2009).

Finally, PV-2A-Cre generates a fusion protein of PV and Cre separated by a self-cleaving linker 2A Madisen et al. (2009). In this case, Cre is expressed at levels almost equal to the gene to which it is paired, meaning that it marks even cells with low mRNA levels.

Because each technique has limitations, we have combined electrophysiological, immunohistochemical, and genetic techniques to create what we hope is a more complete definition of FS inhibitory cell types of the neocortex.

1.0.2 Gap junctions

Traditional intercellular signaling in the brain is done via small molecules, which bind to their downstream receptors eliciting either quick responses directly through ion channels or slower responses via G protein-coupled receptors. Such connections pair cells one-to-one with signals of a definite strength. It is perhaps a shock when it is revealed that like-types of neocortical interneurons also signal via transcellular ion-passing pores in their membranes called gap junctions Galarreta and Hestrin (1999); Gibson et al. (1999).

Gap junctions were first discovered in the mouse heart and liver Revel and Karnovsky (1967). They were so named because of the close proximity of the membranes of neighboring cells across a narrow gap. Eventually, it was discovered that neurons were coupled by such junctions during development Loewenstein (1981). These gap junctions allowed small dyes to pass between cells, allowing researches to visualize clusters of connected cells Connors et al. (1983).

Hexamers of the protein family Connexin (Cx) join together to form the single half of a gap junction channel in a membrane, called a connexon (Figure 3A). Plaques of hemichannel connexons from a pair of cells combine to form the channels of a gap junction (Figure 3B,C).

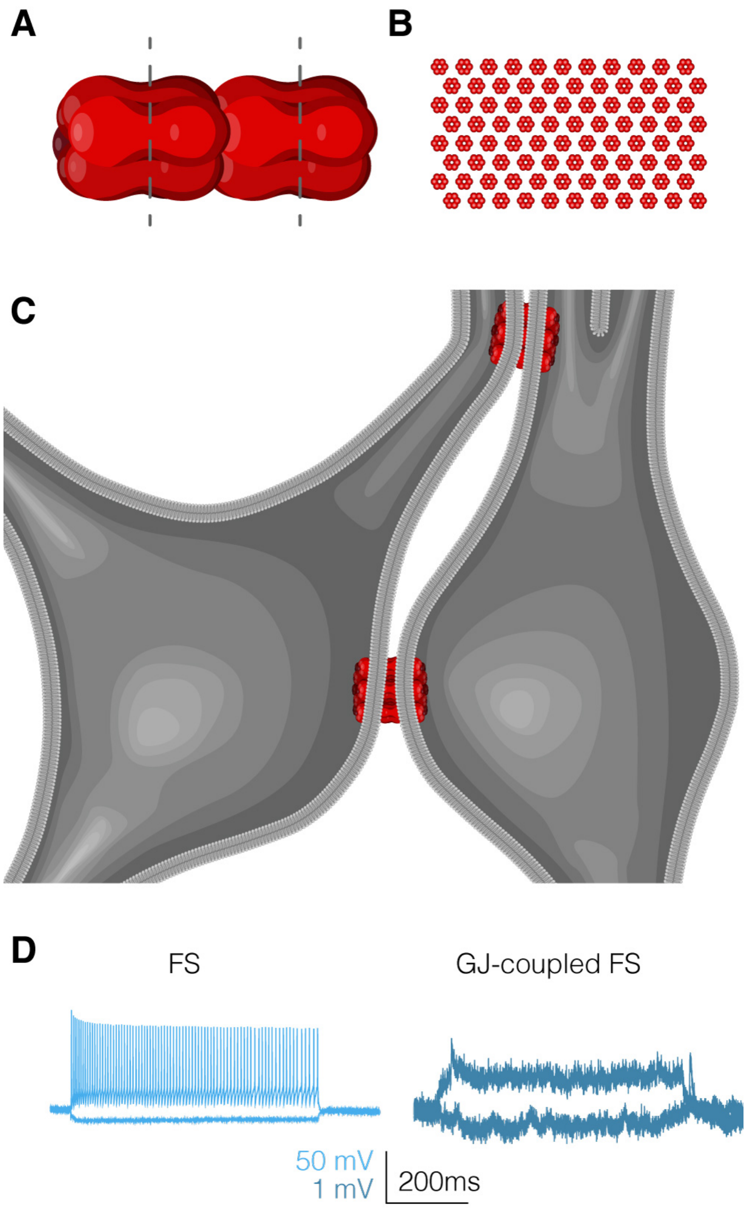

Figure 1.3: (A) Two homohexameric connexons meet to form a pore. Dashed gray lines mark the lipid membrane.(B) Face on, a gap junction is made from a plaque of individual pores. (C) These plaques connect dendro-dendritically (top) somato-somatically (bottom) or dendro-somatically (not shown). (D) Example of signal passed through a weak gap junction. On the left are voltage responses of an FS cell to injected current. On the right are the signals passed through a gap junction to a coupled FS cell. Note that slow membrane changes are passed but spikes are filtered out.

These gap junctions are found widely across the body, including acting to synchronize the beating of the heart. In the heart, waves of depolarization spread between muscle fibers via gap junction channels, including those composed of Cx45 Kumar and Gilula (1996). Of the more than 20 genes that code for connexins, only two are expressed at significant levels in neocortical interneurons, Cx45, and Cx36 Söhl et al. (2005). Not surprisingly, the constitutive knockout of Cx45 is lethal. But, of those three connexins, the dominant neuronal protein is Cx36 and it appears to form gap junctions exclusively of homohexamers Söhl et al. (2005).

In 1999, it was discovered that gap junctions coupled like-types of inhibitory interneurons in the adult neocortex Galarreta and Hestrin (1999); Gibson et al. (1999). More than half of FS cell pairs were coupled to each other, and more than half of putatively SOM-positive cells were coupled to each other. However, LTS and FS cells were rarely coupled. Since then, great numbers of like-types of interneurons have been found to be electrically coupled Hestrin and Galarreta (2005); Simon et al. (2005). Because of the signaling properties of these connections, they became known as electrical synapses.

At first glance, pores between cells would seem to negate the benefit of having multiple cells; if one spikes, doesn't that spike propagate to all of the connected cells? Cx36-based pores are extremely small, only allowing molecules smaller than Lucifer yellow (457 Daltons) through Cruikshank et al. (2005). Because of the small size of ions and gap junction permeability, ions and their resulting currents can pass through. In electronics terms, these connections act as conductors with high resistance between cells Srinivas et al. (1999). The RC circuit formed by membranes and their gap junctions becomes a low-pass filter, synchronizing slow membrane potential variations but attenuating fast changes such as action potentials (Figure 3D, Connors and Long (2004)). Instead of combining a group of cells into a single entity, gap junctions form a unique type of processing: symmetrical bidirectional synapses that pass both positive and negative currents. In so doing, gap junctions pass afterhyperpolarizations, subthreshold activity, and spikelets, synchronizing cells that would otherwise be independent Bennett and Zukin (2004); Long et al. (2005a); Mancilla et al. (2007). This is more broadly defined by the strong frequency-dependence of electrical synapses Gibson et al. (2005).

The spread of the effects of gap junctions was beautifully studied by Amitai et al. (2002).

Through careful measurements of the densities of inhibitory cells and their probabilities of being electrically coupled, they determined that, on average, 5-25 cells are directly coupled to a single cell, and yet the central cell has measurable influence over 22-51 cells via indirect coupling. In this way, a network of like-type inhibitory neurons can listen in on the activity of compatriots far removed.

Soon after discovering neocortical gap junctions, two groups raced to create constitutive knockout mouse lines of the primary gap junction protein Cx36 Deans et al. (2001); Hormuzdi et al. (2001). Both showed a complete abolishment of the Cx36 protein and an extreme decrease in the percentage of electrically coupled cells. Electrophysiological measurements have found an 84% reduction of coupling in the neocortex Deans et al. (2001) and a 97% reduction in the thalamic reticular nucleus (TRN) Landisman and Connors (2005). One recent study of dye-coupling resulted in dramatically different measurements from electrophysiological experiments, suggesting that there is only a 50% decrease in dye-coupling Lee et al. (2014). Nonetheless, the knockout of Cx36 significantly decreases electrical coupling in the brain.

In the quest to understand electrical synapses, drugs have been used to block them temporarily. In comparison to the knockout mouse, the effects are reversible and only active in the presence of the drug. However, they are also nonspecific. A common gap-junction blocker, carbenoxolone, has been found to have dramatic effects on excitatory transmission Beaumont and Maccaferri (2011). Other drugs such as mefloquine increase spontaneous activity and depolarize cells Cruikshank et al. (2004). Because of these nonspecific effects, it is preferable to study electrical synapses in a knockout animal.

However, the constitutive knockout mouse line may not be perfect; there may be compensation for the loss of gap junctions beyond the cells in which they are usually expressed. We have found that there is a significant decrease in the resistance of the never-coupled RS cells in the knockout animal (Chapter 3).

We have worked towards generating a conditional knockout mouse in which Cx36 can be turned off in neocortical interneuronal subtypes late in development via the Cre recombinase. First, we obtained a mouse line in which Cx36 could be conditionally removed Wellershaus et al. (2008). We recorded from pairs of cells in mice without the Cre recombinase expressed– those which should have had the normal complement of Cx36. Instead, they had electrical synapses at only 20% of the rate of normal animals, making them useless for further studies. Quantitative PCR for the Cx36 mRNA confirmed this result. Next, we obtained a conditional Cx36 knockout (unpublished, David Paul) and a conditional Cx45 knockout. Although these mouse lines were not used in this thesis, I have generated conditional knockouts selective for PV and SOM cells of Cx36 and, independently, of both Cx36 and Cx45.

We know that gap junctions can synchronize pairs of neurons as electrical synapses, but what do electrical synapses do for cortical activity more broadly? Combining data from the knockout animal and genome-wide association studies, we can get insight into the roles of gap junctions. Mutations in the Cx36 gene in humans have been linked to an increase in epilepsy, in particular genetically linked epilepsies such as juvenile myoclonic epilepsy Mas et al. (2004). Gap junctions are also potently affected by antimalarial quinine derivatives such as mefloquine Cruikshank et al. (2004); Srinivas et al. (2001). These drugs have potent side effects including vivid, graphic hallucinations, which may be in part due to their effects on gap junctions.

In the mouse, both the insulin-producing pancreatic beta cells and cells in the eye are linked by electrical synapses, which both serve to synchronize the cells Meda (2003) and limit noise in the network Hartveit and Veruki (2012). Mice without gap junctions are unsteady (ataxic) Van Der Giessen et al. (2008) and their circadian cycles are disrupted Long et al. (2005a).

Although we know of many behavioral effects of the knockout of Cx36, the roles of electrical synapses remain tantalizingly elusive. Electrical synapses are unique in that they form the only type of symmetric bidirectional signal between cells and that they pass depolarization and hyperpolarization equally well. One suggestion for a role of these synapses comes from work in the hippocampus, which showed a decrease in the strength of cortical gamma-band oscillations without gap junctions Buhl et al. (2003).

1.0.3 Cortical gamma-band oscillations

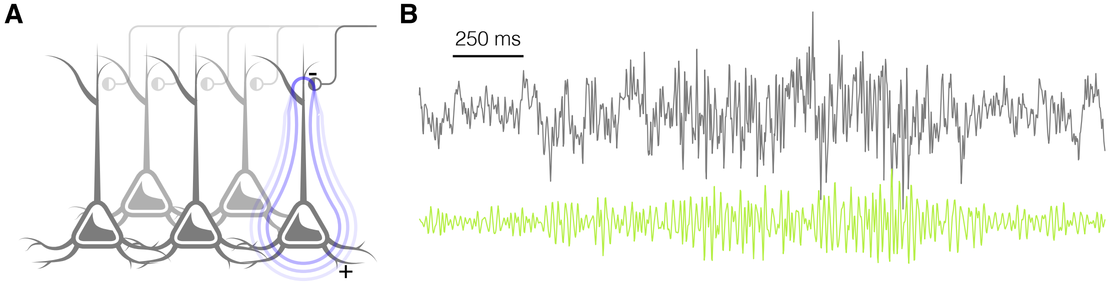

Figure 1.4: (A) Parallel apical dendrites of pyramidal cells generate strong rhythms. A synapse on the apical dendrite creates a dipole with field lines shown in blue. Minus shows an extracellular current sink, plus shows the diffuse extracellular current source. (B) Gamma rhythms from an EEG electrode over the prefrontal cortex of the author in the throes of dissertation generation. Gray is the raw signal, lime green is the signal bandpass filtered between 30 and 80 Hz..

Since 1875, humans have been recording rhythmic pulses of electrical activity from our brains Caton (1875). Amazingly, the synchronous activity of many neurons is sufficient to generate electric fields strong enough to pass through our skulls and skin Buzsáki et al. (2012).

To understand the origin of these fields, one must consider the activity of individual ion channels. An excitatory presynaptic cell releases glutamate into the extracellular space, which binds a fast glutamate receptor (AMPA receptor). The pore of this receptor opens, allowing calcium and sodium to flow inwards and potassium to flow out. This charge locally depolarizes the cell, creating an extracellular current sink Buzsáki et al. (2012). A distributed passive current from the cell soma and other distal regions creates an extracellular current source and from this combination of source and sink we have a dipole Buzsáki et al. (2012) (Figure 4A).

Synaptic currents of small numbers of cells are sufficient to generate small fields detectable by electrodes adjacent to cells, but the electric fields that pass through the skull likely come from aligned synchronous synaptic events across a forest of tree-like pyramidal cells with parallel apical dendrites all extending towards the surface of the brain Buzsáki et al. (2012) (Figure 4A).

One band of EEG frequencies is especially interesting: the gamma band. The gamma band is commonly defined as the frequencies between 20-90 Hz, with variability in the definition in the extremes of the range Adesnik and Scanziani (2010); Buzsáki et al. (2012); Cardin et al. (2009); Moore et al. (2010). Power in the gamma band seems to increase upon attention Lutz et al. (2004) (Figure 4B) and people with schizophrenia show a decrease in their gamma oscillations during perceptual tasks Uhlhaas and Singer (2010). Both of these observations suggest that gamma oscillations may be important in neural computation.

Gamma oscillations are highly localized, often within a region of only 250 μm in diameter Katzner et al. (2009); Paik et al. (2009); Sridharan et al. (2011); Tiesinga and Buia (2009); Xing et al. (2009). Because of the limited spatial resolution of EEGs, targeted recordings have been made from electrodes inserted into the brain.

Early experiments in 1988 showed "stimulus-evoked resonances" in visual cortex within the gamma band evoked by visual stimuli Eckhorn et al. (1988). Quickly thereafter in a one-two punch, the resonances were found to be strongest within a cortical column of cells which collectively respond to similar directions of movement Gray and Singer (1989). Then, separate columns with similar orientation preferences were found to resonate most strongly when both were activated by a stimulus Gray et al. (1989). This finding led the authors to propose gamma-band synchrony as a solution to "the binding problem." How does a percept, a packet of information composed of multiple linked sensations, stay as a unit as it passes through the gauntlet of a persistently active neocortex? It is possible that percepts are linked by their firing closely with a particular phase of the local gamma oscillations Fries (2009); Gray et al. (1989).

In an especially elegant experiment, Fries et al. (2001) recorded from neurons in a higher-order visual region of the primate neocortex termed V4. A monkey was trained to concentrate on one location in the visual field while fixing his gaze upon another. Researchers then asked what differentiated a cell in the brain region being selectively attended to from a cell in the region associated with the direction of its gaze. Neither spike rate nor spike timing differentiated the two cells. The only differentiating factor was that attention increased the spike synchrony with the local gamma band oscillations.

The electrical signals of EEGs come from summed synaptic currents along parallel dendrites, but what cellular processes generate these rhythms? The first models suggested that a paired inhibitory and excitatory cell could generate such rhythms Gray (1994), which no longer seems likely Whittington et al. (2011). Instead, an early hippocampal model of activity relied solely on reciprocal inhibition of inhibitory cells Whittington et al. (1995). This model has since been called interneuron gamma (ING). In this case, the time constant of inhibition was sufficient to alter the rate of oscillations in computational models Whittington et al. (1995). Within two years, the same group proposed an alternative mechanism of gamma oscillations: synchronized inhibition onto excitatory cells generates synchronized excitation onto inhibitory cells Traub et al. (1997). This describes the competing pyramidal-interneuron gamma (PING) model. Differences between the two mechanisms are subtle, but a primary differentiator of the two is that ING leads to a 0 ms phase lag between the firing of excitatory and inhibitory cells, while PING leads excitatory (RS or pyramidal) cells to fire before inhibitory cells.

The type of interneuron required to generate gamma oscillations was suggested soon thereafter to be FS cells Wang and Buzsáki (1996). Since then, it has repeatedly been suggested that gamma oscillations originate with FS, or PV positive, cells rather than LTS or SOM positive cells (e.g. Cardin et al. (2009), Whittington et al. (2011) and references therein, Chapter 4).

We have seen that gap junctions can serve to synchronize cells. Now we have learned that cell synchrony could be an important part of our brain's computations. It is natural to posit that gap junctions are important for gamma-band oscillations. We have investigated the relationship between gap junctions and gamma oscillations and the results are described in Chapters 3 and 4.

1.0.4 Postrhinal cortex

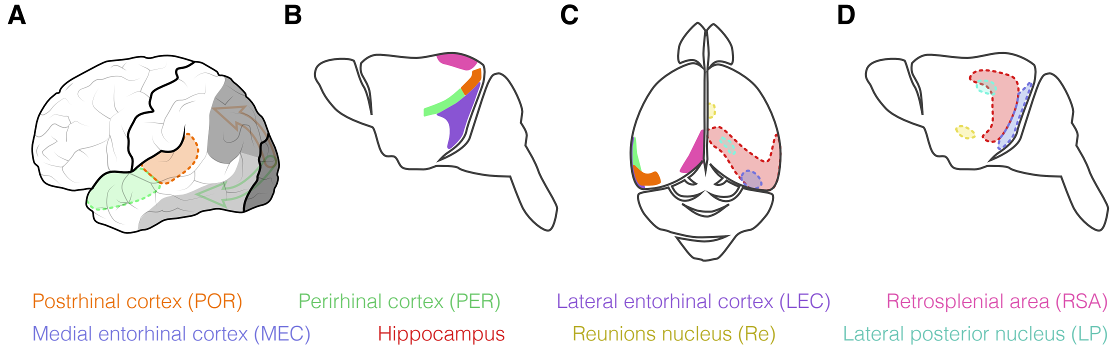

Figure 1.5: Locations of connected regions in mouse and human brains. Dotted transparent regions are within the brain, shaded regions are on the surface. Regions are named at the bottom. (A) Two visual streams in a human brain begin in the occipital lobe and go dorsally to the parietal lobe (orange arrow) or ventrally to the temporal lobe (mint green arrow). POR and PER are on the cortical surface folded towards the midline. Only POR and PER are shown. (B) Regions on the flat or lissencephalic surface of the mouse brain, side view with anterior to the left. (C) Regions on the mouse brain surface (left) or inner structures (right) from above. Anterior is up. (D) Internal regions of the mouse brain.

Visual sensory information passes through a circuitous route on its way to being encoded into a memory. On the way, it passes through circuits of gap-junction-coupled inhibitory cells entrained in gamma-band oscillations within the cerebral cortex. From the preprocessing in the retina through the sensory relay of the thalamus, information from photons passes to ions as it transits to primary visual cortex.

From visual cortex, two parallel and highly interconnected forms of processing begin Lamme et al. (1998); Ranganath and Ritchey (2012) (Figure 5A). One path performs object recognition and is titled the "what" visual stream Nassi and Callaway (2009). This path travels along the bottom or ventral part of the brain through the temporal lobe in primates eventually to the perirhinal cortex (PER), through the lateral entorhinal cortex (LEC), and into hippocampus. A second stream travels along the top or dorsal part of the brain through the parietal lobe to the postrhinal cortex (POR), and later on to the hippocampus by way of the medial entorhinal cortex (MEC) Goodale and Milner (1992); Nassi and Callaway (2009) (Figure 5).

PER and POR are both part of a region called the parahippocampal region (PHR) Burwell et al. (1995). Confusingly, in primates, the POR is called parahippocampal cortex, but is part of the parahippocampal region Burwell et al. (1995). PER and POR lie in a line along the lateral edge of the rodent brain (Figure 5B) and share many properties Beaudin et al. (2012) including extensive interconnection Agster and Burwell (2009); Burwell and Amaral (1998b). The PHR lies on the border of neocortex and a cortical region without six layers, allocortex. The dorsal portion of the PHR contains six distinct layers and thus is neocortex. The allocortical neighbor to the PHR, the entorhinal cortex, is missing layer 4 leading to the descriptive title of the lamina dessicans Pelletier et al. (2004). It's worth noting both that lamination of the dorsal PHR is less distinct than that of primary somatosensory cortex and that lamination of the ventral PHR is nearly nonexistent–neither obviously allocortical nor neocortical. However, local connectivity, cytoarchitectonics, Burwell (2001); Burwell and Amaral (1998b); Furtak et al. (2007) and immunohistochemical reactivity (Chapter 2) demonstrate that PHR is neocortical.

Our attention was drawn to the PHR and the POR in particular due to the extreme decrease in PV staining in the ventral half of POR. Cells expressing PV-IRES-Cre are completely absent from the core of this region. Nowhere in neocortex is this absence more extreme (Chapter 2 and see Glickfeld et al. (2014)). This is not confined only to mice; low PV levels are found in rats Burwell et al. (1995) and in primates Pitkänen and Amaral (1993).

One of the many strengths of the brain is in its flexibility in parallel processing; the two visual streams should not be considered wholly independent, rather they can be compared to two companies with shared executive board members as we shall see when comparing PER and POR Nassi and Callaway (2009). The two-streams hypothesis was formed as a result of experiments done in primates, but anatomical and electrophysiological recordings support the separation of processing in rodents as well Glickfeld et al. (2014); Wang et al. (2011).

The anatomical pathways to PER and POR have been dissected exquisitely Agster and Burwell (2009, 2013); Beaudin et al. (2012); Burwell and Amaral (1998a,b); Burwell et al. (1995); Furtak et al. (2007). Their inputs are varied and many, but POR receives primarily visual input while PER receives cross-modal inputs Furtak et al. (2007).

The easiest way to dissect the roles of POR and PER is via studies in which lesions of small brain regions have been selectively introduced. Lesions of PER led to an inability to perform difficult visual discriminations that require memory Bussey et al. (2003) and to correctly identify objects Murray and Mishkin (1998); Murray et al. (2000). In contrast, lesions of the POR led to an inability for an animal to detect when an object was in an unusual context Norman and Eacott (2005). It appears that PER deciphers complicated objects via multiple senses and passes the information on to the brain's card catalog, the hippocampus, while POR uses primarily visual information to recognize context, and in collaboration with PER, puts objects in context. Putting objects in context is essential to an animal's well-being. A predator on the far side of a river from oneself requires radically different responses from a predator on the near side. Similarly, steel wool and shredded wheat are most easily differentiated not by texture, but rather their context in the toolbox or the cereal box.

Although the visual stream hypothesis is unidirectional, the PHR passes information bidirectionally de Curtis and Paré (2004). It has long been assumed that sensory inputs are processed through sequentially more abstract cortical regions until they reach the PHR. There, they are further processed and passed into the entorhinal and hippocampal systems. Remarkably, the path can be reversed, likely with PHR acting as the cortical gate de Curtis and Paré (2004); Kealy and Commins (2011). This gate has been referred to as the "wall of inhibition," de Curtis and Paré (2004), stopping information flow from neocortex to hippocampus without external activation of PHR. When the path is reversed, information can flow backward through the PHR and into the neocortex Eichenbaum (2000). This reversed path allows for remarkable processing, such as replaying memories while an animal is asleep Ji and Wilson (2007).

POR is described as association cortex, receiving inputs from the pre-processed dorsal visual stream Kondo and Witter (2014). Although its inputs are many, we will focus on three that are particularly relevant (Chapter 2): the lateral posterior nucleus of the thalamus (also lateroposterior, LP), the reuniens nucleus of the thalamus (Re), and retrosplenial area (also retrosplenial cortex, RSA) (Figure 5B-D).

The LP is one of the dorsolateral nuclei of the thalamus. It has connections both with cortex, including POR, and with the superior colliculus Conte et al. (2008). The superior colliculus is a portion of the midbrain that both passes sensory information towards the cortex and motor information out towards muscles; connections with the LP may drive behavior Conte et al. (2008). In particular, lesions in LP have led to contralateral neglect, the inability to attend to objects on the side contralateral to the lesion Conte et al. (2008). This finding suggests that LP plays an important role in directed attention. Notably, LP provides less than 15% of the subcortical inputs to the POR Furtak et al. (2007), but is one of primary inputs to inhibitory cells of the POR (Chapter 2).

Re is a midline thalamic nucleus with promiscuous connections. It is a major source of thalamic input to the hippocampus Vertes et al. (2007) and the thalamic source second only to LP to the POR (Vertes et al. (2007) and Chapter 2). This feature is especially important because although the hippocampus projects strongly to the medial prefrontal cortex (mPFC), the executive center of the brain, both the hippocampus and the PHR receive minimal input in return. Instead, the mPFC projects strongly to Re, which acts as a relay to the hippocampal regions Cassel et al. (2013); Vertes et al. (2007).

RSA is a region of cortex along the midline, notable for a low density of PV-IRES-Cre cells Glickfeld et al. (2014) and parvalbumin staining (data not shown). Unlike LP and Re, which project to both PER and POR, RSA specifically projects to POR Ranganath and Ritchey (2012). fMRI studies have shown that RSA is active in subjections remembering the context of an event (Ranganath and Ritchey (2012); Vilberg and Rugg (2008) and references therein). Studies in rodents have shown that RSA is active during spatial working memory, in particularly when solving a maze Pothuizen et al. (2009). It is further segregated into visual and multimodal regions Pothuizen et al. (2009). Although POR itself is not associated with spatial navigation Burwell et al. (2004), inputs from RSA likely aid POR in defining context.

POR is a fascinating region, forming a gate between hippocampal and neocortical processing. It has broad inputs and outputs, but is striking in its ventral half lacking canonical PV cells. Especially given the bidirectional signaling through the region, it is important to understand how inhibition functions there (Chapter 2).

1.0.5 Goals of this dissertation

In this dissertation, I have addressed two questions. First, how is inhibition altered in a neocortical region lacking canonical FS cells, and second, what role do gap junctions play in neocortical gamma oscillations?

The diminution of PV expression in vPOR had been previously noted Beaudin et al. (2012); de Curtis and Paré (2004), but the extent of this decrease had not been characterized, nor had the effects of the absence of canonical FS interneurons. Measurements of a network lacking PV cells has implications beyond the action of POR. As described above, two mouse autism models lack PV-expressing cells in sporadic patches of neocortex Gogolla et al. (2009), and gamma oscillations entrained by FS cells are altered in patients with schizophrenia Uhlhaas and Singer (2010). Furthermore, I have identified a non-canonical FS cell in vPOR that we now know exists beyond the borders of the canonical FS-cell free vPOR (Chapter 2).

In studying vPOR, I had three sub-aims. First, I had to thoroughly characterize the region immunohistochemically to determine if vPOR had a lower density of inhibitory cells than a region of control cortex, the adjacent dPOR. Next, I determined how inhibition onto RS cells was altered in vPOR through a combination of optogenetic and electrical excitation of groups of inhibitory interneurons. Finally, I asked whether vPOR contained only the known complement of inhibitory cells through paired electrophysiological recordings combined with immunohistochemistry for individual recorded cells.

To determine the effects of gap junctions on gamma oscillations, I took a two-pronged approach. I adapted a known mechanism for generating gamma-oscillations in slices such that I could titrate levels of asynchronous activity relative to gamma-band activity. Using this system, I asked in both primary somatosensory cortex and dPOR whether gamma oscillations were altered in the Cx36 knockout animal relative to its wild-type littermates (Chapter 3)

In parallel, I created a computational model of layer 4 of somatosensory cortex to explore parameters not easily modulated in slices. Cells from a previous model of cortical oscillations were modified to better match my slice data. The cells were connected into a network of neurons almost 900 strong with probabilities based on data from the literature. Finally, I added gap junctions and the ability to selectively remove them. With this model, I could compare the relative importance of FS and LTS cells in the gamma oscillations and the effects of simultaneous competing rhythms (Chapter 4).

Chapter Two

Cortical inhibitory function in the absence of canonical parvalbumin-expressing interneurons

2.0.6 Contributions

Arthur U. Sugden performed the electrophysiology, cell fills, imaging, analysis, and wrote the manuscript. Saundra L. Patrick performed the immunohistochemistry and helped with the imaging. P. Michelle Fogerson injected the rabies and helper viruses. Rebecca D. Burwell identified the slice plane and gave extensive help regarding POR and its inputs. Barry W. Connors directed the work and co-wrote the manuscript.

2.1 Summary

The ventral postrhinal cortex (vPOR), a subset of the parahippocampal region, shows a striking lack of parvalbumin-expressing neurons. Parvalbumin-expressing (PV) cells are the most common type of inhibitory interneuron in the cerebral cortex with a near one-to-one overlap with the fast-spiking electrophysiological phenotype. These cells mediate feedforward inhibition and gamma oscillations, so their absence suggests radically altered inhibitory circuitry. Cell counts demonstrate that there is a decrease in inhibitory cell density in vPOR; other cell types do not compensate with increased densities. While PV cells are absent in vPOR, the dorsal half of POR contains a regular complement of PV cells. Despite vPOR's lack of PV cells, it can generate optogenetically- and electrically-evoked inhibition with equal strength to neighboring PV-containing cortex. vPOR can also generate gamma oscillations. Furthermore, we identified in vPOR a new class of fast-spiking cells, most of which do not express PV but are marked by somatostatin-IRES-Cre. These non-canonical fast-spiking cells (nFS) are differentiated from canonical FS cells of POR not only by PV, but also by their lack of inputs from retrosplenial cortex. nFS cells are not confined only to vPOR, but spread into neighboring canonical PV-containing cortex. vPOR provides a unique window into cortical circuits; it has allowed us to probe the effects of a substantial decrease in inhibitory cell density and

to identify a new group of fast-spiking cells with low or no PV that also exist in neighboring cortex with canonical PV cells.

2.2 Introduction

Three protein markers completely define exclusive classes of neocortical inhibitory interneurons in mouse somatosensory cortex: parvalbumin (PV), somatostatin (SOM), and a serotonin receptor subtype (5HT3aR) Rudy et al. (2010). PV and SOM cells share a common origin in the medial ganglionic eminence (MGE) and show rare overlap in mRNA of less than 5%. In contrast, 5HT3aR cells originate in the caudal ganglionic eminence and their markers do not overlap with MGE-derived cells Rudy et al. (2010). The relative proportions of these classes are consistent across the vast majority of the neocortex, with PV cells comprising 40% of inhibitory interneurons across S1, V1, and frontal cortex Xu et al. (2010).

The three exclusive classes of inhibitory interneurons correspond with identifiable electrophysiological phenotypes Rudy et al. (2010). The fast-spiking (FS) electrophysiological phenotype overlaps nearly completely with PV expression. These cells are marked by low membrane resistance, short time constants, narrow spikes with brief and deep afterhyperpolarizations, and high maximal firing rates. SOM primarily marks low-threshold spiking (LTS) cells, which have relatively high resistance, large spikes, strong spike-frequency adaptation, and can exhibit rebound spiking after hyperpolarization. 5HT3aR cells have heterogeneous firing patterns, but all are physiologically distinct from FS and LTS cells.

As a group, inhibitory interneurons are vital for preventing seizures, regulating temporal and spatial coding, and generating oscillations and synchrony in pyramidal cells. In particular, PV cells have been tightly linked with the generation of gamma oscillations (e.g. Cardin et al.

(2009); Isaacson and Scanziani (2011); Kepecs and Fishell (2014)), which in turn have been linked with attention Fries et al. (2001). In addition, they are essential for thalamocortical feedforward inhibition, initially firing strongly upon excitatory thalamic input and later, during continued activation, depressing Beierlein et al. (2003); Cruikshank et al. (2007); Gabernet et al. (2005).

The parahippocampal region is stationed as a gate for information passing between the neocortex and the hippocampus de Curtis and Paré (2004). In the parahippocampal region, inputs from a variety of sensory systems are integrated and passed to entorhinal cortex and hippocampus if the gate is open. The source of this gating is not entirely understood, but amygdalar input likely encodes object salience and may be the arbiter of PHR gating de Curtis and Paré (2004); Kealy and Commins (2011). Upon being processed by the hippocampus, information can flow along a reciprocal path, through the parahippocampal region to the neocortex Eichenbaum (2000).

The caudal portion of the parahippocampal region is the postrhinal cortex (POR). The POR sits at the border between neocortex and allocortex Suzuki (2010). On the ventral-caudal border of POR lies the parasubiculum and the entorhinal cortex, which have a clear lamina dessicans. This is a sharp transition marked by lamination and the overlap of SOM and PV immunostaining in many inhibitory cells Neske et al. (2015). Rostral to the dorsal-rostral boundary is traditional six-layered neocortex, which continues into POR. Perhaps the most striking aspect of the POR is the substantial decrease of the primary inhibitory interneuronal marker PV in its ventral half. In ventral POR (vPOR), there is an apparently near-complete absence of PV somata and projections. While this has been noted previously Beaudin et al. (2012); de Curtis and Paré (2004), the effects of this absence have gone unstudied.

In addition to the unique roles of PV cells, their near absence in vPOR could radically alter the balance of excitation and inhibition. Given that PV cells are the largest population of inhibitory cells in the majority of the neocortex, one would predict altered inhibition. Here, we have taken advantage of subtle differences in genetic mouse lines with combined electrophysiology and immunohistochemistry of individual cells to identify a new, large population of non-canonical FS cells. Although there is a population of FS cells in vPOR, vPOR continues to have a smaller total complement of inhibitory cells. We have activated subsets of the inhibitory network of vPOR optogenetically and electrically to determine the effects of this decrease of inhibitory cells. Remarkably, we have found equal total inhibition between vPOR and dPOR due to greater inhibition onto inhibitory cells in dPOR than in vPOR.

2.3 Results

2.3.1 Parvalbumin is absent from ventral postrhinal cortex

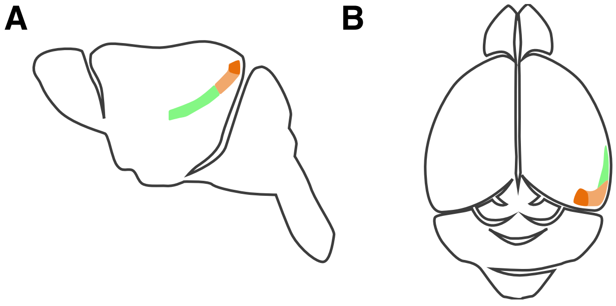

Figure 2.1: Postrhinal cortex (orange and light orange) and perirhinal cortex (green) in the (A) sagittal and (B) horizontal planes. The region in dark orange marks the portion of postrhinal cortex in which individual sagittal sections transect all cortical layers.

Traditionally, the POR has been viewed in coronal sections (e.g. Burwell and Amaral (1998b); Kondo and Witter (2014)). Because of the position and curvature of POR, coronal sections sever laminar connections and show only a subset of POR layers in a single slice. We have identified a 600 μm region of parasagittal slices, located 1300-1900 μm from the lateral edge of the cortex, which includes all cortical layers for POR, and we have confined our experiments to this region. Figure 2.1 shows the parahippocampal region (colored), with

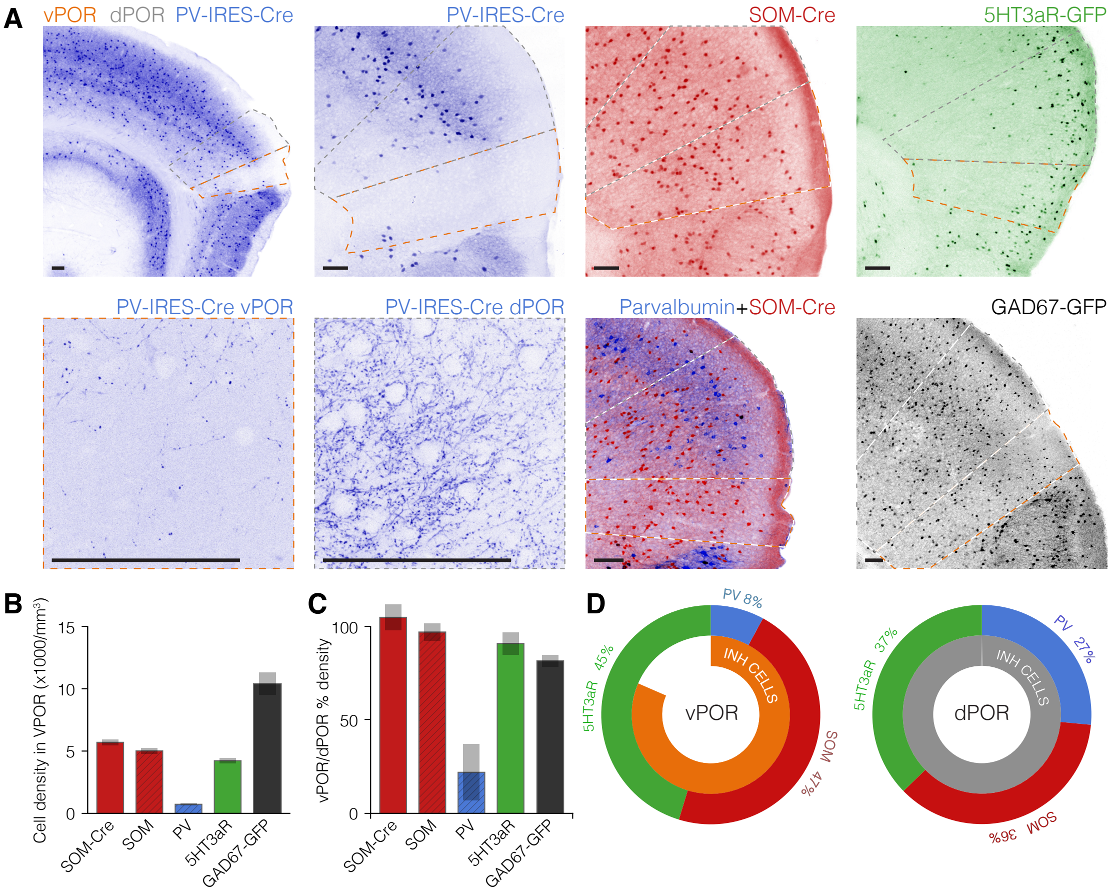

Figure 2.2: PV cells are uniquely missing from vPOR. The remaining cell types have constant densities between the adjacent dorsal POR and vPOR and there is no additional cell type taking the place of PV cells. Scale bars are 100 μm. (A) Psuedocolored images of endogenous fluorescent-protein expression from the genotype listed except for PV immunohistochemistry in Parvalbumin+SOM-Cre. Genotypes used are PV-IRES-Cre; tdTomato, SOM-Cre; tdTomato, 5HT3aR-GFP, GAD67-GFP. (B) Measured densities of inhibitory cell types in vPOR. Diagonal lines are antibody staining. Only PV cells are dramatically decreased in vPOR. Error bars are ±SEM. SOM-Cre N = 7 slices in 2 animals, SOM N = 11 slices in 2 animals, PV N = 17 slices in 2 animals, 5HT3aR-GFP N = 9 slices in 2 animals, GAD67-GFP N = 5 slices in 1 animal. (C) Ratios of densities in B to their respective densities in dPOR. (D) Populations in vPOR versus dPOR.

postrhinal cortex in both dark and light orange and the optimal region in dark orange.

We have combined genetics and immunohistochemistry to identify somata and projections in subsets of interneurons. First, we used a mouse line in which Cre recombinase had been introduced to the PV locus via knock-in downstream of an internal-ribosome entry site (IRES) Hippenmeyer et al. (2005). When it was crossed with the Ai9 tdTomato line Madisen et al. (2009), we saw a profound absence of PV cells in vPOR (Figure 2.2A). In contrast, the dPOR contains PV densities indistinguishable from the adjacent cortex. Confocal images of

PV immunolabeling calibrated to prevent saturation of PV-positive somata across the image showed almost no detectable labeling in vPOR (Figure 2.2A). This absence is not unique to mice; rats show a profound decrease in PV staining in vPOR Burwell et al. (1995) as do primates in the parahippocampal cortex Pitkänen and Amaral (1993). Not only are PV-positive somata largely missing from vPOR, but the PV-positive axons of dPOR do not extend into the region. Furthermore, this decrease is not unique to a particular age. The top left of Figure 2.2A shows a PV-IRES-Cre animal at P106 in which the decrease in tdTomato positive cells was confirmed by immunohistochemistry, while the adjacent image shows a PV-IRES-Cre animal at P25.

To determine the functional implications of the absence of PV interneurons, we have compared vPOR to the control region of the adjacent dPOR.

PV-IRES-Cre cells make up just under a third of interneurons in dPOR (Figure 2.2C-D), so their absence in vPOR could yield profoundly altered inhibitory function. We expected that there would be an increase in the density of either 5HT3aR or SOM cells to maintain the total density of inhibitory cells. Therefore, we compared densities between vPOR and dPOR in SOM-Cre; tdTomato and in 5HT3aR-GFP animals with the ventral/dorsal boundary marked by PV immunohistochemistry. Surprisingly, there was no detectable difference in the density of SOM or 5HT3aR cells between vPOR and dPOR. SOM immunolabeling confirmed that there was no difference in the density of SOM cells between vPOR and dPOR, although SOM immunolabeling marks only 88.0 ± 1.5% of cells expressing SOM-Cre; tdTomato in POR. Although no effective antibody exists towards 5HT3aR cells, expression in the 5HT3aR-GFP mouse line has been confirmed to mark nearly all 5HT3aR cells using in situ hybridizations Lee et al. (2010). So, we conclude that PV cells are less dense in vPOR, but SOM and 5HT3aR cells do not compensate with increased densities.

To confirm that there was no new inhibitory cell type unmarked by PV, SOM-Cre, or

5HT3aR, we measured the density of inhibitory cells marked by a mouse line that expresses GFP from the locus of the primary enzyme that converts glutamate to GABA, Glutamic acid decarboxylase 67 (GAD67) Tamamaki et al. (2003); Taniguchi et al. (2011). This mouse has been previously demonstrated to mark all inhibitory cells in motor cortex Tamamaki et al. (2003), and has since been widely used to label all interneurons (e.g. Gentet et al. (2010); Pfeffer et al. (2013); Yamashita et al. (2013)). Using this GAD67-GFP mouse line, we found a 19% decrease in inhibitory cells in vPOR relative to dPOR (Figure 2.2B). This is similar to the 25% decrease in inhibitory cell density we measure by summing densities from PV, SOM, and 5HT3aR cells.

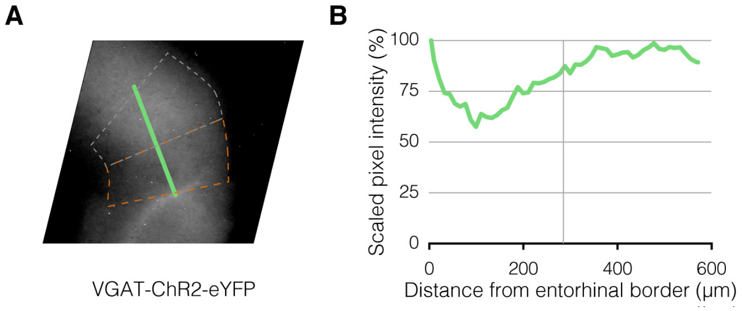

Figure 2.3: VGAT-ChR2-eYFP shows a roughly 25% decrease in fluorescence intensity in vPOR relative to dPOR. (A) Fluorescence image of a 300 μm slice of POR from a VGAT-ChR2-eYFP animal. Orange is vPOR, gray is dPOR, and green marks the line along which the pixel intensity was integrated. (B) Pixel intensity scaled to the entorhinal-vPOR border. Gray vertical line marks the transition from vPOR (below 300 μm) to dPOR (above 300 μm).

We have also confirmed this decrease in overall interneuron density by measuring the relative densities of fluorescently tagged cells in a GAD65-Cre; tdTomato mouse line in dPOR and vPOR Taniguchi et al. (2011). GAD65 and GAD67 are two isoforms of the enzyme required to convert glutamate to GABA. Although this mouse line is only 92% selective Taniguchi et al. (2011), we saw a corresponding difference of 19% fewer inhibitory cells in vPOR relative to dPOR. We also used an independent VGAT-ChR2-eYFP mouse line Zhao et al. (2011), which selectively expresses eYFP conjugated to channelrhodopsin in cellular membranes from the vesicular GABA transporter locus, which is essential for loading GABA into vesicles. Distinguishing somata from processes in this line is difficult due to the membrane expression, but the line marks dendrites and axons effectively. The integrated flux across dPOR and vPOR confirms that vPOR fluoresces at only 75% of the intensity of dPOR (Figure 2.3). Attempts at GABA immunolabeling in a PV-IRES-Cre animal yielded labeling that was incomplete and therefore uncountable. It is worth noting that the VGAT-Cre Vong et al. (2011); tdTomato mouse line, which has not been well characterized in cerebral cortex, did not show the difference in cell density found in the three other lines (vPOR density was 15,600 ± 700. cells/mm^2, dPOR was 16,100 ± 567 cells/mm^2). However, given that all inhibitory cells must express either GAD65 or GAD67 and we have found corresponding decreases in the densities of inhibitory cells in both mouse lines, we suspect that the VGAT-Cre mouse line is not exclusively selective for inhibitory cells. Corresponding with this assumption, the densities of cells are higher in VGAT-Cre than in GAD67-GFP.

To summarize, cell counts demonstrate that GABAergic inhibitory cells in vPOR are about 19% less dense than in dPOR, and this decrease results from the exclusive reduction in number of canonical PV cells.

2.3.2 sIPSCs and optogenetic population inhibition are consistent with densities of interneurons

Given the substantial decrease of inhibitory cell density in vPOR, we determined its consequences on network-level inhibition. To do so, we measured spontaneous inhibitory events (sIPSCs) onto excitatory cells in layer 4 of vPOR and dPOR. In accordance with the lower density of inhibitory cells in vPOR relative to dPOR, there were roughly 40% fewer sIPSCs in vPOR relative to dPOR (Figure 2.4A,C). However, the mean amplitudes of the events of the two regions were indistinguishable (Figure 2.4B).

PV immunostaining and the images of the PV-IRES-Cre animal showed that PV-expressing axons appear to avoid vPOR. This absence could be confirmed by measuring the inhibition

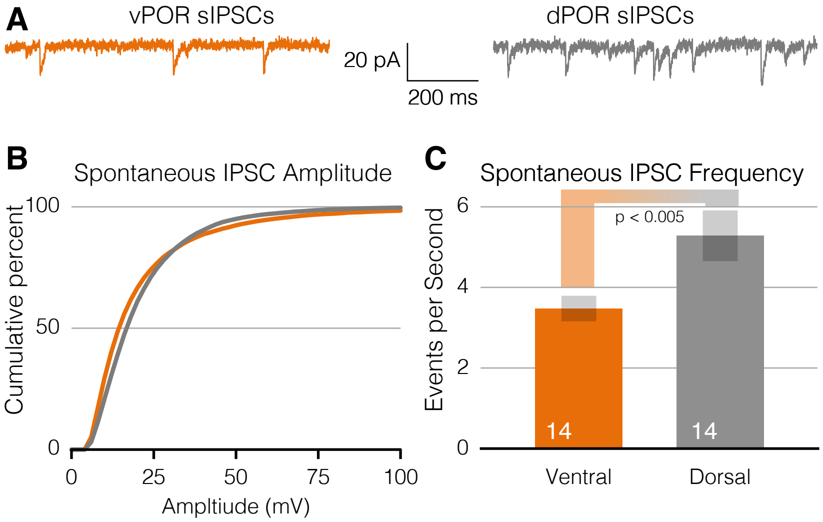

Figure 2.4: Recordings from regular spiking excitatory (RS) cells voltage clamped at -60 mV with a pipette solution containing relatively high chloride. (A) Example recordings of spontaneous IPSCs (sIPSCs) onto RS cells. (B) sIPSCs onto RS cells show no difference in amplitude between vPOR and dPOR (K-S test p-value 0.47). (C) However, the frequency of events is significantly lower in vPOR than in dPOR.

generated by all PV cells onto regular spiking excitatory (RS) cells in vPOR and dPOR. To do so, we expressed the algal light-gated cation protein channelrhodopsin (ChR2) specifically in PV cells. Viral injections cause localized expression and would not yield uniform activation across POR. Therefore, we used a floxed ChR2-eYFP reporter mouse line crossed with PV-IRES-Cre mice to express ChR2 in PV cells uniformly across POR.

We voltage clamped RS cells in layer 4 of vPOR and dPOR at -60 mV with pipettes that contained cesium and a relatively high chloride concentration that resulted in a synaptic reversal potential of -21.5 mV in order to optimally measure strong IPSCs. We blocked glutamatergic signaling with the NMDA receptor antagonist APV and the AMPA receptor antagonist DNQX and activated PV cells with a 5 ms pulse from a blue laser over the recorded cell across three orders of magnitude of stimulating power. This generated IPSCs across nearly all of the stimulus conditions, with IPSC amplitudes increasing with stimulus intensity until saturation was reached.

As expected, the combined optogenetically-evoked IPSCs evoked by PV cells onto RS

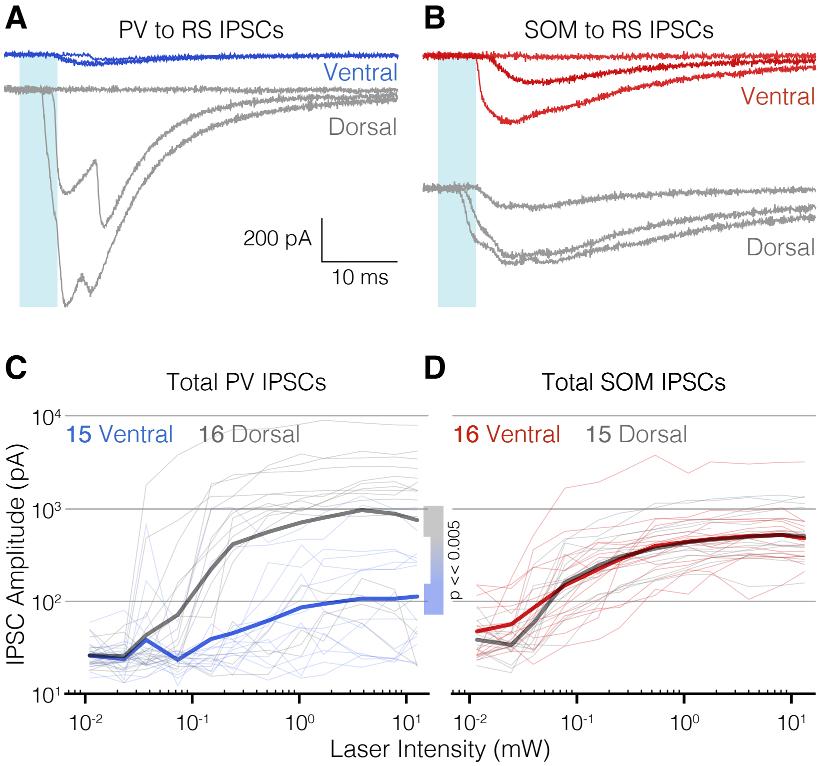

Figure 2.5: Recordings from regular spiking excitatory (RS) cells voltage clamped at -60 mV with a pipette solution containing relatively high chloride. (A-B) Example traces from optogenetic stimulation of total PV-IRES-Cre (A) and SOM-Cre (B) populations onto excitatory cells. Traces are stimulus intensities an order of magnitude apart. Blue bars mark the optogenetic stimulus. (C) Total optogenetic inhibition from PV cells is an order of magnitude lower in vPOR relative to dPOR. (D) Total optogenetic inhibition from SOM cells is indistinguishable between regions rather than compensatorily stronger in vPOR.

cells were an order of magnitude smaller in vPOR than in dPOR, statistically significant at the maximal light intensity with $p << 0.005$ (Figure 2.5A,C). Analysis was performed on both the peak amplitudes and areas of the IPSCs and showed similar results. This decrease was due to GABAergic signaling; 50 μm picrotoxin decreased the response by >95%. This finding demonstrates that axons from PV-IRES-Cre cells from dPOR and the few PV-IRES-Cre cells in vPOR synapse minimally on the RS cells of vPOR. We conclude that the overall inhibition mediated by PV-expressing interneurons is much lower in vPOR than in dPOR.

Is there compensation for the decreased PV cell inhibition in vPOR? We were limited by the lack of a mouse line that expresses the Cre recombinase in all 5HT3aR cells. Conveniently, the majority of 5HT3aR cells are in superficial cortical layers (see Figure 2.2A and

Rudy et al. (2010)). Furthermore, the predominant subtype of 5HT3aR cells, those marked by the neuropeptide VIP Rudy et al. (2010), primarily synapse onto SOM-expressing cells. We confirmed this by measuring inhibition from VIP-Cre; ChR2 cells onto RS cells and found it to be minimal (Figure 2.6). By recording in layer 4 of dPOR and the adjacent region of the minimally-laminated vPOR, we selected cells receiving predominantly SOM and PV-based inhibition.

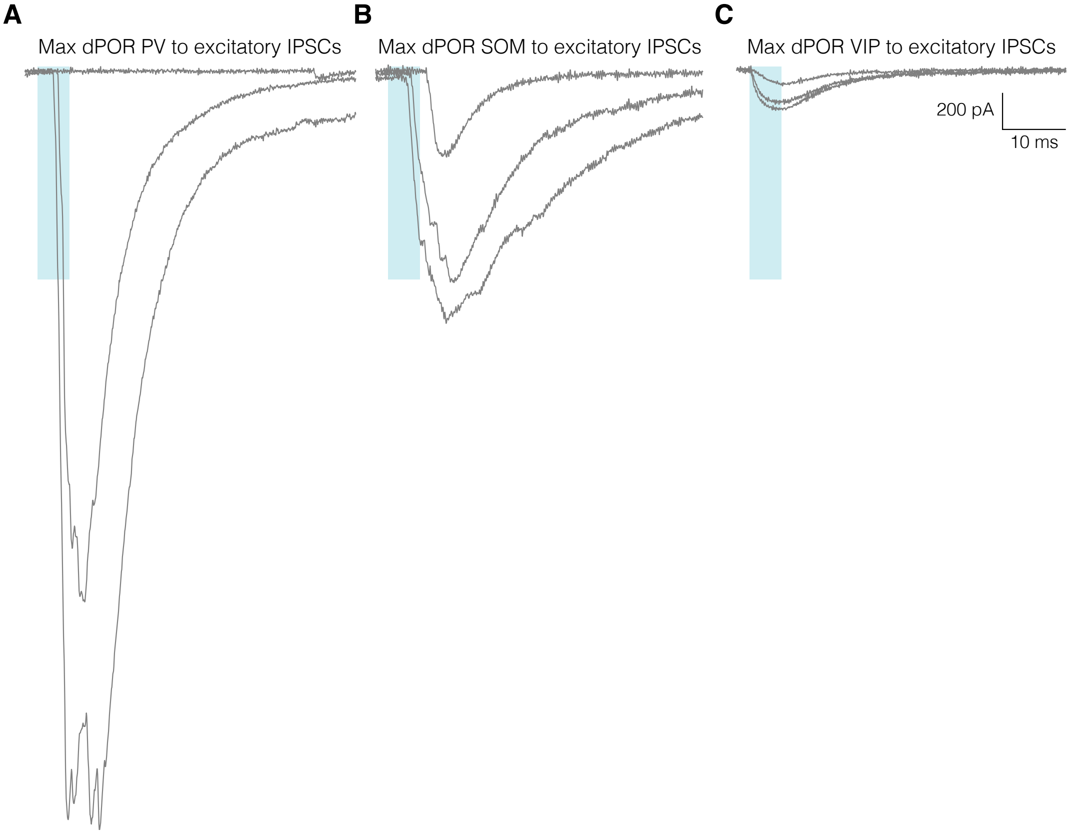

Figure 2.6: VIP cells inhibit RS cells far less than PV and SOM cells. Recordings voltage clamped at -60 mV in a high-chloride pipette solution. 5 ms blue laser pulses of 0.07, 0.51, and 3.82 mW activate local inhibitory cells. Maximal summed IPSCs onto RS cells from (A) PV-IRES-Cre; floxed ChR2-eYFP activation, (B) SOM-Cre; floxed ChR2-eYFP activation, (C) VIP-Cre; floxed ChR2-eYFP activation.

We also measured total inhibition from SOM cells onto RS cells in a SOM-Cre; ChR2-eYFP reporter mouse line and found that responses in vPOR and dPOR were indistinguishable (Figure 2.4B,D). Inhibition from SOM cells was one-third lower in dPOR than inhibition from PV cells (log-means of 505 ± 110 pA and 748 ± 503 pA, respectively), but SOM inhibition was five-fold higher than PV inhibition in vPOR (476 ± 175 pA and 112 ± 67 pA, respectively). As one would expect given the soma and projection densities of SOM shown above, there is not compensation of inhibition by SOM cells onto RS cells.

2.3.3 Total inhibition is equal across POR due to decreased reciprocal inhibition

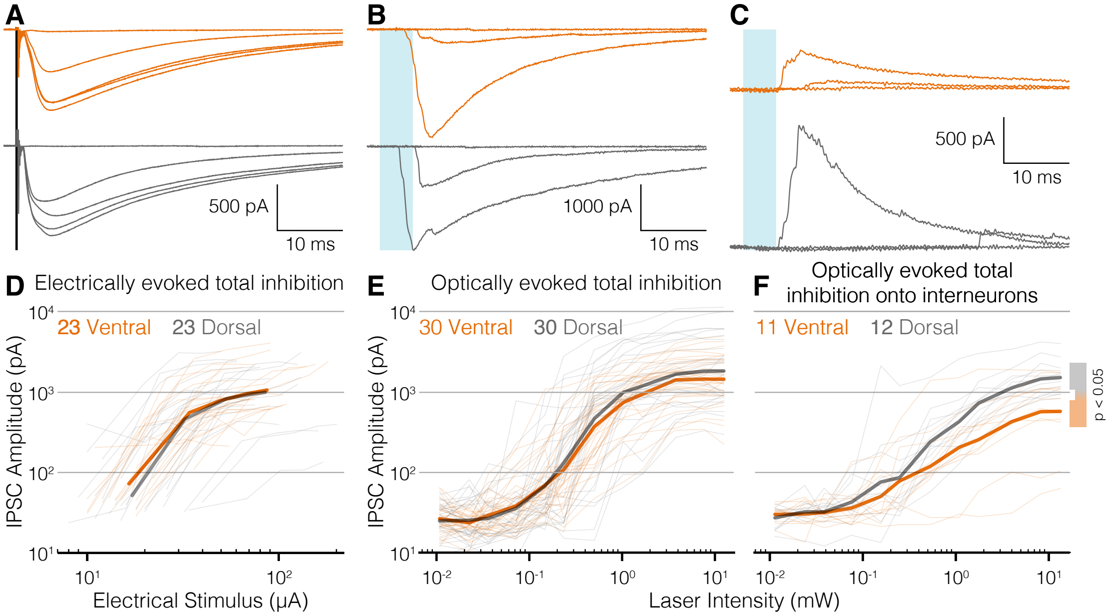

Figure 2.7: Decreased total inhibition onto inhibitory cells in vPOR yields inhibition onto RS cells that is indistinguishable from dPOR. (A-C) Example traces representative of the mean. (A) Black bar marks electrical stimulus; cells were held at -60 mV. (B) Blue bar marks laser stimulus; cells were held at -60 mV. (C) Blue bar marks laser stimulus; cells were held at +20 mV, the reversal potential of ChR2 uncompensated for the liquid-junction potential. (D-F) Dark lines show the log-mean; light lines are individual measurements. Recordings were made under the excitatory blockers DNQX and APV. (D) Electrical stimulation of total inhibitory input onto RS cells shows equal inhibition in vPOR and dPOR. Bipolar stimulation was within 100 μm of the soma. (E) Optogenetic stimulation of total inhibitory input onto RS cells shows equal inhibition in vPOR and dPOR. Channelrhodopsin is expressed exclusively in inhibitory cells in the VGAT-ChR2-eYFP mouse line. (F) Optogenetic stimulation of total inhibitory input onto inhibitory cells shows decreased inhibition in vPOR, likely due to the missing reciprocal inhibition of PV cells.

The sum of network inhibition from PV and SOM networks activated independently would predict a 64% decrease in total inhibition in vPOR relative to dPOR. To test this prediction and activate all inhibitory networks simultaneously, we used either electrical or optogenetic stimulation of all inhibitory cells and measured the resulting IPSCs in RS cells of the two regions.

RS cells were recorded as before with pipettes containing cesium and relatively high chloride in the presence of the glutamatergic blockers APV and DNQX. Cells were stimulated electrically with 0.2 ms shocks from a bipolar electrode placed less than 100 μm radially further away from the pia relative to the recorded cell.

To stimulate optogenetically, we flashed a 5 ms blue laser pulse directly over the recorded RS cell in a VGAT-ChR2-eYFP mouse line that selectively expresses ChR2 in inhibitory cells Zhao et al. (2011). Optogenetically stimulated IPSCs were decreased by >95% by the addition of picrotoxin.

Both electrical and optogenetic stimulation yielded the surprising result that total inhibition was indistinguishable between the two regions (Figure 2.7). This inhibition was likely not from an undetected source; the decreased sIPSC frequency in vPOR (Figure 2.4A-C) suggests that there are fewer inhibitory synapses in vPOR and the decreased fluorescence in vPOR in the VGAT-ChR2-eYFP mouse matches the cell densities we measured above (Figure 2.2). The unchanged amplitude of sIPSCs between vPOR and dPOR suggests that matching inhibition across POR cannot be explained by stronger synapses in vPOR. This is bolstered by equal optogenetically evoked inhibition from SOM cells onto RS cells; SOM cells have equal densities and equal inhibition in vPOR and dPOR and therefore are unlikely to have more release sites in vPOR than in dPOR. In total, one can conclude that fewer cells yield equally strong inhibition in vPOR and dPOR.

An alternate explanation is that although SOM inhibition cannot compensate for the missing PV inhibition, altered reciprocal connections between PV cells and mutual inhibition between PV and SOM networks can compensate. Pairs of probable PV cells in somatosensory cortex within 75 μm of each other have monosynaptic inhibitory connections 65% of the time Deans et al. (2001); Gibson et al. (1999). High PV-to-PV connection probabilities have been found widely Avermann et al. (2012); Galarreta et al. (2008); Pfeffer et al. (2013). But, pairs of probable SOM cells are connected only 0 Gibson et al. (1999) - 15 Deans et al. (2001)% of the time. PV-to-SOM and SOM-to-PV connections are both found roughly 50% of the time Deans et al. (2001). Decreased reciprocal inhibition in vPOR could allow a higher percentage of the interneurons to depolarize to spiking threshold.

Both electrical stimulation and optogenetic stimulation of total inhibition yielded IPSCs with multiple peaks (Figure 2.7A,B). Presynaptic cells presumably spike with widely varying latencies, and at high stimulus intensities a subset of inhibitory cells spike early enough to be able to silence other interneurons. To determine whether inhibition onto inhibitory cells was greater in dPOR than vPOR, we recorded from fluorescently targeted cells in the VGAT-ChR2-eYFP mouse line and optogenetically evoked total inhibition while holding the cell at the reversal potential for ChR2, +20 mV uncompensated for the liquid junction potential, to remove the endogenous ChR2 component. Measurements of total evoked inhibition onto inhibitory cells in vPOR and dPOR showed statistically significantly greater inhibition in dPOR, with a log-average of 1498 pA in dPOR, almost three fold higher than the 569 pA of vPOR (Figure 2.7F).

At the maximal stimulus amplitude, combined PV and SOM inhibition onto RS cells is 1.9× greater in dPOR than in vPOR. At the same power, total inhibition onto inhibitory cells is 2.6× greater in dPOR than in vPOR (1500. ± 262 pA and 569 ± 174 pA, respectively). It appears that total inhibition from the entire inhibitory cell network is equal between vPOR and dPOR because vPOR lacks a subset of reciprocally-inhibitory PV interneurons.

2.3.4 A parvalbumin-independent population of fast-spiking cells

Are the electrophysiological properties of SOM-Cre; tdTomato cells in vPOR the same as those in dPOR? The electrophysiological properties of PV cells are an important part of neo-

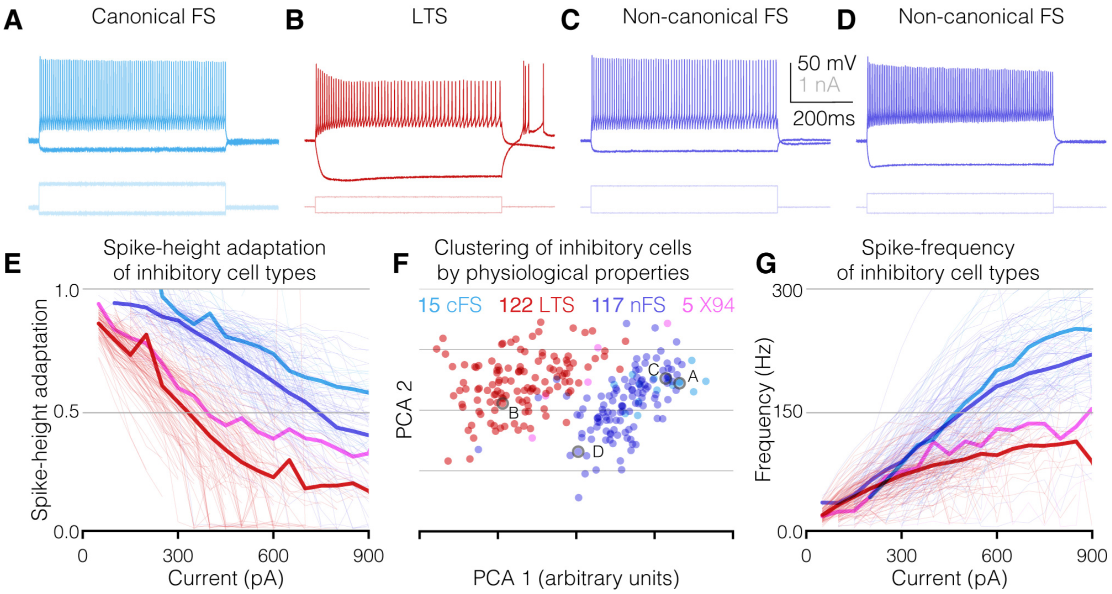

Figure 2.8: FS cells in the putative PV-free POR (A-D) Example electrophysiological traces of cell types in POR at -150 pA and 200 pA above rheobase. (A) Canonical FS (cFS) cells are PV-IRES-Cre; tdTomato positive, express PV strongly, and are absent from vPOR. (B) LTS cells are identified by SOM-Cre; tdTomato and are SOM positive. (C-D) FS cells identified in the nearly PV-free vPOR that non-canonical (nFS). (E) Spike-height adaptation over 600 ms differentiates LTS cells from all FS cells. nFS cells largely overlap with cFS cells of dPOR while X94 cells overlap with LTS cells. (F) Principal component analysis of intrinsic characteristics (resistance, rheobase, sag, spike-frequency adaptation, spike-height adaptation, spike width, spike height, and tau) separates LTS cells from nFS cells, even those identified via SOM-Cre; tdTomato. nFS cells overlap with cFS cells and X94 cells group with LTS, not nFS cells. Lettered cells are those from A-D. (G) Spike frequency over 600 ms separates cell classes similarly to spike-height adaptation.

cortical circuits, being key to feedforward inhibition and gamma oscillations Cardin et al. (2009); Cruikshank et al. (2007). It is important to determine if the inhibitory network of vPOR can function without fast-spiking properties. To answer this question, we recorded from SOM-Cre; tdTomato cells in current clamp.

FS cells have clearly different properties from LTS cells. They have lower resistance, a higher rheobase, higher spike-frequencies, and have minimal spike-height and spike-frequency adaptation. In contrast, LTS cells have high resistance, a sag upon hyperpolarization, action potentials following hyperpolarization, and dramatic adaptation of spike-height and spike-frequency during repetitive spiking. For each recorded cell, we injected -150 pA of current and stepped by +50 pA until the cell went into depolarization block or we reached 1 nA of injected current. Using the criteria described above, we segregated the cell types by their

Table 2.1: Electrophysiological properties of cell types

	nFS	LTS	cFS	X94
Resistance (MΩ)	151 ± 6.4	357 ± 13.6	107 ± 11.5	213 ± 63.9
Rheobase (pA)	225 ± 9.2	69 ± 3.6	333 ± 24.7	170 ± 60.4
Membrane potential (mV)	-69.6 ± 0.58	-59.9 ± 0.61	-71.2 ± 1.1	-65.0 ± 1.2
Hyperpolarizing Sag (mV)	1.0 ± 0.10	5.1 ± 0.30	1.3 ± 0.18	2.3 ± 1.04
Spike frequency adaptation slope	0.28 ± 0.0074	0.21 ± 0.0064	0.24 ± 0.0088	0.20 ± 0.0487
Spike height (mV)	72 ± 0.64	83 ± 0.46	68 ± 2.77	81 ± 0.96
Spike height adaptation slope	0.07 ± 0.0024	0.16 ± 0.0057	0.04 ± 0.0039	0.10 ± 0.0159
Spike width (ms)	0.31 ± 0.0045	0.42 ± 0.0064	0.24 ± 0.0097	0.31 ± 0.0271
Tau	6.8 ± 0.76	28.0 ± 1.48	4.7 ± 0.30	13.5 ± 3.02

properties and only included those cells in which a determination of their type could be made (Table 1). Measurements of nFS cells include both those that grouped with cFS cells (Figure 2.8F) and those with mixed phenotypes.

To our surprise, fluorescently targeted recordings of SOM-Cre; tdTomato positive cells across POR showed that 29/142 or 20.4% of fluorescing cells have an FS electrophysiological phenotype. In dPOR, 8/39 cells or 20.5% were FS cells and 21/82 or 20.4% were FS cells in vPOR. The remaining cells have the LTS electrophysiological phenotype (Figure 2.8B). Of the FS cells, a subset have mixed properties of LTS and FS cells, as in Figure 2.8D.

Many of the FS cells in vPOR were electrophysiologically indistinguishable from canonical FS cells labeled by PV-IRES-Cre. Because SOM-Cre; tdTomato-positive FS cells did not have traditional PV immunolabeling, but were partially labeled by SOM immunohistochemistry, they define a group of FS cells independent of traditional PV labeling. We have termed these FS cells non-canonical FS (nFS) because they have little or no PV expression, in contrast to the strongly PV-expressing canonical FS (cFS) cells. High-resistance FS cells with little spike-height and spike-frequency adaptation were included in the nFS category, as in Figure 2.8D.

We have compared the intrinsic characteristics of nFS cells, the SOM-positive LTS cells, and PV-positive cFS cells measured in POR. In addition, we have compared the X94 mouse line, which has been shown to mark a subset of more FS-like SOM cells Ma et al. (2006). Spike-height adaptation over a 600 ms current step separates all FS cells from LTS and X94 cells dramatically (Figure 2.8E). Other characteristics further divide the groups, including spike frequency (Figure 2.8G) and resistance, rheobase, sag, spike-frequency adaptation, spike-width, and tau. We combined all of these measurements and identified the axes along which the cells vary maximally via principal component analysis. In this analysis, the LTS cells clearly form a separate group from the nFS and cFS cells, which clump together.

nFS cells make up a substantial group of FS cells marked by SOM-Cre; tdTomato in a region without canonical PV expression. But, to establish with certainty that nFS cells are PV-negative, we filled nFS cells and LTS controls for 1-2 minutes with biocytin and Alexa488, fixed the tissue, and immunolabeled for SOM, PV, or both (Figure 2.9). All filled cells were recorded in the core of vPOR to avoid a possible overlap with cFS cells.

In contrast to our images that span dPOR and vPOR, imaging of PV immunolabeling of filled cells at high magnification with maximal sensitivity showed that 30% of cells in vPOR expressed low levels of PV, albeit at levels an order-of-magnitude less than in dPOR (Figure 2.2, 2.9A). More surprising was a large population of nFS cells that expressed no detectable SOM or PV (Figure 2.9A-B). A third subset of nFS cells expressed SOM (Figure 2.9C).

nFS cells expressing low levels of PV, normal levels of SOM, or neither had electrophysiological phenotypes varying between the high-resistance FS phenotype seen in Figure 2.8D to canonical FS phenotypes. However, each group contained FS cells with phenotypes indistinguishable from cFS cells (Figure 2.9E-H).

Given that PV expression has been so tightly linked with the fast-spiking interneuron

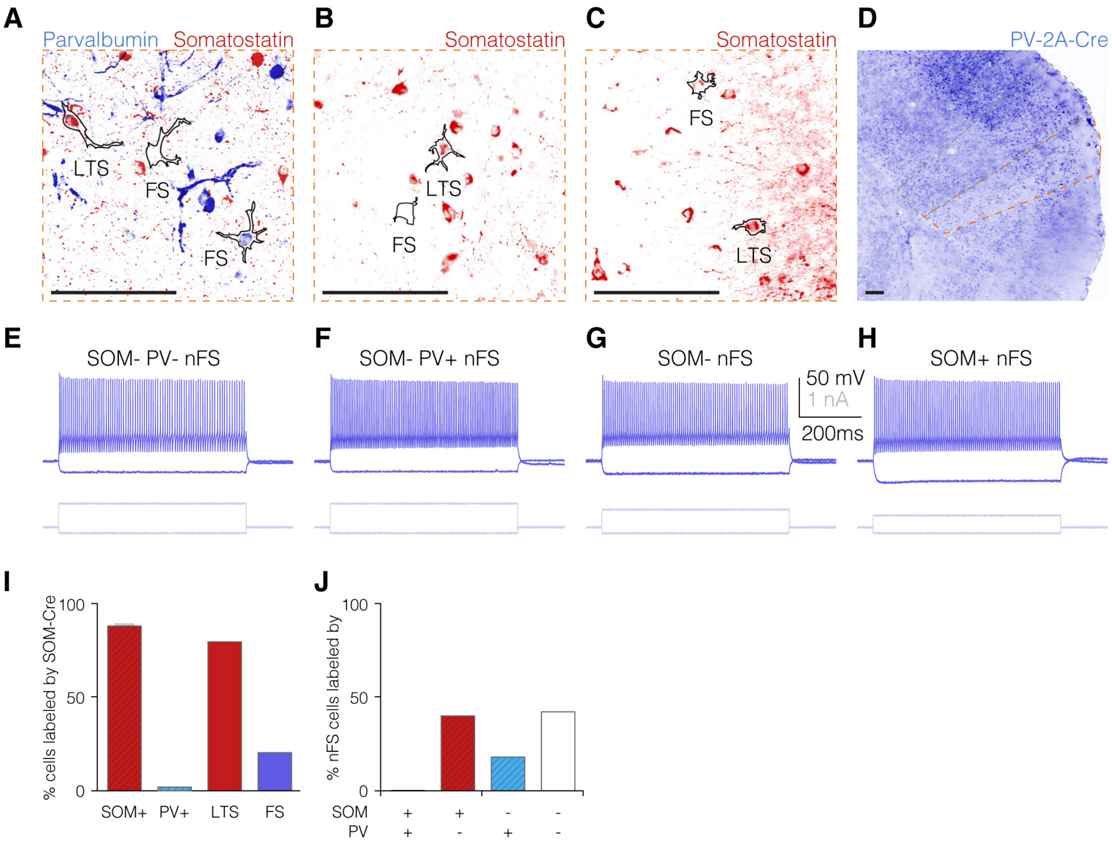

Figure 2.9: nFS cells do not contain canonical levels of PV. They can be PV-positive, SOM-positive, or neither. (A-C) Cells filled in vPOR for 1-2 minutes. Cells in a single image filled ±5 seconds. Blue is PV labeling, red is SOM labeling. (A) Three adjacent inhibitory cells of a VGAT-ChR2-eYFP animal: SOM-positive LTS cell, SOM- and PV-negative FS cell, and PV-positive FS cell. (B) Adjacent SOM-Cre; tdTomato cells are a SOM-positive LTS cell and a SOM-negative FS cell. The tdTomato signal remained strong, confirming a lack of washout. (C) Adjacent SOM-Cre; tdTomato cells are a SOM-positive FS cell and a SOM-positive LTS cell. The tdTomato signal remained strong. (D) PV-2A-Cre marks many excitatory neurons in addition to inhibitory neurons. (E-H) Traces at -150 pA and 200 pA above rheobase of the FS cells in A-C. (I) Overlap of immunohistochemistry and electrophysiologically determined cell types in the POR of the SOM-Cre; tdTomato genotype. SOM+ N = 768/870 cells across two animals, PV+ N = 1/222 across 4 animals, LTS N = 114/142, FS N = 29/142. (J) Expression patterns of nFS cells. SOM+PV- determined from I, SOM-PV+ N = 8/27, SOM- PV- N = 19/27.

phenotype in cerebral cortex (Rudy et al. (2010) and references therein), we wondered how closely related nFS cells were to cFS cells. The PV-IRES-Cre animal we used in Figure 2.2 expresses Cre at a lower level than PV, given that the internal ribosome entry site has a low efficiency Madisen et al. (2009). In contrast, a mouse line generated with the self-cleaving linker 2A separating PV and Cre was claimed to yield a near one-to-one expression of Cre relative to PV Madisen et al. (2009). We recorded from cells marked with PV-2A-Cre crossed with the Ai9 tdTomato reporter and found that the majority of labeled cells were RS cells (Figure 2.9D), so we discounted its use for localizing low levels of PV mRNA.

To quantify the expression patterns of nFS cells, we first examined the PV and SOM immunoreactivity in a SOM-Cre; tdTomato animal at high magnification. We have found that 88% of SOM-Cre; tdTomato cells are SOM immuno positive (Figure 2.2, 2.9I). PV marked only 1/222 SOM cells, or 0.45%. Of those cells marked by SOM-Cre; tdTomato, all are either LTS (115/145 or 79.6%) or FS (30/145 or 20.4%). Because all LTS cells are SOM positive, 40% of nFS cells marked by SOM-Cre must be SOM immuno positive and the remaining 60% are SOM immuno negative (Figure 2.9J). No cells were marked by both SOM and PV (0/27) and those marked exclusively by PV make up one-third of the SOM immuno negative nFS cells (8/27), or 18% of nFS cells (Figure 2.9J). In summary, nFS cells are marked by low levels of PV protein (18%), the SOM protein (40%), or neither (42%).

2.3.5 nFS cells receive depressing synapses and support gamma oscillations

nFS cells make up roughly one fifth of the FS network in dPOR, but are nearly the complete FS network in vPOR. Given the populations determined above (Figure 2.2, 2.9), cFS and nFS cells make up roughly 35% of the inhibitory cells in dPOR, but only 17% of the inhibitory cells of vPOR.

Excitatory synapses onto canonical FS are consistently depressing synapses, while those onto LTS cells are facilitating Beierlein et al. (2003); Reyes et al. (1998). Similarly, FS-to-RS synapses are usually depressing, while LTS-to-RS synapses are on average flat, but vary widely. One measure of short-term depression or facilitation is the paired-pulse ratio. A pair of stimuli, in this case electric shocks, are elicited in rapid succession. The amplitude of the second response is divided by the first. Resulting values below one indicate short-term depression, while those above indicate facilitation. Given that vPOR has only half of the FS

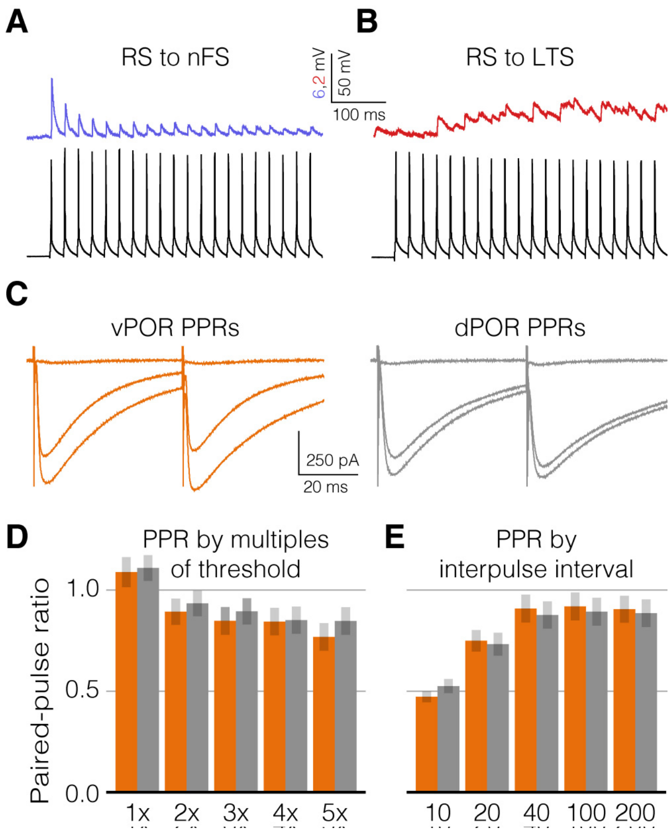

Figure 2.10: nFS cells have network properties similar to canonical PV FS cells. (A) Like RS-to-cFS connections, RS-to-nFS connections are depressing. (B) In contrast, RS-to-LTS connections are facilitating. (C) Example paired-pulse ratios stimulated with a bipolar electrode in the presence of extracellular glutamatergic blockers APV and DNQX. Examples with interpulse interval of 50 ms at 1×, 3×, and 5× threshold with N of 16 in vPOR and 16 in dPOR. (D) Varying multiples of threshold do not differentiate vPOR and dPOR. (E) Varying paired-pulse interval does not differentiate vPOR and dPOR.

cell population of dPOR, we would have expected that the paired-pulse ratio of inhibition from all inhibitory cells would be greater in vPOR than in dPOR.

We recorded from pairs of cells in which one expressed SOM-Cre; tdTomato and the other had an RS phenotype, and found that excitatory synapses onto nFS cells were depressing (2/2 measured) while those onto LTS cells were facilitating (2/2 measured, Figure 2.10C,D). Notably, connection probabilities in POR were dramatically lower than those in barrel cortex. Rather than seeing RS-to-SOM-Cre; tdTomato chemical connections at the somatosensory rate of 40-60% measured by Gibson et al. (2005) and Avermann et al. (2012), we found only 4/48 connections or just over 8% across POR. Cell fills confirmed that we did not consistently transect the axon with our slice plane, and we found connection probabilities in barrel cortex

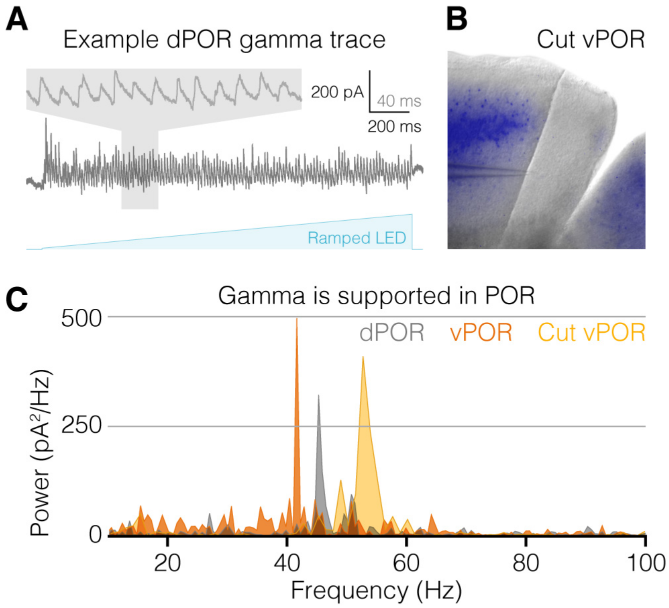

Figure 2.11: nFS cells support gamma oscillations. Isolated vPOR sustains gamma oscillations without canonical PV cells. Three-second light ramps over slices selectively expressing ChR2 in RS cells yields strong, rhythmic activity. (A) Example trace of RS cell voltage-clamped to -40 mV. (B) vPOR was isolated with a scalpel from dPOR and entorhinal cortex. (C) Example power spectra from dPOR, vPOR, and isolated vPOR from the slice in B. Peak frequencies and powers are highly dependent on viral expression and can't be directly compared between regions.

similar to those previously reported (data not shown). The low probability of finding nFS cells in SOM-Cre; tdTomato led to few nFS-SOM connections, although one pair of nFS cells in dPOR was reciprocally chemically connected and gap-junction coupled.

Table 2.2: Connection probabilities of SOM-Cre; tdTomato cells in POR

	From: RS	nFS	LTS
To: RS		4/14	5/34
nFS	2/14	4/8	1/5
LTS	2/34	0/5	0/14

We measured an overall paired-pulse ratio for IPSCs similarly to measurements of total inhibition above. A bipolar electrode was placed less than 100 μm radially below (away from the pia) a putative RS cell, which was being recorded with a pipette solution containing cesium and relatively high chloride to maximize measurements of IPSCs. We blocked excitatory transmission with the glutamate receptor blockers APV and DNQX. We found the minimal level of stimulation that would yield responses at least 50% of the time, which was deemed threshold. We then varied the pair of stimuli by intensity (1-5× threshold) or interpulse interval (10-200 ms).

Measurements of the paired-pulse ratio showed no significant differences between the networks of vPOR and dPOR (Figure 2.10C-E). Although the vPOR network contains fewer FS cells, the total inhibition had the same level of short-term depression at all tested intervals.

Next, we asked whether larger-scale network properties were maintained in vPOR. Ramps of light over neocortex selectively expressing ChR2 in RS cells yield strong gamma-band oscillations Adesnik and Scanziani (2010). We injected an AAV2/9-CamKIIα-C1V1-eYFP virus into POR, which is predominantly expressed in RS cells. Then, we ramped a white LED with a spot size of roughly 150 μm over the course of three seconds to a maximum power ranging between 0.001 and 10 mW.

This photostimulation generated strong, rhythmic activity in the gamma band in RS cells (30-80 Hz, Figure 2.11A). The peak power of the rhythmic activity depended on viral expression and stimulus intensity. Our virus preferentially expressed in dPOR relative to vPOR as measured by eYFP fluorescence, but it had less preference for dPOR than an AAV5-CamKIIα-ChR2-eYFP virus, which gave unusably low expression in vPOR. Because of this tropism, we were not able to compare absolute powers between vPOR and dPOR, but instead could only assess whether gamma oscillations were present.

We isolated the network of vPOR using scalpel cuts across all neocortical layers and at least 300 μm beyond (Figure 2.11B). Slices from 4/4 animals maintained gamma oscillations in vPOR prior to cuts and 2/2 animals with cuts fully separating vPOR from the cFS-containing regions dPOR and vPOR maintained strong gamma oscillations as in Figure 2.11C.

2.3.6 Only cFS cells get input from retrosplenial cortex

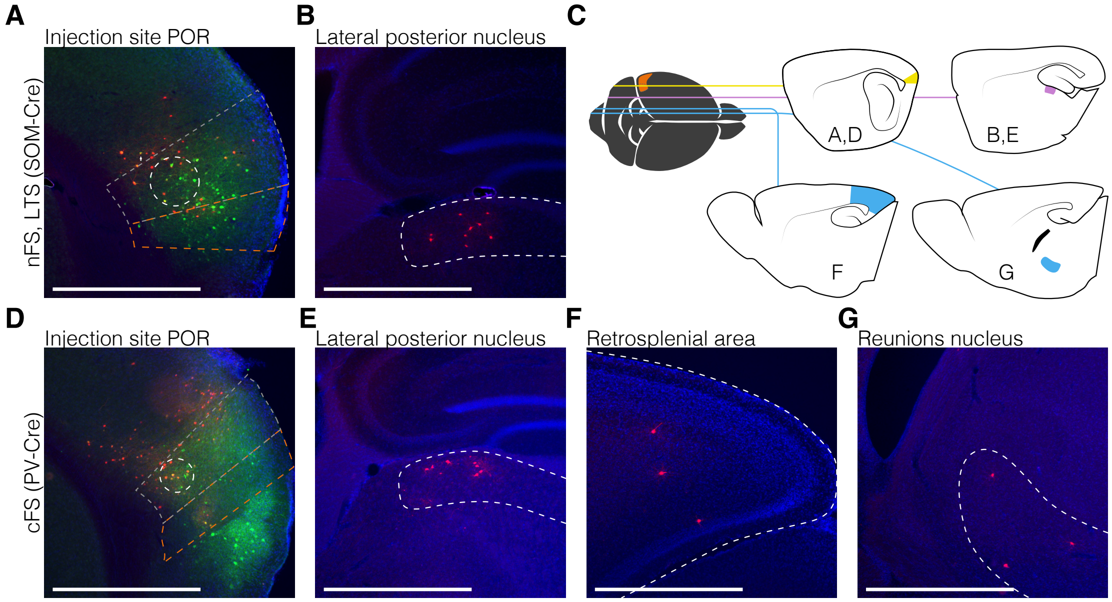

Figure 2.12: Rabies injections of posthrinal cortex. Green is a floxed helper virus expressing rabies glycoprotein and the avian receptor TVA. Red is rabies virus. Yellow cells are doubly-infected postsynaptic cells. Blue is DAPI. Orange dotted line is vPOR, gray dotted line is dPOR. White dotted lines are named regions except for A and D. (A-B) Inputs to nFS and LTS cells in SOM-Cre animals. (A) Injection site of mouse 1 dorsal/ventral boundary of POR. White circle contains the majority of yellow cells. (B) Presynaptic cells from the lateral posterior nucleus of the thalamus. (C) Color-coded schematic of presynaptic cells. Yellow is the injected region, purple marks areas of presynaptic cells to both cFS and nFS cells, blue marks inputs only to cFS cells. (D-G) Inputs to cFS cells in PV-IRES-Cre animal. (D) Injection site in mouse 2 in dPOR. White circle contains the majority of yellow cells. (E) Presynpatic cells in the laterposterior nucleus of the thalamus. (F) Presynaptic cells from retrosplenial cortex. (G) Presynaptic cells in the Reuniens nucleus of the thalamus.

Many nFS cells of the POR are indistinguishable from cFS cells by their intrinsic electrophysiological characteristics, their local connections, and their roles in network oscillations. Given that they differ so greatly in their PV and SOM expression, we hypothesized that they would differ in their inputs from other regions.

To determine inputs to cFS and nFS cells, we injected rabies virus into PV-IRES-Cre and SOM-Cre animals respectively. Injections in the SOM-Cre mouse line identified inputs to either LTS or nFS cells and those in PV-Cre line identified inputs solely to cFS cells.

First, we injected into the dorsal/ventral POR boundary a Cre-dependent helper virus expressing the rabies glycoprotein, the avian receptor TVA, and GFP Kohara et al. (2014); Wall et al. (2010); Wickersham et al. (2007). After allowing 21 days for expression, we injected a G-deleted rabies virus driving mCherry expression into the same stereotactic coordinates. Initial rabies infections were confined to GFP-expressing cells and all other mCherry-expressing cells are inputs synapsing onto POR inhibitory cells (Figure 2.12). Brains were sliced in the parasagittal plane so that we could determine which layers were injected in POR. All five injections were accurate within 100 μm.

In 2/2 injected SOM-Cre animals, presynaptic cells were labeled immediately rostral to the dPOR(Figure 2.12A), in perirhinal cortex, and in the lateral posterior nucleus of the thalamus (LP, Figure 2.12B).

In 3/3 injected PV-Cre animals, presynaptic cells were labeled immediately rostral to the dPOR(Figure 2.12D), in perirhinal cortex, the diagonal band of Broca, LP (Figure 2.12E), the retrosplenial area (RSA, (Figure 2.12F), and the reuniens nucleus of the thalamus (Re, Figure 2.12G).

Both PV-Cre and SOM-Cre postsynaptic cells shared some inputs. The immediately rostral neocortex (Figure 2.12A,D) and the perirhinal cortex were both expected given the extensive communication between these regions Agster and Burwell (2009); Burwell and Amaral (1998b). Inputs from perirhinal cortex were at the lateral, caudal, and dorsal extreme of the sagittal sections. Longer-range inputs to both postsynpatic targets were confined primarily to LP (Figure 2.12B). The POR is primarily a visual associational area and so projections from LP are not unexpected Furtak et al. (2007).

PV-Cre cells had additional inputs from regions that did not send projections that synapsed on SOM-Cre cells. In all PV-Cre animals, the Reuniens nucleus of the thalamus (Re) had cells that synapsed onto PV-Cre-expressing cells of dPOR (Figure 2.12G). However, the cell populations labeled in Re were small, on the order of 3-6 cells per animal. We found no cells in Re in 2/2 SOM-Cre animals, but we cannot rule out Re-to-SOM-Cre connections. Re plays a fascinating role in hippocampal input; Re acts as a processing station between medial prefrontal cortex (mPFC) and the parahippocampal region and hippocampus Cassel et al. (2013); Vertes et al. (2007). It has been shown that there are few inputs from mPFC directly to the postrhinal cortex Vertes et al. (2007), but many neurons from Re to hippocampus and the parahippocampal region appear to be targets of mPFC cells. So, these inputs may represent mPFC input to POR.

The greatest differentiating factors between inputs to PV-Cre- and SOM-Cre-expressing cells were inputs from RSA (Figure 2.12F). Previous work showed that RSA is strongly and reciprocally connected with POR, but not with the adjacent perirhinal cortex Ranganath and Ritchey (2012). 3/3 PV-IRES-Cre animals had cells spread across much of RSA, encompassing a region of up to 200 μm medial-laterally as seen in Figure 2.12F. 0/2 SOM-Cre animals had cells expressing in this region.

2.4 Discussion

vPOR lacks canonical PV-positive FS cells. Parvalbumin immunohistochemistry and the PV-IRES-Cre knock-in animal both show profoundly low expression in vPOR compared to adjacent cortical areas. This absence is confirmed by optogenetic stimulation of total PV cell inhibition onto excitatory cells, and the absence continues into adulthood. This absence of PV inhibitory cells is not compensated for by an increase in density of the remaining two types of cells, SOM-positive or 5HT3aR-positive. It is also not compensated for by an increase in inhibition from SOM cells; total SOM inhibition onto excitatory cells is unchanged between regions. Correspondingly, there is a decrease of spontaneous IPSCs in vPOR.

Across frontal cortex, primary visual cortex, and primary somatosensory cortex, the percentage of PV cells differs by less than 3% Xu et al. (2010). vPOR is an extreme outlier in neocortical PV cell density. Two other regions have decreased PV density, although not necessarily to the same degree: ventral perirhinal cortex and lateral RSA Glickfeld et al. (2014).

Although vPOR has a lower density of inhibitory cells than dPOR, it is missing an inhibitory cell type with strong reciprocal chemical connections Deans et al. (2001); Gibson et al. (1999). Total evoked inhibition onto excitatory cells elicited optogenetically or electrically is indistinguishable between the regions. It is fascinating that the organization of the cortical network is such that the absence of cPV cells does not affect total evoked inhibition onto excitatory cells.

FS cells exist in vPOR, although the region lacks PV-IRES-Cre; tdTomato cells and strong PV-immunolabeled cells. We have identified a new group of FS cells which have little-to-no PV, and often have SOM in its stead (nFS cells). This group is found in both vPOR and dPOR and may be found elsewhere across neocortex. Many of these cells have electrophysiological properties indistinguishable from PV-IRES-Cre expressing FS cells, although some have combinations of characteristics of FS and LTS cells.

These cells would be easy to miss in regions with cFS cells. Profiling cells by mRNA expression, such as in work by Lee et al. (2010), might not be able to distinguish between nFS and cFS cells because both might express PV mRNA. Others have identified FS cells in the SOM-Cre mouse line Hu et al. (2013), but found afterwards that these cells express PV protein. Depending on the level of PV expressed, these could be nFS cells or transient expression of SOM during the development of a cFS cell. We predict that these cells might be found across neocortex, but especially in regions with fewer PV-IRES-Cre cells such as the lateral band of RSA and the ventral band of perirhinal cortex.

nFS cells appear to behave similarly in a network to cFS cells. RS-to-nFS connections are depressing as are RS-to-cFS connections, in contrast to RS-to-LTS connections. They support traditional network activity such as strong gamma oscillations elicited with an optogenetic ramp, although they have lower connectional probabilities than in somatosensory cortex. Gamma oscillations are thought to play an important role in binding percepts together as they pass through the neocortex Fries (2009). This appears to be the first instance of gamma oscillations generated from a group of cells of which less than 10% express PV.

It seems improbable that such a drastic region of cFS cells absence would persist across mammalian evolution if it were not essential. However, the nFS inhibitory network is surprisingly similar to the cFS network in its intrinsic properties and local connections. We identified a factor which substantially differentiates these cell types; injections of rabies virus to show differences in presynaptic inputs to cFS and nFS cells. cFS cells were labeled by the PV-Cre animal, while a combined population of nFS and LTS cells were labeled by the SOM-Cre animal. By finding regions in the SOM-Cre animal that did not express cells, where they did strongly in the PV-Cre animal, we could identify regions that selectively project to cFS cells but not nFS cells.

Our experiments suggest that cFS and nFS cells both receive inputs from LP. The LP has been implicated in visual attention Posner and Petersen (1990), and combined input from visual cortical areas and LP onto PV-Cre and SOM-Cre cells of POR can join to process information before it is passed on to entorhinal cortex and hippocampus.

However, only cFS cells receive inputs from RSA. Activity in the primate homologue of POR is associated with both memory coding and retrieval, but activity in RSA is specifically increased during memory retrieval Ranganath and Ritchey (2012). POR acts as a gate for the flow of information to the hippocampus from neocortex de Curtis and Paré (2004) and POR receives input from a region that is activated when information flows from the hippocampus to neocortex. Perhaps inhibition specific to cFS cells of dPOR is important for its gating.

One other factor differentiates nFS cells from cFS cells: their PV expression. Recently, it has been shown that PV levels in basket cells can change upon experience Donato et al. (2013). Decreased PV levels are associated both with decreased GAD67 levels and increased synaptic plasticity. It is possible that nFS cells make up a group of cells with actively modulated PV. These cells could have enhanced synaptic plasticity relative to their PV FS neighbors. We hope that future studies examine vPOR for active regulation of PV. One candidate is microRNA-298, which has binding sites in PV predicted both by sequence conservation and binding energy. Surprisingly, this miRNA has a similarly strong binding site in the GAD67 transcript, which could explain the coregulation of PV and GAD67 identified in Donato et al. (2013).

In summary, we have found that the ventral portion of postrhinal cortex (vPOR) has a significantly lower density of inhibitory cells than the adjacent control cortex. This is due to the exclusive absence of canonical parvalbumin-expressing fast-spiking (cFS) cells. vPOR continues to have equal inhibition to control cortex due to decreased reciprocal inhibition. This cFS-cell free region made it possible for us to identify a population of low-to-no PV-expressing fast-spiking cells which are found also in the neighboring control cortex. This new type of FS cell supports similar network dynamics to cFS cells, but receives different inputs.

2.5 Experimental Procedures

Electrophysiology Mice aged P18-P26 were anesthetized and two 300 μm parasagittal slices 1300-1900 μm from the lateral edge of the cortex were taken in ice-cold artificial cerebrospinal fluid (ACSF) and maintained in ACSF composed of 126 mM NaCl, 3 mM KCl, 1.25 mM NaH_2PO_4, 2 mM $MgSO_4$, 26 mM $NaHCO_3$, 10 mM dextrose, and 2 mM $CaCl_2$. The ACSF was carbogenized with 95% O_2/5% CO_2. Whole-cell recordings were conducted at 32°C with either a potassium-based pipette solution composed of 130 mM K-gluconate, 4 mM KCl, 2 mM NaCl, 10 mM HEPES, 0.2 mM EGTA, 4 mM ATP-Mg, 0.3 mM GTP-Tris, and 14 mM phosphocreatine-Tris (pH, 7.25; 290 mOsm) or a cesium-based pipette solution for measuring total IPSCs composed of 54 mM Cs-gluconate, 56 mM CsCl, 1 mM CaCl2, 1 mM MgCl2, 10 mM EGTA, 10 mM HEPES, 5 mM QX-314, 4 mM ATP-Mg, 0.3 mM GTP-Tris, and 14 mM phosphocreatine-Tris (pH 7.25; 290 mOsm). Slices were visualized through a Nikon Eclipse 600FN with DIC and fluorescence was activated by a Mightex LED. Recordings were made with two Axoclamp-2B amplifiers and digitized with a Digitidata 1440 and a computer running PClamp 10. 50 μm APV and 20 μm DNQX were used to block excitatory transmission during optogenetic and electrical stimulation of inhibition and 50 μm picrotoxin was used to determine that putative inhibitory transmission was GABAergic.

Data analysis Basic analysis was performed in Clampfit and more advanced analysis, including fitting spike-height adaptation and principal component analysis, was performed with our open-source software designed for analyzing electrophysiological data found at `https://bitbucket.org/asugden/simpliphys`. Data presented were not compensated for the liquid junction potential of 14 mV.

For PCA, we determined spike-height and spike-frequency adaptation slopes relative to input current. Spike-height adaptation slope refers to the slope of the best fit line to the plot of spike-height adaptation by current (example Figure 2.8A). Similarly, spike-frequency adaptation slope refers to the best fit line of the plot of spike-frequency adaptation by current.

Peak amplitudes of optogenetically- and electrically- evoked IPSCs were calculated as the minimum of the current within a 100 ms window after stimulation.

Log-means were used to measure the mean of a logarithmic plot, while simple means were used for non-logarithmic plots. Means yield similar results, but are more strongly biased by outliers with exceptionally high amplitudes.

One-tailed Student's t-tests were used on IPSCs resulting from the maximal light intensity to determine the differences between population IPSC amplitude in optogenetic experiments.

Optogenetic and electrical stimulation Channelrhodopsin was primarily expressed using mouse lines encoding ChR2. For experiments with genetically-encoded channelrhodopsin, we activated the cells with 5 ms pulses of light from a blue laser (447 nM) through a 40x water-immersion lens. The laser spot was focused to have peak power across a spot 50 μm in diameter. For the gamma experiments, we stereotactically injected an AAV2/9-CamKIIα-C1V1-eYFP at P10-P12 and let it express for 10-12 days. vPOR was isolated with a scalpel and a light microscope and confirmed with fluorescence in a PV-IRES-Cre; tdTomato animal. 3 second ramps of whole-field light from a white led (150 μm from a Mightex LCS-5500-03-22) were given through a 40x water-immersion lens. Electrical stimulation was provided with a twisted bipolar electrode located within 100 μm of the recorded cell deeper along a line tangent to the pia.

PV and SOM immunohistochemistry Mice (Som-Cre-Tomato,PV-Cre-Tomato) age P20-25 were used for most immunohistochemical work. For immunohistochemistry of older animals, P105 animals were used. For the younger animals, 800 um slices cut in the saggital plane were fixed by transfer to 4% paraformaldehyde overnight. Slices were changed to 30% sucrose, 0.1 M phosphate buffer until resectioned at 40 ?m. Older animals were perfused with Ice-cold heparinized Saline followed by 4% paraformaldehyde. All tissue was washed twice in 0.1 sodium phosphate (PB) followed by 3 washes in PB with 0.15 M NaCl, pH 7.4 (PBS). Sections were incubated in blocking solution (0.1% Tween, 0.25%, Triton X-100, 10% normal goat serum in PBS) for 1 h for nonspecific binding, then incubated in blocking solution containing primary antibody containing either or both mouse monoclonal anti-parvalbumin antibody

(Swant, Switzerland, clone 235, 1:2000) or rabbit polyclonal anti-somatostatin (Peninsula San Carlos, CA T4103, 1:1000) for 2-3 days with rotation at 4¡C. Following primary incubation, tissue was rinsed 5 times at 5 min each rinse in PBS and then preblocked for 45 min in blocking solution as above. Tissue was incubated goat anti-mouse or rabbit IgG Alexa 647, Alexa 633. Alexa 488 (Molecular Probes, 1:500 for 2 h at room temperature, rinsed three times in PBS, 10 min each, followed by two rinses of PB. All sections were mounted from 0.01 M PB and coverslipped using Vectashield (Vector, H-1000). Photomicrographs of immuno-stained slices were taken using a Zeiss confocal Microscope (LSM 520).

Immunohistochemistry for identification of short cell fills in VGAT-ChR2-eYFP and SOM-Cre VGAT-ChR2-eYFP mice age P20-25 were used for characterization of YFP positive cells. Cells were quickly filled with traditional pipette solution also containing Alexa 488 and biocytin (pH 7.25, 290 mOsm). Immediately following the fills, the 300 um slice was placed in 4% fix for 45 minutes followed by 3, 10 minute rinses of 0.1 M sodium phosphate and 0.15 M NaCl, pH 7.4 (PBS).The decreased time of filling and fixation and quick washes enhanced the recovery of fluorescent signal. When all filling, fixing and washes were complete, all slices were washed twice in PBS. Sections were incubated in blocking solution (0.1% Tween, 0.25%, Triton X-100, 10% normal goat serum in PBS) for 1 hour for inhibition of nonspecific binding, then incubated in blocking solution containing primary antibodies (mouse monoclonal anti-parvalbumin antibody [Swant, Switzerland, clone 235, 1:2000] and rabbit polyclonal anti-somatostatin [Peninsula San Carlos, CA T4103, 1:1000]) and Strepaviden Alexa 488 (Molecular Probes, OR, 1:500) overnight at room temperature. Following primary and Strepaviden incubation, tissue was rinsed 5 times at 5 min each rinse in PBS and then preblocked for 45 min in blocking solution as above. Tissue was incubated goat anti-mouse IgG Alexa 647 and goat anti-rabbit IgG Alexa 647 (Molecular Probes, OR, both at 1:500 for 2 hours at room temperature, then rinsed three times in PBS, 10 min each, followed by two rinses of 0.1 M sodium phosphate 7.4 (PB). All sections were mounted from 0.01 M PB with appropriate orientation of filled cells up and coverslipped using a thin circle of vaseline as a border surrounding the slice with Vectashield (Vector, H-1000) within that border. Photomicrographs of immuno-stained slices were taken using a Zeiss confocal Microscope (LSM 520)

Immunohistochemistry for the rabies injection in PV-Cre and Som-Cre mice Either Som-Cre or PV-Cre animals were used for double injection in the vPOR of AAV2-flex-sTpEpB and EnvA-GDeltaRabies-mCherry viruses spaced 3 weeks apart. Five days after the second injection, animals were perfused with Ice-cold Saline followed by 4% paraformaldehyde. Brains were hemi-dissected 1 mm to the left of the midline and placed in 4% paraformaldehyde overnight. They were changed to 30% sucrose/ 0.1M phosphate solution until resection 26-30 hours later. The right hemisphere of all animals was sliced saggitally at 60 um. All sections were collected sequentially until midline was passed. Tissue was rinsed three times for 10 minutes each rinse in 0.1 sodium phosphate and 0.15 M NaCl, pH 7.4 (PBS). Sections were incubated in blocking solution (0.1% Tween, 0.25%, Triton X-100, 10% normal goat serum in PBS) for 1 h for nonspecific binding, then incubated in blocking solution containing the primary antibody rabbit-anti-GFP (Molecular Probes, OR, A6455 at 1:500) overnight with rotation at 4¡C. Following primary incubation, tissue was rinsed 4 times at 10 min each rinse in PBS and then incubated in goat anti-rabbit IgG Alexa 488, (Molecular Probes, OR, at 1:500) for 2-3 hours at room temperature, rinsed three times in PBS, 10 min each, followed by two rinses of 0.1 sodium phosphate pH 7.4 (PB). All sections were mounted from 0.01 M PB and coverslipped using Vectashield with Dapi (Vector Labs, Burlingame, CA H1200). Photomicrographs of immunostained slices were taken using a SPOT Camera (Spot Software, version 4.7, Diagnostic Instruments) mounted to a Nikon microscope (Nikon Eclipse, E600).

Visualization of 5HT3aR-GFP histology The 5HT3aR-GFP transgenic animal was perfused with ice-cold heparinized saline followed by 4% paraformaldehyde. The hemidissected brain was placed in fixative overnight until cryoprotected in 30% sucrose the following day. Tissue was saggitally sliced at 40 um and washed 3 times 0.1 M sodium phosphate (PB). All sections were mounted from 0.01 M PB and coverslipped using Vectashield (Vector Labs, Burlingame, CA, H-1000).

Mouse lines To mark subsets of inhibitory cells, we used a tdTomato reporter animal (B6.Cg-Gt(ROSA)26Sor$^{\mathrm{tm9(CAG\text{-}tdTomato)Hze}}$/J or a channelrhodopsin reporter animal (B6;129S-Gt(ROSA)26Sor$^{\mathrm{tm32(CAG\text{-}COP4H134R/EYFP)Hze}}$/J), combined with expression of the Cre recombinase. Cre-expressing lines include GAD2-Cre (Gad2$^{\mathrm{tm2(cre)Zjh}}$/J), Parvalbumin-Cre (B6;129P2-Pvalb$^{\mathrm{tm1(cre)Arbr}}$/J), Somatostatin-Cre (Sst$^{\mathrm{tm2.1(cre)Zjh}}$/J), VGAT-Cre (Slc32a1$^{\mathrm{tm2(cre)Lowl}}$/J). In addition, we used the 5HT3aR-GFP line (MMRRC: Tg(Htr3a-EGFP)DH30Gsat/Mmnc), the GAD67-GFP mouse line, courtesy of Dr. Maria Picciotto Tamamaki et al. (2003), and the VGAT-ChR2-eYFP line (B6.Cg-Tg(Slc32a1-COP4H134R/EYFP)8Gfng/J).

Chapter Three

Network gamma oscillations in neocortex do not require gap junctions

3.0.1 Contributions

Arthur U. Sugden performed the recordings, injections, and wrote the manuscript. Scott J. Cruikshank and Shane R. Crandall performed initial recordings of high-titer virus. Barry W. Connors directed the project and co-wrote the manuscript.

3.1 Summary

Gap junctions connect neighboring cortical interneurons, yet their role in the neocortex remains poorly understood. Extensive measurements of paired cells have shown that gap junctions can synchronize the firing of interneurons by rapidly and symmetrically conducting ionic current. Rhythmic synchrony has been repeatedly linked with cortical processing, in particular in the gamma band (30-80 Hz oscillations). Here, we hypothesized that because gap junctions can synchronize cells, neocortical fast-spiking cells have gap-junctions, and fast-spiking cells have been implicated in gamma oscillations, the knockout of gap junctions would alter gamma-band oscillations. We generated gamma oscillations optogenetically in layer 4 of primary somatosensory cortex and in layer 4 of an associational cortical region, postrhinal cortex. To determine if gap junctions were required specifically when inhibitory cells had varied inputs, we expressed channelrhodopsin in a subset of inhibitory cells. By titrating the relative drive of inhibitory and excitatory cells, we could modulate the level of arrhythmic background activity, which could increase the role of synchronizing gap junctions. Surprisingly, across gamma oscillations generated with varying levels of inhibitory drive, there was no dependence on gap junctions.

3.2 Introduction

Gap junctions are extensive in the neocortex, coupling roughly 50% of inhibitory interneurons with neighboring interneurons of the same subtype Galarreta and Hestrin (1999); Gibson et al. (1999). They are also effective, passing on average 10% of their slow voltage signals to the downstream cell Connors and Long (2004). Gap junctions are dynamic, turning over on average four to 24 times per day, many times faster than the average membrane protein turnover of 1 day McCracken and Roberts (2006); Pereda (2014). While it is clear that gap junctions can dramatically affect signaling in interneurons, their roles in the greater neocortical network are poorly understood.

Gap junctions comprise clusters of pores formed of two hemichannels, each containing six subunits that connect pairs of cells. Gap junctions in vertebrates are members of the connexin (Cx) family of proteins, coded by about 20 different genes Söhl et al. (2005). Hemichannels from separate cells join to form a channel that connects the intracellular domain of one cell with that of its partner. Those channels allow ions and small molecules up to about 1000 Daltons to pass through, although pore sizes vary with connexin composition Evans and Martin (2002). Electrically coupled cortical interneurons are connected dendro-dendritically, dendro-somatically, or somato-somatically. Neuronal gap junctions are also called "electrical synapses", and they pass ionic current rapidly and bidirectionally. This can strongly synchronize the spikes and subthreshold activity of connected cells Bennett and Zukin (2004); Mancilla et al. (2007).

Half of the connexin subtypes are expressed in the central nervous system, but only Cx36 and Cx45 are known to be expressed extensively in neurons Connors and Long (2004). Cx36 was found to be widely and exclusively expressed Condorelli et al. (2000) in neuronal gap junctions via freeze-fracture electron-microscopy Rash et al. (2000). These findings motivated the creation of a Cx36 constitutive knockout mouse line in which the Cx36 gene was replaced with reporter genes including LacZ Deans et al. (2001). LacZ expression in the cortex implied that Cx36 was found only in inhibitory interneurons Deans et al. (2001). Cortical expression begins in the second postnatal week and continues throughout maturity Long et al. (2005a). The Cx36 knockout mouse has shown that the loss of Cx36 nearly abolishes electrical synapses in every brain structure in which it has been studied, suggesting it is a key component of the vast majority of electrical synapses (e.g. Ref. Deans et al. (2001); Landisman and Connors (2005); Long et al. (2005b)). The Cx36 knockout mouse loses 97% of its electrical coupling in neurons of the thalamic reticular nucleus (TRN) Landisman and Connors (2005), 100% of its electrical coupling in somatostatin-expressing cortical interneurons (SOM cells) Deans et al. (2001), and 83% in parvalbumin-expressing interneurons (PV cells) Deans et al. (2001). It is worth noting that recent measurements of dye-coupling of interneurons in the TRN showed higher residual coupling, although there remains at least a 50% decrease in coupling Lee et al. (2014).

Inhibitory interneurons comprise only 10-30% of neocortical neurons Rudy et al. (2010) but they play essential roles in the network. Inhibition suppresses runaway excitation and thus seizures Isaacson and Scanziani (2011); Trevelyan et al. (2006). Inhibitory interneurons also increase the dynamic range of circuits and tune network dynamics Isaacson and Scanziani (2011); Rudy et al. (2010). Recent work suggests that all neocortical inhibitory interneurons fall into three subtypes defined by expression of distinct proteins Rudy et al. (2010): the serotonin 5HT3a receptor identifies 30%, the calcium-binding protein PV defines 40%, and the neuropeptide SOM marks the final 30%. Electrophysiologically, PV cells are mostly fast-spiking (FS) interneurons and SOM cells show a low-threshold spiking (LTS) behavior Rudy et al. (2010). PV cells are interconnected via electrical and chemical synapses and synapses with excitatory neurons show synaptic depression in each direction Beierlein et al. (2003); Gibson et al. (1999). Pairing electrical synapses with chemical synapses in PV cells can yield opposite effects on the same target cell with different timescales, which can have complicated dynamic consequences Hayut et al. (2011). LTS cells, on the other hand, are connected only by electrical synapses and, while chemical synapses from LTS cells to excitatory neurons show synaptic depression, synapses from excitatory neurons to LTS cells are strongly facilitating. Through GABAergic synapses, networks of PV cells and LTS cells can inhibit one another Gibson et al. (1999).

The knockout of Cx36 leads to a wide array of behavioral phenotypes. Mice are less coordinated (unpublished data, Burwell RD & Connors BW), their vision is seriously impaired Deans et al. (2002), and they have a circadian rhythm deficit Long et al. (2005a). They also show learning deficits. When conditioned to an eye-puff with a tone, Cx36 knockout animals are unable to properly time a tone-evoked eye-blink Van Der Giessen et al. (2008). Similarly, when challenged with a ladder with mobile rungs, the Cx36 knockout animal has difficulty learning to associate a tone with a moving rung and stumbles Van Der Giessen et al. (2008). Learning deficits extend to object recognition; knockout animals are unable to recognize objects after a delay of only 15 minutes Frisch et al. (2005). The loss of Cx36 also increases anxiety. Animals in a light-dark box experiment spend less time in light areas Zlomuzica et al. (2012).

The cerebral cortex generates oscillations, which were first measured in 1875 Caton (1875) and quickly shown to be associated with different behavioral states Caton (1877). Since then, cortical oscillations including theta (4-12 Hz) and gamma (30-80 Hz) have been linked to attention Fries et al. (2001); Gray et al. (1989), but the origins and functions of these rhythms remain only partially understood. PV interneurons have been repeatedly linked to the mechanisms of gamma rhythms Cardin et al. (2009); Traub et al. (1996b); Whittington et al. (2011).

Recently, it was demonstrated that pulsed optical stimulation of PV cells can drive the cortical network with strong resonance in the gamma frequency range, peaking around 40

Hz Cardin et al. (2009). The observation that PV cells are highly electrically coupled Gibson et al. (1999) raises the question of whether gap junctions play a role in the generation of neocortical gamma oscillations. There is ample evidence that gap junctions are essential for normal gamma oscillations in hippocampus. The deletion of Cx36 led to a decrease in gamma-band EEG power in vivo and the kainate in vitro model of gamma oscillations Buhl et al. (2003); Hormuzdi et al. (2001). Furthermore, in neocortex in vitro, gap junctions were necessary for synchronizing SOM cells in rhythms induced by the metabotropic glutamate receptor (mGluR1a) agonist ACPD Beierlein et al. (2000).

Necortical gap junctions likely play a role in human health. First, mutations in the gene that encodes Cx36 may cause some forms of epilepsy. Juvenile myoclonic epilepsy, which accounts for 5-10% of epilepsy cases, has a strong genetic component Mas et al. (2004). Linkage analysis has identified four mutations within the Cx36 gene, none of which led to coding changes but all of which are predicted to alter the structure of the folded mRNA and thus protein expression Mas et al. (2004). By understanding the network effects of Cx36, we may gain insight into the possible role of gap junctions in epilepsies. Second, quinine and its derivatives such as mefloquine block gap junctions Cruikshank et al. (2004); Srinivas et al. (2001). These drugs have been used widely to prevent malaria, and they are associated with vivid dreams and occasionally hallucinations and psychosis. Third, people undergoing their first schizophrenic episodes under no medication show a decrease in gamma oscillations during perceptual tasks (for review see Uhlhaas and Singer (2010)). As electrical coupling of PV-expressing interneurons is suggested to play a role in gamma oscillations Cardin et al. (2009); Sohal et al. (2009), defining the role of electrical coupling in gamma oscillations may lead to a better understanding of psychiatric disorders.

Gamma oscillations can be induced optogenetically in slices without a temporally biased method such as pulsing the driving light at 40 Hz. Rather, excitation of cortical excitatory cells via a slow optogenetic ramp naturally generates rhythmic gamma-band activity Adesnik and Scanziani (2010). This suggests that the mechanism by which gamma is generated in vivo remains intact in slices. By recording in vitro, we have unparalleled access to individual cells and can measure subthreshold activity in a large number of cells. This has proven essential, given that the gamma power in our optogenetic model can vary by orders of magnitude even among closely spaced cells (e.g. less than 100 μm apart).

Experimental and theoretical studies have suggested that gamma oscillations can be generated by at least two distinct network phenomena: interneuron gamma (ING) or pyramidal-interneuron gamma (PING) Bartos et al. (2007); Isaacson and Scanziani (2011); Tiesinga and Sejnowski (2009); Whittington et al. (2011). In ING, the reciprocal inhibitory connections between FS cells enforce a synchrony onto the networks of FS and RS cells. In PING, synchrony of excitatory cells produces volleys of excitatory activity, which in in turn lead to synchronized inhibition.

In this study, we measured the extent to which gap-junction mediated synchrony of neocortical interneurons affected local gamma oscillations, as generated via an optogenetic ramp in Cx36 wild-type (WT) and knockout animals (Cx36KO). While a constitutive knockout has ample time in which the network may compensate for the gene's loss, previous experiments have demonstrated that common gap-junction blockers have important nonspecific effects, especially for network activity. Carbenoxolone has extensive non-specific effects. For example, one study showed that carbenoxolone affected 4-aminopyridine induced seizures, while mefloquine did not Beaumont and Maccaferri (2011); Connors (2012). Mefloquine is not without side effects either, as it increases spontaneous synaptic activity, depolarizes cells slightly, and can change the shape of afterhyperpolarizations in excitatory cells Behrens et al. (2011); Cruikshank et al. (2004). Furthermore, the Cx36 knockout mouse model has been thoroughly characterized (e.g. Beierlein et al. (2003); Deans et al. (2001); Long et al. (2005a,b); Postma et al. (2011)) and remarkably little compensation for the loss of Cx36 has been identified. Given that few if any changes have been attributed to compensation for the loss of Cx36 rather than to the loss itself, the Cx36KO line is an excellent model in which to measure the effect of gap junctions on network oscillations.

Multiple studies have demonstrated the import of gap junctions in neocortical cell synchrony. Surprisingly, we found no effect of the knockout of gap junctions on optogenetically induced gamma oscillations in somatosensory cortex. We confirmed these findings in a distant neocortical region of association cortex, the postrhinal cortex. Next, we hypothesized that our gamma model had sufficiently extreme rhythmicity that gap junctions were unnecessary. To decrease the rhythmicity to physiological levels, we increased the ratio of inhibitory-to-excitatory optogenetic stimulation such that the inhibitory cells might depend more greatly on gap junctions. We determined once again that there was no effect on optogenetically induced gamma oscillations.

3.3 Results

3.3.1 Optogenetic excitatory ramps produce strong rhythmic oscillations across neocortex

Previous work demonstrated that gamma oscillations could be generated in slices by in utero electroporation of channelrhodopsin timed to select for layer 2/3 excitatory cells of primary visual cortex Adesnik and Scanziani (2010). However, many of the previous measurements of gap-junctional coupling have been made in layer 4 of primary somatosensory cortex, due in part to the ease with which cell types can be selected by size. Therefore, we identified a virus that reliably expressed across cortical layers and regions without damage. We used a construct designed to selectively express in excitatory cells, AAV2/9-CamKIIα-C1V1-eYFP Yizhar et al. (2011), diluted such that it expressed on average one viral particle per cell. C1V1

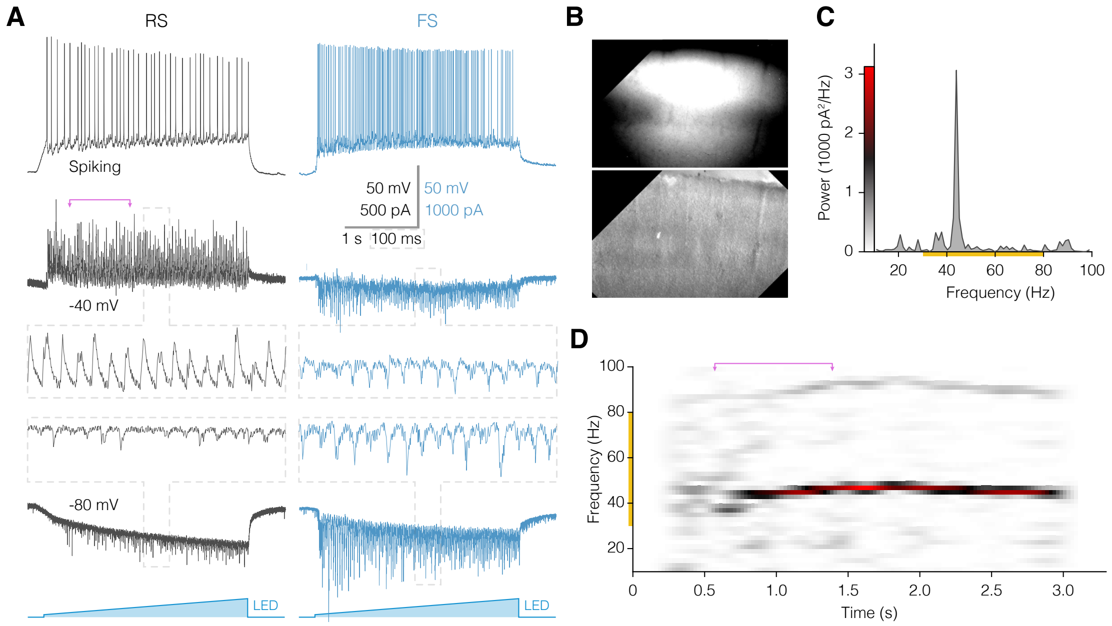

Figure 3.1: 3-second LED ramps over slices of neocortex, both in somatosensory and postrhinal cortices, with a virus selectively expressed in excitatory cells yield strong gamma oscillations. Pink arrows mark the analyzed 0.8 s with maximum gamma-band power. Yellow bands on frequency axes mark the gamma-band range. (A) Example RS and FS cells during a ramp. Each shows a current clamp trace, a voltage clamp trace at -40 mV, and a voltage clamp trace at -80 mV. (B) Example somatosensory cortex injection of AAV2/9-CamKIIα-C1V1 after 12 days expression and matching DIC image. (C) Power spectrum of the strongest 0.8 seconds of gamma band power of RS cell from A voltage clamped at -40 mV. (D) Spectrogram of RS cell from A voltage clamped at -40 mV.

is a redshifted channelrhodopsin construct that combines parts of *Volvox* channelrhodopsin VChR1 and traditional *Chlamydomonas* channelrhodopsin ChR1 to yield a construct with very high currents at low light intensities Yizhar et al. (2011).

The virus was initially purified by the UPenn Vector Core to a titer of 5.8×10^12 infections particles per milliliter. Infections with the full-titer virus caused cortical damage by seven days of expression. All recorded excitatory cells at this titer were photosensitive, so the multiplicity of infection (MOI) or the number of infectious viral particles per cell on average was indeterminable. We diluted the virus sixfold such that the MOI was between 1 and 2. Of the recorded cells in layer 4, 18.5% were not photosensitive, which, via the Poisson distribution, yields an MOI of 1.7 ($P(0) = e^{-MOI}$). This implies that 31.2% of cells were infected by 1 viral particle, 26.3% of cells were infected by two particles, and only 24% of cells were infected by more than 2 particles. At this dilution, there was no damage after 13 days of expression.

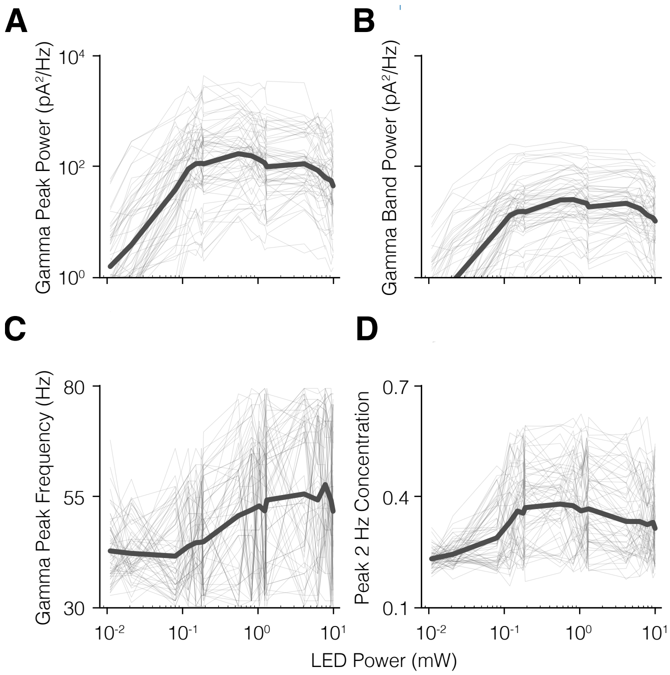

Figure 3.2: 20 intensities of light were tested per cell. Fourier analysis was performed on strongest 0.819 seconds to avoid frequency drift. (A) Amplitude of the peak 2 Hz bin. (B) Averaged 30-80 Hz power. (C) Frequency of the peak 2 Hz bin. (D) Ratio of amplitude of peak 2 Hz bin to the 30-80 Hz band power.

Although the eYFP expression was stronger in layers 2/3 and 5 than in layer 4, the majority of cells in layer 4 were photosensitive.

We recorded from FS cells to determine their activity during optogenetic ramps, then selected for excitatory cells marked by their regular-spiking (RS) pattern. RS cells were used to compare gamma-band power. To activate the channelrhodopsin only locally, we stimulated slices with an LED with a 150 μm spot diameter. Cells were recorded in current clamp and voltage clamped at -40 mV and -80 mV using a potassium electrode solution (Figure 3.1A). Holding the cells at -80 mV isolated excitatory currents, while -40 mV gave a mixture of inhibitory and excitatory currents. The majority of RS cells expressed C1V1 and spiked in response to the optical ramp stimuli when recorded in current clamp, as in Figure 3.1A. However, their synaptic currents during ramp stimuli were predominantly inhibitory. These currents were highly rhythmic, as shown in the inset of Figure 3.1A. Recordings were made from the expression pattern shown in Figure 3.1B. Optogenetic ramps of light over three seconds produced strong gamma oscillations across more than an order-of-magnitude of stimulus intensities (Fig 3.1B-C).

Currents onto FS and RS cells were remarkably complementary. The majority of currents recorded from FS cells were excitatory, as demonstrated by voltage clamping at -80 mV (Figure 3.1A). In contrast, RS cells received predominantly inhibitory currents.

Over the course of the three-second light ramp, the gamma oscillations changed in frequency and in power. A stable example is shown in Figure 3.1D, but even in this case the peak frequency shifted by over 2 Hz during the ramp. Therefore, we confined our analysis to the 0.8 seconds over which the gamma-band power was strongest. Rarely did the peak frequency bin shift by 2 Hz or more over 0.8 seconds.

Recording oscillations over such a wide range of stimulus intensities exposes a fascinating property of the network: as the stimulus increases towards the optimal intensity, the peak frequency stays constant at just over 40 Hz, while the peak power increases (Figure 3.2A, C). At the optimal intensity, there's an inflection point in the graphs of the peak frequency and the peak power. The peak power stops increasing and remains relatively constant, while the frequency starts to shift upwards. This correlates with the peak of the concentration of power in the strongest bin relative to the rest of the gamma power (Figure 3.2D). In these experiments, gamma-band power (Figure 3.2B) was tightly linked to the peak 2 Hz bin, given that the power in the peak bin was up to 70% of the total gamma power. This can be seen in both the spectrogram (Figure 3.1D) and power spectrum (Figure 3.1E) of the example trace from Figure 3.1A.

In short, optogenetic ramps with selective excitation of RS cells produce strong oscillations in the gamma band across a wide range of stimulus intensities.

3.3.2 Gamma power in somatosensory cortex is independent of gap junctions

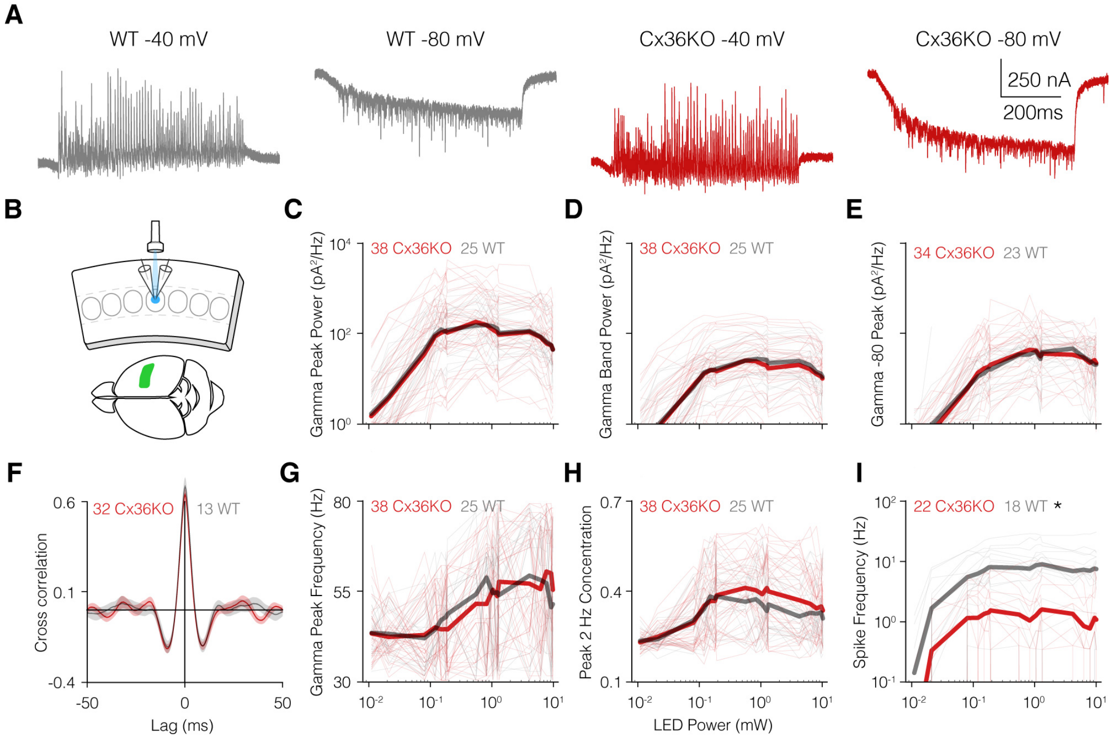

Figure 3.3: Gamma does not depend on gap junctions in somatosensory cortex. Dark bars are the mean or log-mean for log-axis plots. (A) Example recordings from WT and Cx36KO animals. (B) Paired recordings were done in somatosensory cortex (green) of RS cells while optogenetically stimulating with an LED. (C) Gamma power in the peak 2 Hz bin, voltage clamped at -40 mV and across three orders-of-magnitude of stimulus intensities, is indistinguishable between Cx36KO and WT. (D) Gamma-band (30-80) Hz power at -40mV is indistinguishable. (E) Gamma peak power at -80 mV is indistinguishable. (F) The cross-correlation between pairs of RS cells are indistinguishable. (G) The gamma peak frequency by power is indistinguishable. (H) The concentration in the peak 2 Hz bin is indistinguishable. (I) RS Spike frequencies across the entire ramp in current clamp are dramatically and significantly ($P = 0.0018$) higher in WT than in Cx36KO. Plotted is the mean, to include cells that didn't spike.

Copious data have suggested that gap junctions synchronize neocortical interneurons. So, we asked whether this inherent network oscillation required gap junctions in layer 4 of somatosensory cortex (Figure 3.3A,B).

The peak gamma power of currents in RS cells measured at -40 mV was indistinguishable between WT and Cx36KO (Figure 3.3C). Gamma power ranged widely; individual cells recorded within 100 μm of each other sequentially could vary by an order of magnitude. However, we recorded animal pairs on the same day to match expression times, and we confirmed that the fluorescence of layer 4 (an example is in Figure 3.1B) matched between littermate pairs. As described above, eYFP expression was greater in layers 2/3 and 5 than in layer 4. We have determined our infection rate for layer 4 and we used a small stimulus diameter to confine the gamma oscillations to layer 4 thus trying to minimize the input of the adjacent layers. Next, we compared the photocurrents measured below the threshold of synaptic activity (WT 27.5± 1.9 pA over 25 cells in 3 animals, Cx36KO 27.1 ± 8.3 pA over 38 cells in 4 animals). None differed significantly.

To determine whether genotype influenced the distribution of power across gamma frequencies, we compared the average power across the 30-80 Hz gamma band (Figure 3.3D). However, there was no discernible difference. The purely excitatory activity measured at -80 mV onto RS cells was similarly indistinguishable (Figure 3.3E).

We thought perhaps the cross-correlation between the inhibitory events onto pairs of RS cells would distinguish between WT and Cx36KO. If gap junctions served to synchronize spike timing at a fine scale, we might expect that the width of the cross-correlation peak would be tighter in WT than Cx36KO. However here, too, we found no significant difference (Figure 3.3F). Neither the peak frequency, nor the concentration in the peak 2 Hz bin distinguished the two genotypes(Figure 3.3G,H).

One ancillary measure dramatically differed between WT and Cx36KO: the rates at which RS cells were firing. Excitatory cells in the WT animal ($N = 16$) spiked at an average rate of 11.3 ± 2.2 Hz at the stimulus intensity that generated the peak gamma power, five times faster than the Cx36KO rate of 2.5 ± 0.67 Hz ($N = 22$, $P = 0.0018$, Figure 3.3I). The decreased firing rate of this subpopulation of Cx36KO neurons corresponded with a decrease in RS cell resistance from 248 ± 15.4 MΩ to 197 ± 10.1 MΩ ($P = 0.0078$). However, the population of RS cells with high spike frequencies and low resistances were unusual. Comparisons of the resistances of all RS cells recorded in somatosensory cortex were not different between WT and Cx36KO (224 ± 9.2 MΩ across 62 cells and 216 ± 7.6 MΩ across 78 cells, respectively, P = 0.25).

Surprisingly, there were few measurable differences between the gamma oscillations of WT animals expressing Cx36 and their age-matched siblings in which the protein had been knocked out (Cx36KO). The only measures by which we could detect a difference between Cx36KO and WT animals were the increased spike frequency and resistance of RS cells in the WT animal.

3.3.3 Gamma power in postrhinal cortex is independent of gap junctions

Even with our small activation diameter, the laminar pattern of expression in somatosensory cortex could have created competition between different mechanisms of gamma generation across layers. Given the extensive evidence suggesting that gamma oscillations play a role in synchronizing neighboring inhibitory cells, we moved to a radically different neocortical region with less extreme lamination, dorsal postrhinal cortex, in which to measure the effects of gap junctions on gamma oscillations. Postrhinal cortex is a component of the parahippocampal region Burwell and Amaral (1998b) that provides input to entorhinal cortex. The ventral portion of postrhinal cortex has unusual inhibitory interneurons, including reduced parvalbumin staining (de Curtis and Paré (2004) and Chapter 2), but the dorsal half contains the normal complement of parvalbumin cells.

As in somatosensory cortex, we injected the same virus diluted at a 1-to-6 ratio to maintain slice health and to yield an MOI under 2. This dilution produced strong activation and expression in dorsal postrhinal cortex (Figure 3.4A-C). The altered lamination of postrhinal cortex led to an even expression across the layers (Figure 3.4C). This was specific to dorsal

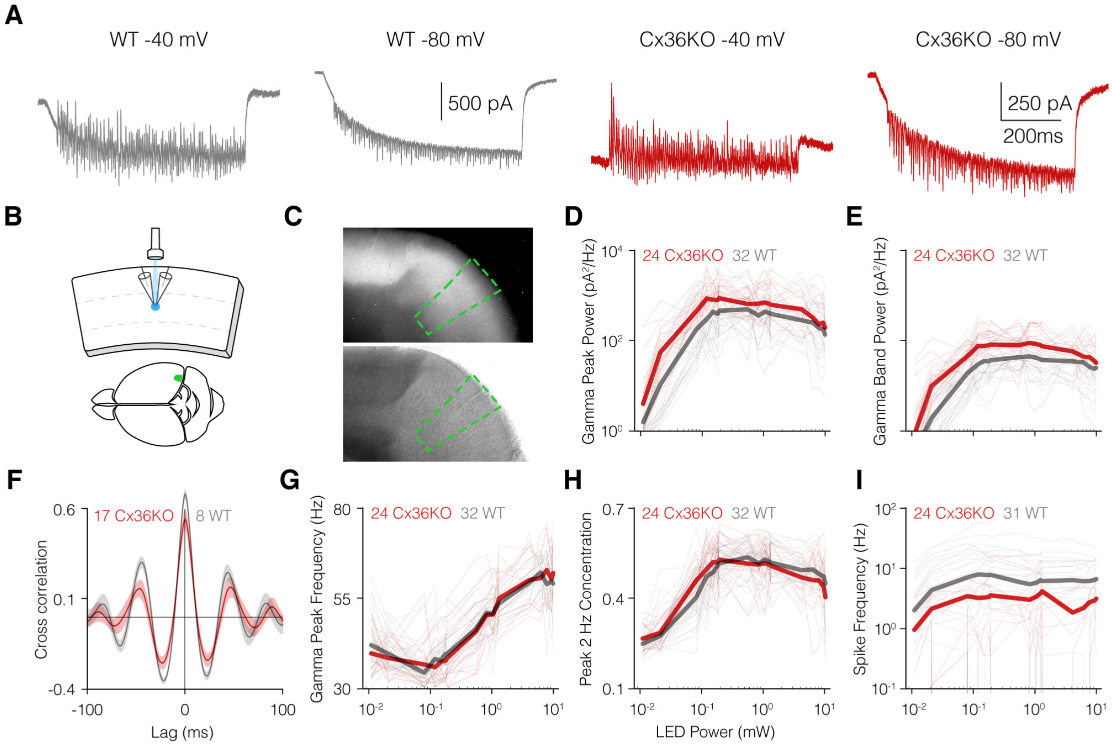

Figure 3.4: Gamma does not depend on gap junctions in postrhinal cortex. Dark bars are the mean or log-mean for log-axis plots. (A) Example recordings from WT and Cx36KO animals. (B) Paired recordings were done in postrhinal cortex (green) of RS cells while optogenetically stimulating with an LED. (C) Photographs of fluorescence from the injection shows that layer 4 has similar expression to the neighboring layers. Green marks the recording region in the dorsal postrhinal cortex. (D) Gamma power in the peak 2 Hz bin, voltage clamped at -40 mV and across three orders-of-magnitude of stimulus intensities, is statistically indistinguishable between Cx36KO and WT. (E) Gamma-band (30-80) Hz power at -40mV is indistinguishable. (F) The cross-correlation between pairs of RS cells are indistinguishable. (G) The gamma peak frequency by power is indistinguishable. (H) The concentration in the peak 2 Hz bin is indistinguishable. (I) Spike frequencies across the entire ramp in current clamp are not-significantly higher in WT than in Cx36KO. Plotted is the mean, to include cells that didn't spike.

postrhinal cortex; along the anterior border of the injection (the bottom right of the image), the expression begins to express selectively lower in layer 4. Animals were matched for expression level and photocurrents in layer 4 RS cells (WT 30.2± 7.4 pA over 32 cells in 4 animals, Cx36KO 26 ± 9.9 pA over 24 cells in 3 animals) and were not significantly different.

Consistent with our results from somatosensory cortex, we could identify no ways in which the light ramp yielded statistically significant differences between WT and Cx36KO animals in voltage-clamped RS cells of layer 4. The gamma power of the peak 2 Hz band voltage clamped at -40 mV showed no detectable differences (Figure 3.4D). The average Cx36KO power was slightly higher than that of WT animals, although this is not statistically significant. When the data from the somatosensory cortex and postrhinal cortex are combined, this difference is completely eliminated. Although WT and Cx36KO show no differences, gamma power in postrhinal cortex is significantly greater than in somatosensory cortex ($P << 0.005$). This may be due to network differences between the regions.

Gamma-band power measured at -40 mV shows no difference (Figure 3.4E). This is because the power is concentrated at the peak frequency (Figure 3.4H), so the band power tracks with the peak power. The cross-correlogram shows no large differences between WT and Cx36KO genotypes (Figure 3.4F) and a quantification of the cross correlogram peak, width, and side-lobes by stimulus intensity shows no differences (not shown).

Unlike our recordings in barrels, postrhinal cortex did not show a difference in spike frequency during gamma activity (Figure 3.4I). Correspondingly, there is no significant difference in RS cell resistance (WT 271 ± 24.7 MΩ in 25 cells, Cx36KO 231 ± 21.3 MΩ in 38 cells, $P = 0.17$). This is another strong confirmation that our results are not due to compensation in the Cx36KO animal.

3.3.4 Increased inhibitory stimulation blocks gamma oscillations

During exploratory experiments in which we determined that a full-titer virus dramatically damaged the tissue, WT neurons appeared to have stronger gamma power than Cx36KO neurons in somatosensory cortex. Expression after seven days appeared equal across layers, unlike the expression in animals with a diluted virus. After we extensively tested healthy tissue and found no difference in the strength, frequency, inhibitory/excitatory components, and cross-correlations of RS cells during gamma oscillations, we hypothesized that the full-titer difference came either from real differences in gamma generation due to laminar compe-

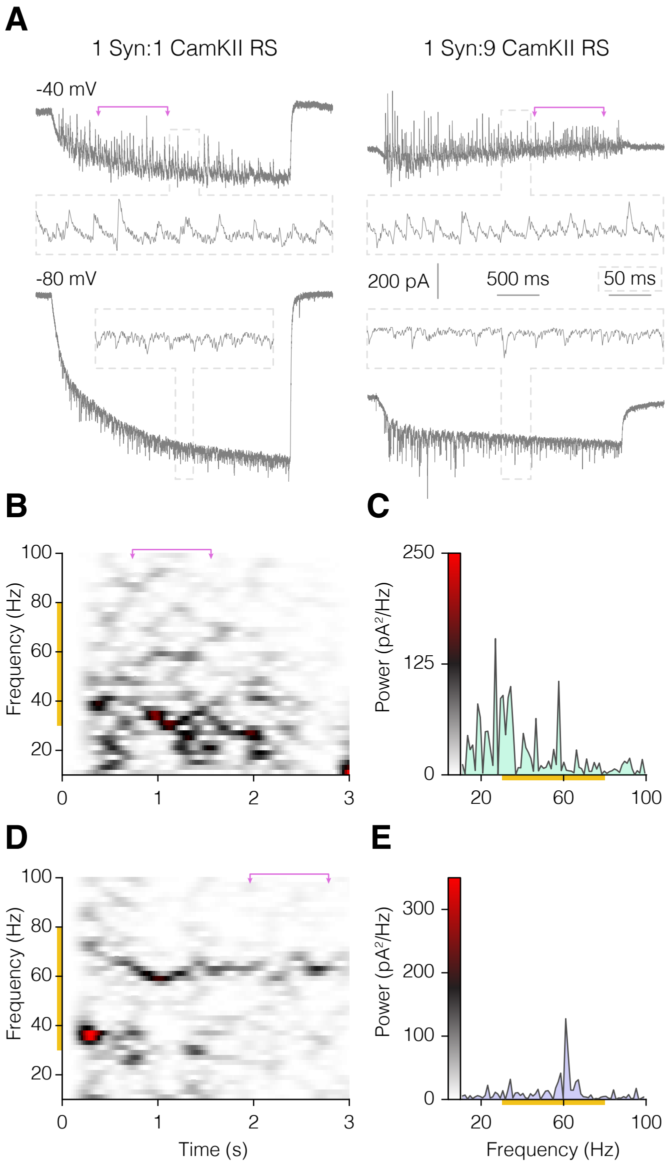

Figure 3.5: Increasing drive to inhibitory cells disrupts gamma oscillations. Pink arrows mark the analyzed 0.8 s with maximum gamma-band power. Yellow bands on frequency axes mark the gamma-band range. (A) Example traces of an RS cell with (left) equal parts synapsin-driven channelrhodopsin and CamKIIα-driven channelrhodopsin and (right) 1 part synapsin-channelrhodopsin to 9 parts CamKIIα channelrhodopsin voltage clamped during a 3-second optogenetic ramp. (B) Spectrogram of -40 mV 1:1 trace from A. (C) Spectrum of peak region from B. (D) Spectrogram of -40 mV 1:9 trace from D. (E) Spectrum of peak region from D.

tition, increased expression in inhibitory cells, or from sensitivity to virus due to a range of other problems experienced by the Cx36KO animal such as diabetes Meda (2003). We considered increased expression in inhibitory cells the most likely explanation because the CamKIIα promoter was selected to express exclusively in excitatory cells, but it expresses intermittently at low levels in inhibitory cells. When full-titer virus was used, most inhibitory interneurons

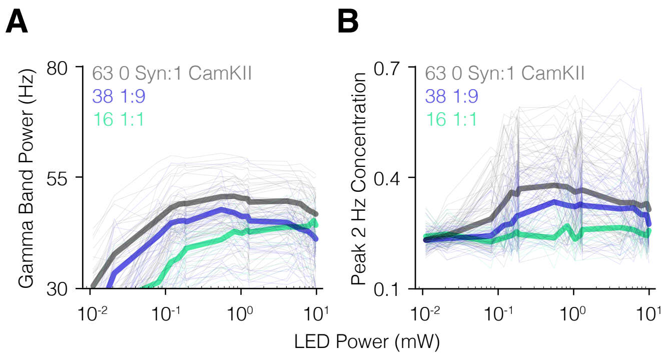

Figure 3.6: Increasing drive to inhibitory cells continues to generate power in the 30-80 Hz band, but disrupts gamma oscillations. (A) Activity is generated between 30-80 Hz. (B) This activity is arrythmic; it is not concentrated in the peak 2 Hz bin.

were photosensitive.

We tested laminar competition due to unequal expression by recording in a region in which expression was equal across layers, posthrinal cortex, and found no difference by genotype. So, we next tested whether increased drive of inhibitory cells would reveal gap-junction-dependent effects on gamma oscillations. To do so, we combined a virus that expresses in all cell types, AAV2/9-hSyn-ChR2-eYFP with the virus we had been using that preferentially expressed in excitatory cells, AAV2/9-CamKIIα-C1V1-eYFP. The viruses were matched for titer and serotype, but we continued to use the AAV2/9-CamKIIα-C1V1-eYFP to bias stimulation towards excitatory cells. We also used matching fluorescent proteins because of the tendency for red fluorescent proteins to be sequestered Asrican et al. (2013). Measurements from inhibitory cells confirmed that inhibitory cells were photosensitive.

We used a dilution series of viral mixtures. From 1 hSyn-ChR2: 0 CamKIIα-C1V1 through 5:1, 1:1, 1:3, 1:9, and up to the original 0:1 hSyn-ChR2 to CamKIIα-C1V1 mixture. Only the last two mixtures produced consistent peaks in the gamma band. We have selected two of these mixtures, 1 hSyn-ChR2:1 CamKIIα-C1V1 and 1 hSyn-ChR2:9 CamKIIα-C1V1, to compare (Figure 3.5).

Example traces from an RS cell in the 1 hSyn-ChR2:1 CamKIIα-C1V1 mixture show strong synaptic activity during the ramp, as do example traces driven by the mixture with greater excitatory drive, hSyn-ChR2: 9 CamKIIα-C1V1 (Figure 3.5A). Activity of the 1:1 mixture was arrhythmic and never coalesced into gamma oscillations (Figure 3.5B,C). In contrast, slightly increasing excitatory drive by increasing the mixture to 1 hSyn-ChR2: 9 CamKIIα-C1V1 generated gamma oscillations (Figure 3.5D,E). However, these oscillations were weaker than those generated in animals with exclusively CamKIIα-C1V1 and these oscillations in the 1:9 dilution fluctuated in and out.

These differences are most visible when comparing the band power and peak concentration of different viral combinations. Each viral mix generates activity in the gamma band (Figure 3.6A), but only as the ratio of excitatory to inhibitory drive increases does the synchronous activity becomes both more periodic and more narrow-band (Figure 3.6B). The increased activity due to an optogenetic stimulus leads to power within the gamma band in the 1 hSyn-ChR2: 1 CamKIIα-C1V1 mixture, although it is not rhythmic (Figure 3.6B). There are no differences between Cx36KO and WT animals in this non-rhythmic activity.

First, we tried to address the wide variation of measured gamma powers across neurons within a single animal. By measuring sequential bouts of gamma within a cell with the same stimulus intensity, we could compare the within-cell variability to that of cells measured sequentially. Cell-to-cell variability dominated trial-to-trial variability in the measurements (Figure 3.7A).

The rhythms driven by a greater percentage of inhibitory-to-excitatory cells remained independent of gap junctions. The 1 hSyn-ChR2: 9 CamKIIα-C1V1 mixture shows very similar results to the 0 hSyn-ChR2: 1 CamKIIα-C1V1 mixture shown in Figures 1-3.4, although the peak powers are lower. Peak gamma power and gamma band power were indistinguishable (Figure 3.7C,D). The frequency of the oscillations and the rhythmicity of excitatory currents were similarly matched (Figure 3.7G,H). Other measurements such as cross-correlation and

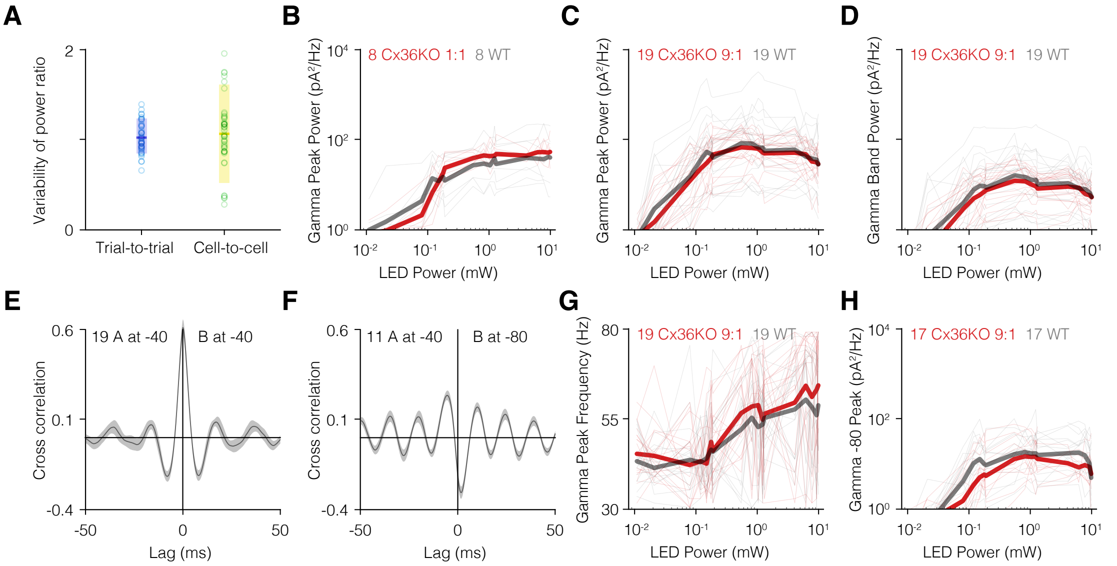

Figure 3.7: Increasing inhibitory drive does not make gamma depend on gap junctions. Dark lines are log-mean on log axes. (A) Cell-to-cell variability is much greater than trial-by-trial variability as measured by the ratio of the log peak power of sequential measurements. Thick purple and yellow lines are mean, purple and yellow regions are the 10-90 percent intervals. (B) Gamma peak power is minimal in a 1:1 synapsin-channelrhodopsin to CamKIIα-channelrhodopsin mixture. (C) Increasing the mixture to 1 synapsin-channelrhodopsin to 9 CamKIIα-channelrhodopsin yields gamma oscillations, but no distinguishable difference between Cx36KO and WT. (D) Gamma-band power shows no detectable differences. (E) Cross-correlogram of the synaptic currents of neighboring RS cells held at -40 mV shows strong correlation with exactly 0 ms lag in a 1:9 mix of viruses. (F) Cross-correlogram of one RS cell held at -40 mV and the other at -80 mV shows that excitation precedes inhibition by 5.4 ms. (G) Gamma peak frequency is indistinguishable between Cx36KO and WT genotypes with the 1:9 viral mixture. (H) Excitation measured at -80 mV is indistinguishable between genotypes.

concentration in the peak band showed the same lack of dependence on gap junctions.

Given the increased inhibitory drive in this optogenetic 1 hSyn-ChR2: 9 CamKIIα-C1V1 gamma model, we wanted to determine if we were shifting a putative PING model (in the 0 hSyn-ChR2: 1 CamKIIα-C1V1 condition) to an ING model (in the 1 hSyn-ChR2: 9 CamKIIα-C1V1 condition). In previous studies, gamma oscillations driven purely by reciprocal inhibition had 0 ms phase lag between inhibitory and excitatory cell firing Traub et al. (1996a). One can determine the relationship between inhibition and excitation in a single cell by measuring the lag in the cross-correlogram across a pair of cells. First, we measured Lag(E_1, I_2)–the lag in the cross-correlogram inhibition, voltage clamped at -40 mV, and excitation, voltage-clamped at -80mV. Then we measured Lag(E_1, E_2), the lag between excitation and excitation. The vast majority of synaptic activity onto RS cells at -40 mV was inhibitory, and space clamp issues associated with our potassium pipette solution precluded recording at more depolarized voltages. Based on the equation Lag(E_1, I_1) = Lag(E_1, I_2) - Lag(E_1, E_2), we calculated that inhibition lags excitation in excitatory cells by 5.4 ms Okun and Lampl (2008).

Although a viral mixture does not affect the dependence of gamma oscillations on gap junctions, we have developed a mechanism to titrate the rhythmicity of network activity in vitro by mixing nonselective viruses or those selective for inhibitory cells with viruses selective for excitatory cells. We can further titrate the power of these rhythms by varying the optogenetic stimulus and viral dilution.

3.4 Discussion

We have modified an original technique for generating gamma oscillations optogenetically such that we can stimulate oscillations in layer 4 of two disparate regions of neocortex (Figure 1). We further expanded the system to have fine control over the amplitude and the rhythmicity of these oscillations by changing the relative drive of inhibitory and excitatory cells (Figure 4). This mechanism for generating gamma has considerable advantages over induction by drugs such as carbachol and kainate. First, gamma oscillations in vivo are localized to small regions, on the order of 250 μm in diameter Katzner et al. (2009); Paik et al. (2009); Sridharan et al. (2011); Tiesinga and Buia (2009); Xing et al. (2009). Drugs require bath application and affect the entire slice, while optogenetically-evoked gamma is easily localized by spot size and position. Second, gamma oscillations are intermittent, unlike drug-induced oscillations which can take many minutes to begin or terminate Fries et al. (2001); Lu et al. (2012). Optogenetic gamma can be activated with millisecond precision. Third, likely because of the long-term activity, kainate-induced oscillations are maximally strong only at unphysiologically low temperatures in submerged recording chambers, where their peak frequency lies below the gamma range Lu et al. (2012). In contrast, the oscillations we have induced were recorded at near-physiological temperatures and they maintained in vivo-like peak frequency and power.

With these tools, we have asked whether gap junctions play a role in the natural 40 Hz oscillation derived from simple asynchronous depolarization of excitatory cells. Studies of the coupling of pairs of interneurons in neocortex have suggested that gap junctions serve to synchronize them (e.g. Beierlein et al. (2000); Deans et al. (2001); Gibson et al. (1999, 2005); Long et al. (2005a); Mancilla et al. (2007)) while measurements of gamma in hippocampus, both under kainate in vitro and more naturally in vivo, have shown differences between the gamma power of Cx36KO and WT animals Buhl et al. (2003); Hormuzdi et al. (2001). Given these results, we predicted that optogenetically induced gamma oscillations would be significantly decreased in the neocortex of Cx36KO mice.

Recordings of gamma oscillations from somatosensory and postrhinal cortices revealed almost no differences between genotypes (Figure 2, 3). Given the ease with which these oscillations are generated, it appears that we have tapped into an intrinsic and important part of the cortical network. Our results imply that some mechanisms of gamma generation in neocortex in vivo do not depend on gap junctions. However, certain other gamma oscillations may rely on gap junctions: those in the presence of strong arrhythmic activity, competing rhythms, or rhythms generated by a more purely ING mechanism.

We tested whether increased arrhythmic activity would force the gamma oscillations to rely in part or in whole on gap junctions (Figure 5). First, we characterized activation of the total network of excitatory and inhibitory cells by injecting a virus with no preference for neuronal type (Figure 4). This generated purely arrhythmic activity. Then, by titrating the mixture of the nonselective and excitatory cell-preferring viruses, we found a point at which gamma oscillations began. Nevertheless, even in this regime there was no dependence on gap junctions.

The relative timing of inhibitory and excitatory synaptic inputs onto RS cells suggests a consistent lag of inhibitory cell firing of about five milliseconds (Figure 5). This in turn suggests that the optogenetic gamma mechanism is an E-I or PING rhythm Traub et al. (1996a), which is bolstered by our ability to eliminate gamma oscillations by increasing inhibitory drive. It remains possible that an ING mechanism of gamma generation in neocortex would be gap-junction dependent.

The remaining mechanism by which gap junctions may serve to strengthen gamma oscillations is in the presence of competing rhythms. The work of Buhl et al. (2003) demonstrates just such a case in hippocampus; the gap-junction dependence of gamma oscillations is modulated by the theta phase. We have attempted to address this case with a computational model (Chapter 4).

3.5 Experimental Procedures

Electrophysiology Animals were all Cx36KO Deans et al. (2001) or their wild-type littermates. Mice aged P20-P25 were anesthetized and two 300 μm slices 1300-1900 μm from the lateral edge of the cortex were taken in ice-cold artificial cerebrospinal fluid (ACSF) and maintained in ACSF composed of 126 mM NaCl, 3 mM KCl, 1.25 mM NaH_2PO_4, 2 mM $MgSO_4$, 26 mM $NaHCO_3$, 10 mM dextrose, and 2 mM $CaCl_2$. The ACSF was carbogenized with 95% O_2/5% CO_2. Whole-cell recordings were conducted at 32°C with a potassium-based pipette solution composed of 130 mM K-gluconate, 4 mM KCl, 2 mM NaCl, 10 mM HEPES, 0.2 mM EGTA, 4 mM ATP-Mg, 0.3 mM GTP-Tris, and 14 mM phosphocreatine-Tris (pH, 7.25; 290 mOsm). Slices were visualized through a Nikon Eclipse 2200FN with DIC and fluorescence was activated by a Mightex LED. Recordings were made with two Axoclamp-2B amplifiers and digitized with a Digitidata 1440 and a computer running PClamp 9.0.

Optogenetic and electrical stimulation Channelrhodopsin was expressed using one of two viruses, either an AAV2/9-hSyn-ChR2-eYFP (UPenn Vector Core, titer of 3.4e13 diluted 1:35) or an AAV2/9-CamKIIα-C1V1-eYFP (UPenn Vector Core, titer of 5.8e12, diluted 1:6). Injections of only AAV2/9-CamKIIα-C1V1-eYFP were allowed to express for 10-12 days. The combined viruses were recorded only at 9 days of expression.

We activated the cells with a 3 s ramp of whole-field illumination from a white led (150 μm from a Mightex LCS-5500-03-22) through a 40x water-immersion lens.

Data analysis Basic analysis was performed in Clampfit and more advanced analysis, including spectra and spectrograms were performed with our open-source software designed for analyzing electrophysiological data found at
`https://bitbucket.org/asugden/simpliphys`.

The LED turned on only after reaching a threshold voltage. The time of this voltage was measured experimentally and used for generation of the spectrum of the gamma oscillations. The 819.2 ms in which the peak total gamma-band power were analyzed for the plots in this paper in order to select for a region with consistent frequency. Comparison of the entire 3-second ramp showed no differences from those shown in the paper. Gamma-band power was averaged across each of the frequency bins.

Chapter Four

A model of optogenetically induced gamma oscillations in neocortex

4.0.1 Contributions

Arthur U. Sugden programmed the model and wrote the manuscript. Nathan Vierling-Claassen and Stephanie R. Jones provided advice on the design and implementation of the model. Barry W. Connors directed the project and co-wrote the manuscript.

4.1 Summary

Canonical signaling among neurons of the neocortex acts via chemical synapses, but inhibitory interneurons of like-types can also communicate via gap junctional coupling. This coupling is extensive, measurably linking activity between one cell and perhaps fifty of its neighbors. The total gap junctional conductance also halves the input resistance of each inhibitory cell. In addition, this coupling serves to synchronize interneurons, partially through low-pass filtered afterhyperpolarizations. Although the synchronizing effect of paired coupled cells has been extensively recorded and modeled, the effects of gap junctions on gamma-band activity of the neocortex have not been measured prior to this dissertation. We created a model of layer 4 of mouse somatosensory cortex that incorporates interneuronal gap junctions and generates optogenetic gamma-frequency activity. We used the model to explore the effects of interneuron gap junctions and other factors on gamma activity.

4.2 Introduction

The importance of gap junctions and their signaling was introduced above (Chapter 3). In short, neocortical gap junctions are small pores formed of homohexamers of the protein connexin36 (Cx36). Unlike many other gap junction proteins, Cx36 is minimally voltage sensitive, thus acting as a simple resistor between cells under physiological conditions Srinivas et al. (1999). The RC circuit formed by the gap junctions and their cells acts as a low-pass filter, strongly attenuating spikes, but passing a large proportion of slower voltage deflections such as afterhyperpolarizations (AHPs) Mancilla et al. (2007). Synchronization between cells comes from a combination of the remaining spikelets and slow AHPs Mancilla et al. (2007).

We took a two-pronged approach to determine the effect of neocortical gap junctions on gamma oscillations. First, we modified a system by which we could generate strong, rhythmic activations in cortical slices Adesnik and Scanziani (2010) such that we could titrate the level of arrhythmic activity versus gamma-band activity (Chapter 3). The key strength of this method is that it relies on a non-rhythmic input to cells and can be used to generate oscillations in vivo and in vitro. In concert, we created the first computational model of these optogenetically induced gamma oscillations. To do so, we modified a previous model of rhythmic activity in the neocortex Vierling-Claassen et al. (2010) to better match the conditions we measure in layer 4 of somatosensory-cortical slices. With the model, we can make predictions about the effects of gap junctions under various conditions that are difficult to generate experimentally.

A multitude of computational models have been created to simulate the origin of cortical oscillations (see Buzsáki and Wang (2012) and enclosed references). Further models have been created to examine the role of gap junctions in neocortical oscillations LeBeau et al. (2003); Mancilla et al. (2007); Traub et al. (1996a). Models without gap junctions were able to generate gamma-band oscillations, although they were not used to test whether gap junctions had an effect in these rhythms. In contrast, models with gap junctions predicted that gap junctions help synchronize cells, and may be required for normal generation of gamma oscillations LeBeau et al. (2003).

Our recordings of gamma oscillations were in layer 4 of somatosensory cortex, which is predominantly made up of the inhibitory fast-spiking (FS) cell marked by the calcium binding protein parvalbumin, the inhibitory low-threshold spiking (LTS) cell marked by the neuropeptide somatostatin, and excitatory cells Rudy et al. (2010). FS cells are thought to be essential for gamma oscillations Cardin et al. (2009); Traub et al. (1996b); Whittington et al. (2011), while LTS cells may play a role in theta (4-12 Hz) oscillations given their propensity for generating slower rhythms Long et al. (2005a). Most FS cells are morphologically distinct from LTS cells in that they primarily synapse on excitatory cells with baskets of synapses around the soma Rudy et al. (2010). The remaining subset of FS cells are chandelier cells, but they are of much lower density than basket cells (compare Taniguchi et al. (2013) to Chapter 2 Figure 4.1) and we are thus not modeling them. Excitatory cells, which will be denoted as regular-spiking (RS), make up 80-85% of somatosensory cortex layer 4, while the remaining cells are 50% FS cells, 35% LTS cells, and 15% of a mixed group of cells marked by the serotonin receptor 5HT3aR Rudy et al. (2010).

With our model, we suggested that LTS cell synapses play a minimal role in FS-cell generated gamma oscillations. However, we identified a difference between the model's predictions and the slice recordings that suggests that the decreased resistance of RS cells in the Cx36 knockout animal may be a part of a homeostatic mechanism to compensate for the loss of gap junctions.

4.3 Experimental Procedures

4.3.1 General modeling methods

Simulations were performed using the NEURON simulation environment Carnevale and Hines (2006) with the implicit Euler integration method, a time step $\delta = 0.025$, and the temperature set at 30°C for the temperature-dependent sodium channel.

We modified LTS and FS cells from the model of Vierling-Claassen et al. (2010) in order to improve the AHP shapes, such that they might be more realistically passed through simulated gap junctions. We combined these updated cells with the original excitatory cell model in a network of a 500 μm by 500 μm region of tissue. Both inhibitory cell networks had optional gap junctions with probabilities based on paired recordings and filled cells. The connections between cell types were derived from experimental slice data. This network produces strong 20-80 Hz oscillations. We further refined the model to represent the synaptic noise found in a slice and to have connection strengths and shapes similar to those measured in slice.

Connection strengths measured in slices of somatosensory cortex vary by up to a factor of four Avermann et al. (2012); Beierlein et al. (2003); Deans et al. (2001). We modeled a network of the minimal and maximal connection strengths and found that a network modeled on the distance dependence and connection strengths of Avermann et al. (2012) generated oscillations dependent primarily on LTS cells, while a network modeled on the connection strengths of Beierlein et al. (2003) yielded oscillations dependent primarily on FS cells. In so doing, we demonstrated that the optogenetic model of gamma oscillations preferentially activates only a single network of inhibitory cells.

4.3.2 Cells were optimized for AHP shape

RS cell

Our excitatory cell is unchanged from that of Vierling-Claassen et al. (2010), which in turn is based on a minimal model designed by systematically reducing compartments while testing for consistent properties Bush and Sejnowski (1993) (Figure 4.1B). Currents in the cell were created by Mainen and Sejnowski (1996), who in turn derived them from measurements by Huguenard et al. (1988) and Hamill et al. (1991) (Figure 4.1C,D). Mature excitatory cells are

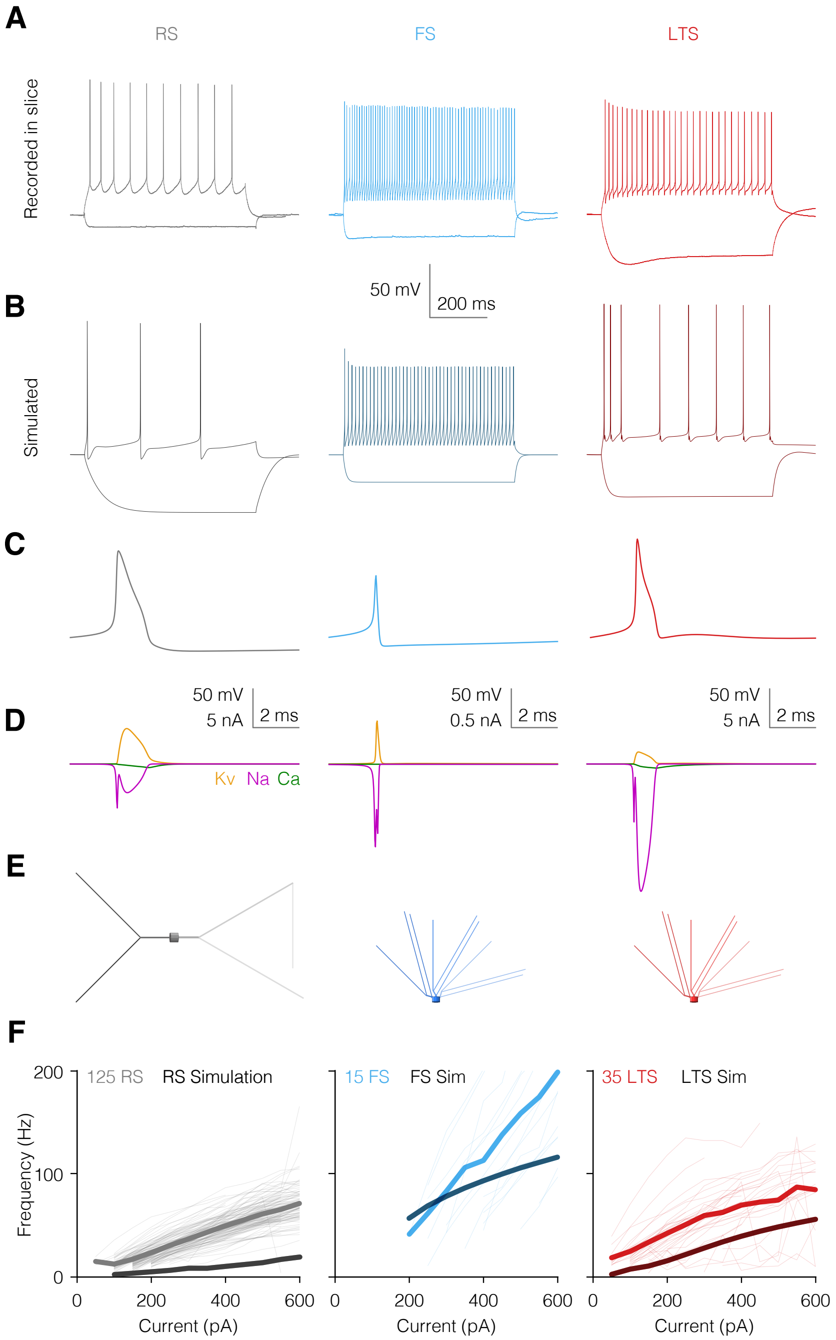

Figure 4.1: Modeled cell characteristics of isolated cells. (A) Slice recordings of an RS, FS, and LTS cell hyperpolarized by -150 pA and depolarized by 200, 300, and 150 pA of current, respectively. (B) Simulation of each cell type with matching parameters. Simulated cells were tuned for AHP shape rather than spike height. (C) Expanded single spike of each cell type. (D) Dominant currents during the simulation of the depolarization and repolarization phases of the action potential. (E) Diagram of the simulated cell drawn to scale. The apical trunk (right of soma) of the RS cell is 35 μm. (F) The frequency-current curve shows that our model cells are similar to real cells, although with lower spiking rates than average. Number (125, 15, 35) refers to the number of recorded cells of each type.

not coupled by gap junctions, and thus their spike shapes should not affect our results. Most important to us was that the cell could be a part of a network that could generate strong oscillations Vierling-Claassen et al. (2010) and that its resistance matched previous measurements. The cell has a resistance of 178 MΩ, which is in close agreement with previous reports Deans et al. (2001).

This cell contains only eight compartments, but the compartments are long, which aids in differentiating input from FS basket cells to the soma and other inputs to the dendrites (Figure 4.1E).

One factor clearly differentiates the modeled RS cell from one in a slice: the frequency-current (FI) curve of the simulated cell shows that its spike rates are lower than those recorded in slice (N=125 recorded cells, Figure 4.1F). The sodium channel we used is dominant in the modeling field (e.g. Bahl et al. (2012); Kampa and Stuart (2006); McCormick et al. (2007); Yu et al. (2008)), having been fit carefully to real data Mainen and Sejnowski (1996). Because of its fitting, we cannot simply modify the m and h gates, although it appears in the RS cell that the activation gate m opens at too hyperpolarized a threshold and the inactivation gate has too long of a tau (Figure 4.2). Two other sodium channels broadened the spikes unreasonably and were discarded. Without a better experimentally justified sodium channel, we chose to have lower FI curves for all cell types and to expect gamma oscillations at slightly lower frequencies. We defined gamma oscillations within 20-80 Hz, as is done in vivo Cardin et al. (2009) and was done in previous models using the same channels Vierling-Claassen et al. (2010).

FS cell

The FS cell is adapted from Vierling-Claassen et al. (2010), which in turn is based on the morphology of the aspiny cell described in Mainen and Sejnowski (1996). To this cell, we replaced the sodium channel with one created specifically for fast spiking cells by Golomb

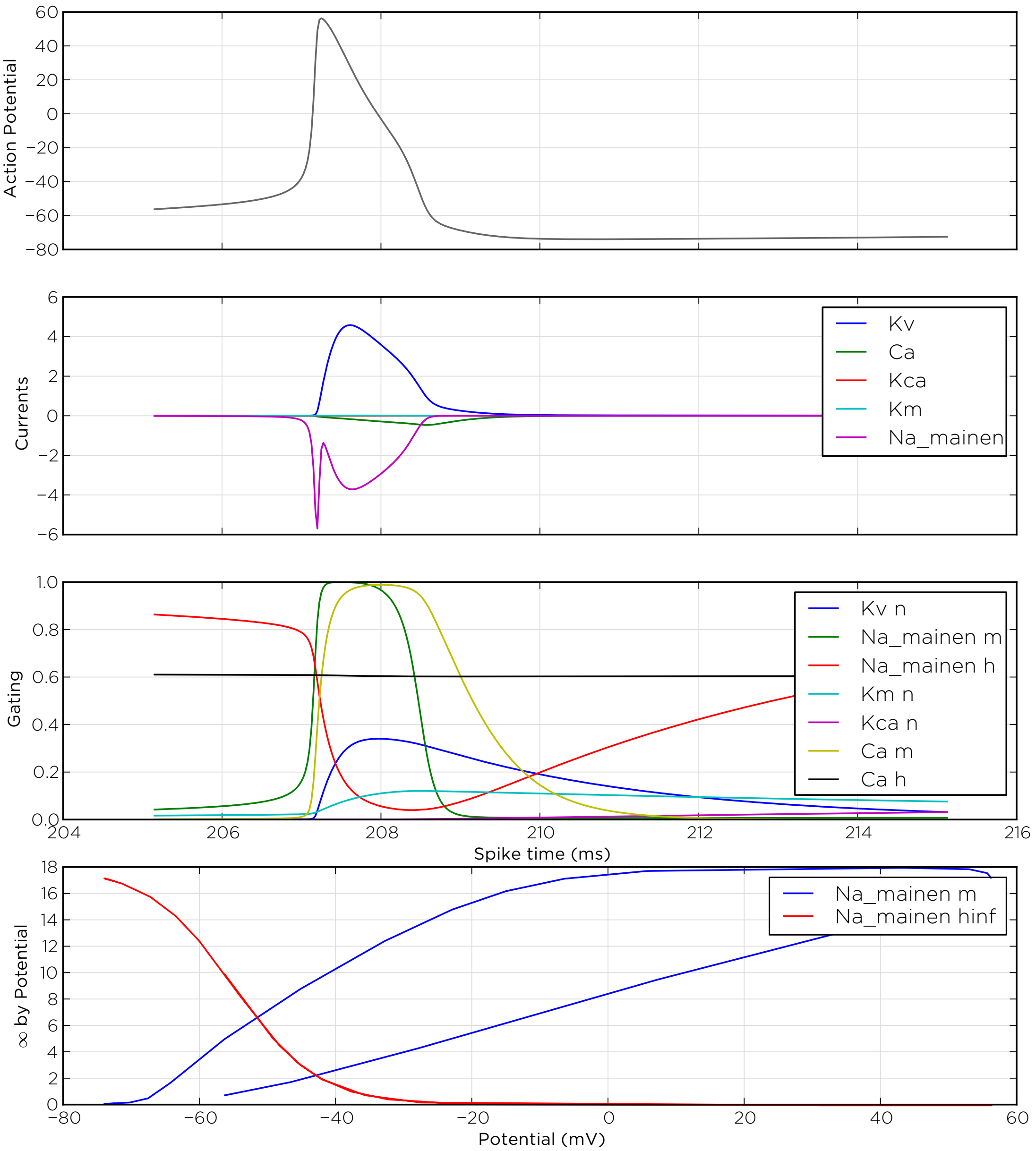

Figure 4.2: Currents and gates during an action potential of the modeled RS cell. From top, action potential, major currents during the action potential, major gates during the action potential, m_∞ and h_∞.

et al. (2007) and added a Kv3 channel created for globus pallidus neurons Günay et al. (2008). Kv3.1 channels are known to play a role in fast spiking Chow et al. (1999), and including this channel narrowed the spike significantly (Figure 4.1B,C). Key to this benefit was a low level of activation of the Kv3 channel at the resting potential of the cell. We modified sodium channel expression to be consistent throughout the cell. The narrow action potential (Figure 4.1D) was not possible to generate given the sodium channel included in Vierling-Claassen et al.

(2010), so these changes have dramatically improved the AHP shapes of our FS cells (Figure 4.1B,C).

As in the RS cell, we did not replicate the 200 Hz firing rates with 600 pA of current injection that we measured in recorded FS cells (FS cell in Figure 4.1F). Instead, we tried to match the relative FI curve between each of the cell types. As determined by the spike-frequency adaptation, spike-height adaptation, spike-width, and resistance (Figure 4.1B), our model cell is similar to an FS cell in a slice. The simulated cell has a resistance of 173 MΩ outside of a network, which is reduced by 55% when in a gap-junction coupled network to 77 MΩ, similar to previous measurements Deans et al. (2001).

LTS cell

The LTS cell has been similarly adapted from Vierling-Claassen et al. (2010). Its morphology is identical to that of the FS cell, except that its axon projects to different parts of the RS cell. Here, we added the Kv3 channel, in this case to replicate Kv3.2 channels in somatostatin-positive cells Chow et al. (1999). Its inclusion formed the AHP with multiple inflection points specific to LTS cells. The resistance is 281 MΩ outside of a network and drops by 55% in a gap-junction coupled network, exactly the same as the FS cells, to 126 MΩ matching previous reports Deans et al. (2001).

The conductances and other parameters of each of the channels in the cells is described in Table 1. The entire model and its cells have been made available at `https://bitbucket.org/asugden/l23-network`.

Table 4.1: Intrinsic parameters for the three cells. Citations are 1. Mainen and Sejnowski (1996) 2. Golomb et al. (2007) 3. Günay et al. (2008) 4. Traub et al. (2003)

	RS		FS		LTS	
	Soma	Dendrites	Soma	Dendrites	Soma	Dendrites
$\bar{g}_{Na}$ [1] (pS/μm^2)	5000	5000			7000	7000
$\bar{g}_{Na}$ [2] (pS/μm^2)			0.7	0.7		
$\bar{g}_{Kv}$ [1] (pS/μm^2)	800	800	1500	400	350	350
$\bar{g}_{Kv3}$ [3] (pS/μm^2)			100,000	30,000	3000	3000
$\bar{g}_{Leak}$ (pS/μm^2)	0.4	0.4	1.2	1.2	0.7	0.7
$\bar{g}_{Ca}$ [1] (pS/μm^2)	40	30			30	30
$\bar{g}_{KCa}$[1] (pS/μm^2)	40	20			8	8
$\bar{g}_{M}$ [1] (pS/μm^2)	10	10				
$\bar{g}_{T}$ [4] (pS/μm^2)					2	2
$\bar{g}_{h}$ [4] (pS/μm^2)					0.01	0.01
E_{Na} (mV)	60				75	
E_K (mV)	-75		-65		-60	
E_{Leak} (mV)	-65		-73		-74	
$\tau_{r,Ca}$ (ms)	100				200	
$vshift_{Na}$ (mV)	-10				-18	

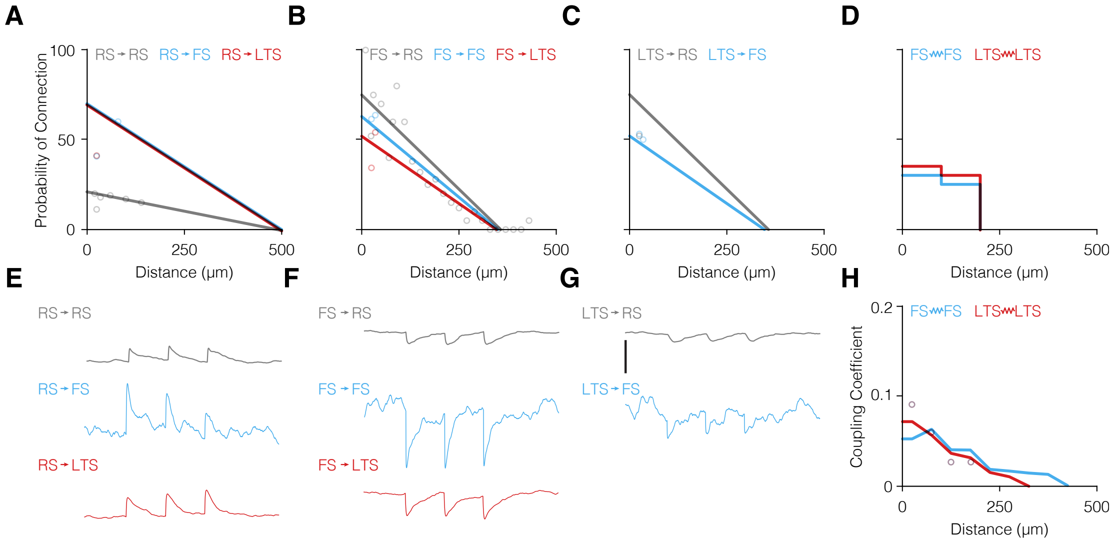

Figure 4.3: Chemical and electrical connection probabilities for the network. Lines are equations from which we compute connection probabilities. Dots are data from previous work. (A) Connection probabilities from RS cells. Connections to FS and LTS cells overlap. Data points from Avermann et al. (2012); Gibson et al. (1999); Lefort et al. (2009). (B) Connection probabilities from FS cells. Data points from Avermann et al. (2012); Deans et al. (2001); Gibson et al. (1999); Packer and Yuste (2011). (C) Connection probabilities from LTS cells. Deans et al. (2001); Gibson et al. (1999). (D) Connection probabilities for gap junctions are fit to coupling coefficients in H. (E-G) 3 PSPs delivered at 10 Hz, displayed at the average size for each connection type. (G) LTS cells do not connect to other LTS cells in mice in Deans et al. (2001). (H) Average coupling conductance by distance for pairs of cells with measurable conductances (above 0.01). Data points from Amitai et al. (2002).

4.3.3 Connection probabilities were derived from experiments

Chemical connections

Available data on chemical connection probabilities are both inconsistent and rarely summarize all possible chemical connections between RS, FS, and LTS cells. We assembled measurements from five groups that had consistent results: Gibson et al. (1999), Deans et al. (2001), Lefort et al. (2009), Packer and Yuste (2011), and Avermann et al. (2012). These parameters measuring chemical connections may be different between cortical regions; measurements made in primary visual cortex gave substantially different connection probabilities Pfeffer et al. (2013). When data were limited or missing, we assumed that excitatory cell connections had the same maximal distance of 500 μm based on distance-dependent data out to 150 μm from Avermann et al. (2012) (Figure 4.3A). Similarly, inhibitory cells all project no further than 350 μm, based on extensive distance-dependent measurements of FS to RS chemical connections performed by Packer and Yuste (2011) (Figure 4.3B, C). We set the probabilities of RS-to-FS and RS-to-LTS connections to be equal and have done the same for FS-to-RS and LTS-to-RS connections, and for FS-to-LTS and LTS-to-FS connections. To better match the dynamics previously found in slices, RS-to-FS connections are depressing, while RS-to-LTS connections are facilitating Beierlein et al. (2003). Although other connection types have short-term dynamics, they are less consistent than RS-to-inhibitory connections. Therefore, we set the remaining connection types to be constant.

The chemical synapses (Figure 4.3E-G) were adapted from Vierling-Claassen et al. (2010). First, the 20-80% rise times of both EPSPs and IPSPs were sped up dramatically, such that they better matched data from measures of paired cells (Table 1) Avermann et al. (2012); Beierlein et al. (2003); Deans et al. (2001). To match measurements of IPSP rise times, we had to create two different $\mathrm{GABA_A}$ receptors, one for excitatory cells and a second for inhibitory cells. However, by using only one receptor for all inhibitory cells, we had to optimize the fit to real data between both FS and LTS cells. In improving the rise time of all PSPs, we also improved the half-width of PSPs so that they better matched real recordings.

Next, after the receptor profiles were set, we adjusted synaptic strengths such that they matched those measured in slice by two different groups (Table 1). Those based on Avermann et al. (2012) are denoted L for the low-strength network, while those connections based on the work of Beierlein et al. (2003) and Deans et al. (2001) are denoted H for being higher in strength. PSP amplitudes measured by the two groups were sufficiently different that we separately simulated both networks.

To limit the degrees of freedom within the simulation, each connection has a fixed strength. However, we inject modeled synaptic noise into each compartment as a stochastic Ornstein-Uhlenbeck process, exactly as was used previously Vierling-Claassen et al. (2010). This process can be imagined as a random walk of a dog on an elastic leash tethered to a position zero. Because those simulations were designed to reproduce in vivo-like conditions and ours simulate brain slices in a traditional artificial cerebrospinal fluid, we decreased the strength of the noise such that RS and LTS cells have only subtle input, while FS cells have substantial noise.

Table 4.2: Average chemical connection strengths of a weak-connection and strong-connection network. References are 1. Avermann et al. (2012) 2. Beierlein et al. (2003) 3. Deans et al. (2001)

		From RS Sim/Literature	FS Sim/Literature	LTS Sim/Literature
To RS	Amplitude$_L$ (mV)	0.38/0.37 ^{1}	-0.55/-0.52 ^{1}	-0.50/-0.49 ^{1}
	Amplitude$_H$ (mV)	1.23/1.10 ^{2}	-1.05/-1.10 ^{2}	-0.48/ ^{2}
	Rise time (ms)	1.18/0.88 ^{2}	1.30/1.50 ^{2}	3.19/2.10 ^{2}
	Half-width (ms)	16.2/12.3 ^{2}	21.8/24.0 ^{2}	24.4/22.6 ^{2}
To FS	Amplitude$_L$ (mV)	0.84/0.82 ^{1}	-0.51/-0.56 ^{1}	-0.33/-0.37 ^{1}
	Amplitude$_H$ (mV)	2.00/2.20 ^{2}	-1.72/-1.75 ^{3})	-1.05/-1.00 ^{3}
	Rise time (ms)	0.34/0.37 ^{2}	0.45	0.42
	Half-width (ms)	7.3/4.9 ^{2}	7.8	7.8
To LTS	Amplitude$_L$ (mV)	0.31/0.39 ^{1}	-0.90/-0.83 ^{1}	
	Amplitude$_H$ (mV)	0.31/0.30 ^{2}	-1.85/-1.75 ^{3}	
	Rise time (ms)	0.89/0.86 ^{2}	0.75	
	Half-width (ms)	15.5/8.9 ^{2}	14.0	

Electrical connections

Determining the connection parameters of gap junctions is more difficult than the chemical connections because the measurement of a pair of electrically coupled neurons can include both direct connections and indirect connections through the network. Thankfully, previous work has estimated the total number of connected cells via careful measurements of the density of inhibitory cells combined with the probability of electrical connections Amitai et al. (2002). These estimates suggest that cells are measurably (coupling coefficient greater than

0.01) coupled to between 22 and 51 other cells, with direct connections to between only 5 and 25 direct connections.

We connected only nearby cells (Figure 4.3D), given that dye filling shows the majority of coupling between cells to be in proximal dendrites Fukuda (2007). For FS cells, 30% of like-type interneurons within a radius of 100 μm were coupled with a strength of 2 nS, within the range of direct connections predicted previously Amitai et al. (2002). 25% of cells between 100 μm and 200 μm were coupled at a strength of 1.5 nS. This led to an average of 12.6 connections for FS cells, well within the range of 5-25 described above. These values produced an excellent fit to distance-dependent measurements of coupling conductances (Figure 4.3H).

LTS cells were electrically coupled at a rate of 35% out to a radius of 100 μm with a strength of 1.0 nS and coupled at a rate of 30% out to a radius of 200 μm with a strength of 0.5 nS. This generated a very similar match to previous data on coupling conductances (Figure 4.3H) and yielded 15 average gap junctions per cell.

With these distance-dependent connection probabilities, we generated a two-dimensional model of 27×27 RS cells, 9×9 FS cells, and 9×9 LTS cells, all centered on the same point. Inhibitory cells are spaced by 50 μm, while excitatory cells lie 18 μm apart. Because the connections are probabilistic, there is no need to randomize the spacing.

To avoid outliers in both chemical and electrical connection probabilities, we constrained the numbers of chemical and electrical connections to be fixed across simulations.

Randomness has been carefully inserted into the network. All randomness depends on a single seed number assigned to the program at its start. Each connection type, chemical and electrical, derives a new seed number from the original one such that the exact same network can be generated in multiple runs, except for differences selected by the user. In this way, we can test the effects of gap junctions in a network without disrupting the chemical connections.

Optogenetic stimulation

Gamma oscillations can be generated in slice by ramping light over a region with the excitatory cells preferentially expressing channelrhodopsin Adesnik and Scanziani (2010). Peak gamma powers in barrel cortex increased until an inflection point, at which point they roughly flattened off (Chapter 3 Figure 3C). This point corresponds to about 0.18 mW of light. The mean photocurrent at the minimal optogenetic stimulus intensity (0.004 mW) was 27.5 pA. Combining the two, the optogenetically-induced photocurrents at the optimal light power are roughly 1200 pA.

During our simulated ramp, we injected a random current rising to 1200 ± 800 pA into our excitatory cell network. This random current was then linearly scaled by distance. Although each cell in the simulated network received a random current, each individual cell received the same current across successive simulations. Our optogenetic stimulation in vitro passes through a high-power objective with a field-of-view of roughly 150 μm and spreads beyond this field of view (data not shown) Thus, we modeled the light spread as approaching zero at a distance of 250 μm from the recorded cell, with all negative values set to 0. The simulated optogenetic ramp created maximally strong gamma oscillations in the middle of the ramp, rather than at the beginning or end, confirming our selection of photocurrents.

In experimental measurements of the optogenetic ramp, it was determined that the virus used to infect excitatory cells also yielded substantial expression in inhibitory cells (Chapter 3). To simulate this, we injected 300 ± 800 pA into the inhibitory cell network, again linearly scaled by distance. This yielded strong oscillations in the synaptic events onto an RS cell (Figure 4.4).

In the case of the ramp with preferential drive to inhibitory cells, we injected a random current of 600 ± 800 pA into each excitatory cell, which was linearly scaled by distance as above. Into the inhibitory cells we injected 1200 ± 800 pA, linearly scaled by distance.

Finally, we included the decreased resistance of RS cells that we measured in animals in which Cx36 had been knocked out (Chapter 3). Here too, we have conflicting results. There have been no reported changes to the amplitudes of IPSPs onto RS cells in the Cx36 knockout animal. However, in visual cortex, miniature and evoked IPSCs onto undetermined targets were not significantly different between wild-type and knockout animals Postma et al. (2011). Given the differences in synaptic connections between visual and somatosensory cortices, we will focus only on recordings from somatosensory cortex. We increased the currents associated with each synapse such that it generated an equal-amplitude PSP onto an RS cell. This was as simple as scaling the currents recorded from the voltage-clamped RS cell. RS cells in the wild-type animal had an average resistance of 248 MΩ, while those in the Cx36 knockout animal had an average resistance of 197 MΩ, yielding a scale factor of 1.26 of the currents in the network without gap junctions.

4.4 Results

4.4.1 Low connection strengths generate LTS-dependent oscillations

One of the benefits of modeling our network is that we can selectively remove gap junctions without disrupting the drive to any cell in addition to leaving its chemical synapses as they were. Therefore, we can precisely determine the role of gap junctions in the model. A second benefit is that we can record from every cell in the model simultaneously. We voltage clamped the central RS cell at -40 mV so that the data could best be compared with Chapter 3. The

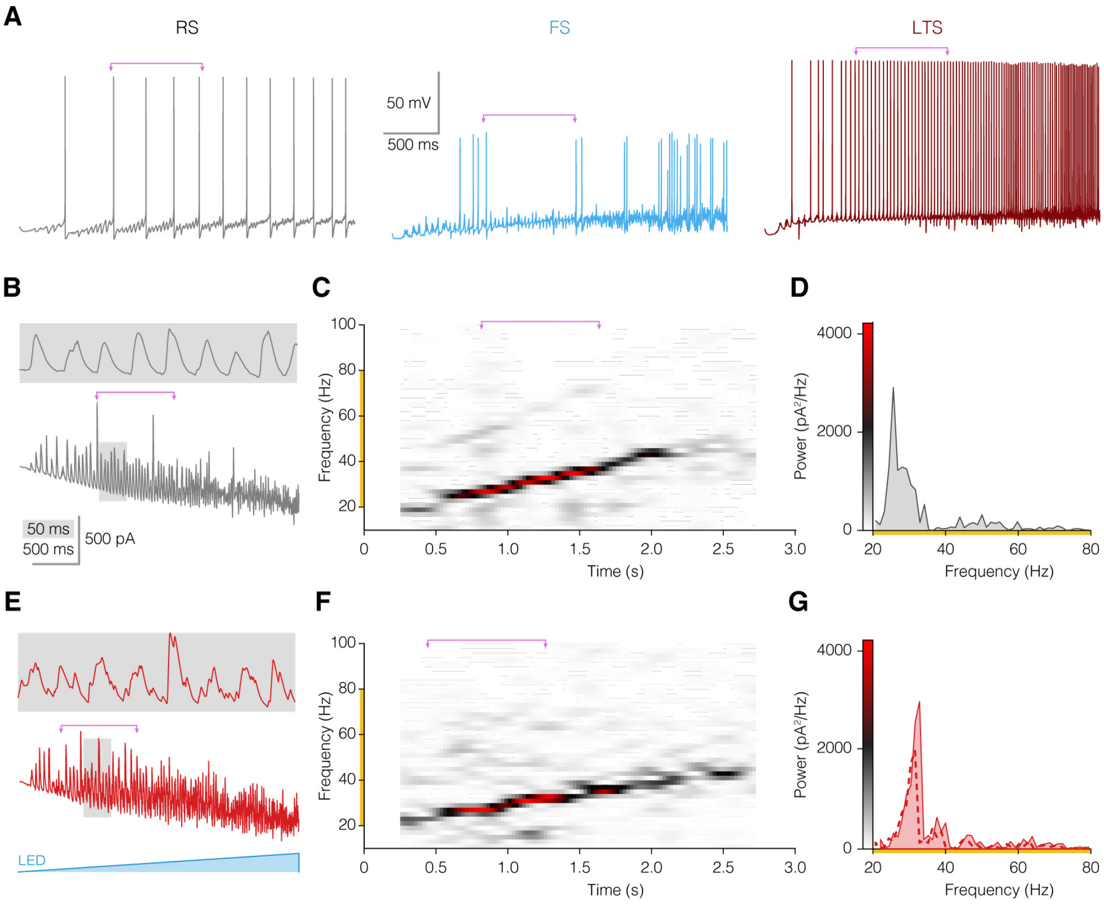

Figure 4.4: Simulation of optogenetic ramp with low connection strengths with and without gap junctions. Magenta arrows mark the region of strongest integrated gamma band power (20-80 Hz). (A) Example traces of an RS, FS, and LTS during the ramp with gap junctions. The selected FS cell was that which spiked most. (B) Example trace of the central RS cell voltage-clamped at -40 mV with a ten-fold zoom inset. (C) Spectrogram of the trace from B. Powers are shown along Y-axis of D. (D) Power spectrum of the strongest 819 ms marked in magenta in A-C. (E) Example trace from the identical network except that it lacks gap junctions. (F) Spectrogram of E. Powers are shown along Y-axis of G. (G) Power spectrum of magenta from F. The dotted line is the spectrum without including the lower resistance of RS cells.

remaining cells were current clamped so that we did not disrupt their firing.

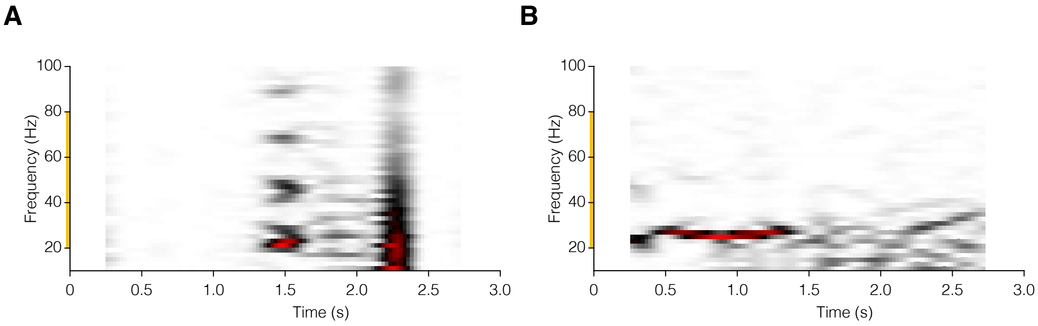

Figure 4.5: Removal of LTS cells completely eliminates gamma oscillations in the low-amplitude connection model. (A) Example trace from low-amplitude model without LTS cells. The broadband noise is a small number of IPSCs from FS cells. (B) Example trace from high-amplitude model without LTS cells. Gamma oscillations remain.

A simulated optogenetic ramp with Model L, made up of the low connection strengths described above, generated oscillations in the low gamma-band range (20-40 Hz, Figure 4.4). The ramp elicited spiking from RS cells and LTS cells, but failed to generate significant activity in the FS cells (Figure 4.1A). During the time with the strongest gamma-band power, marked in magenta (Figure 4.4), only 27/81 FS cells spiked more than twice. In addition, selective removal of LTS cells completely abolished gamma-band activity (Figure 4.5).

The central voltage clamped RS cell showed strong, rhythmic, primarily inhibitory currents (Figure 4.4B). A spectrogram of the PSCs showed that the frequency of the oscillations was proportional to the instantaneous amplitude of the stimulus as it ramped up (Figure 4.4C). This result was inconsistent with slice experiments where frequency remained constant at the optimal stimulus intensity (Chapter 3 Figure 1D). Peak powers were similar to those we found in slices (Figure 4.4D, Chapter 3 Figure 1C).

When we selectively eliminated gap junctions from the model, we found remarkably few differences. The inhibitory waveform showed slightly more high-frequency events without gap junctions (Figure 4.4E), but otherwise was similar. The spectrogram showed the same stimulus intensity-frequency relationship (Figure 4.4F) and the resulting power was similar (Figure 4.4G). However, this was entirely dependent on modeling the decreased resistance of RS cells, and thus the stronger synaptic currents onto them.

4.4.2 High connection strengths generate FS-dependent oscillations

In work done by Cardin et al. (2009); Wang and Buzsáki (1996); Whittington et al. (2011), it is FS cells, not LTS cells, that generate gamma-band oscillations. In order to try to model those predictions, we matched the synaptic strengths to results from Beierlein et al. (2003) and Deans et al. (2001). We used the identical protocol described above, including identical

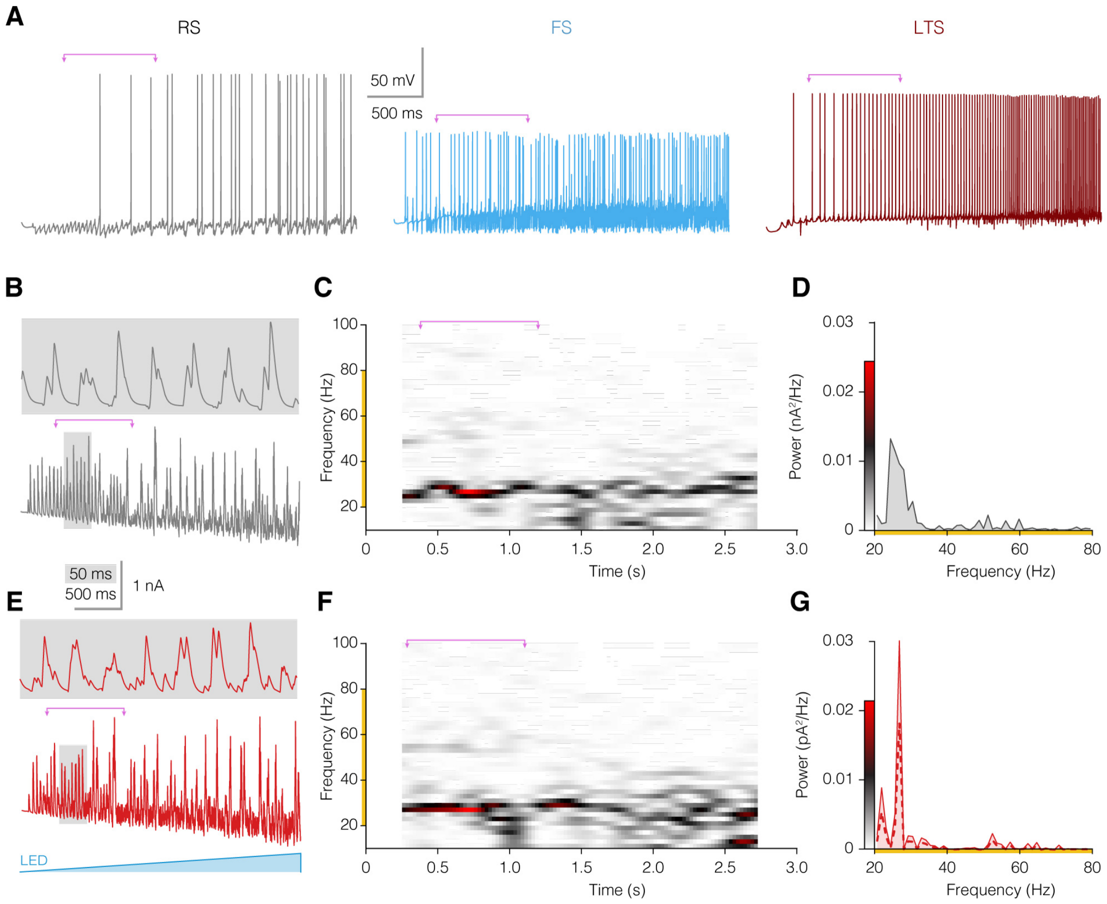

Figure 4.6: Simulation of optogenetic ramp with high connection strengths with and without gap junctions. Magenta arrows mark the region of strongest integrated gamma band power (20-80 Hz). (A) Example traces of an RS, FS, and LTS during the ramp with gap junctions. (B) Example trace of the central RS cell voltage-clamped at -40 mV with a ten-fold zoom inset. (C) Spectrogram of the trace from B. Powers are shown along Y-axis of D. (D) Power spectrum of the strongest 819 ms marked in magenta in A-C. (E) Example trace from the identical network except that it lacks gap junctions. (F) Spectrogram of E. Powers are shown along Y-axis of G. (G) Power spectrum of magenta from F. The dotted line is the spectrum without including the lower resistance of RS cells.

optogenetic drive to each of the cells. In Model H, we changed only the strengths of chemical synapses to those of the high-amplitude network in Table 1.

In contrast to the low-amplitude network, Model L, described in the previous section, this simulation generated FS-dependent gamma oscillations (Figure 4.6). RS cells received rhythmic input primarily from FS cells during the peak period of the gamma oscillations (Figure 4.6A). LTS cells spiked during this period, but their selective elimination did not affect the oscillations (Figure 4.5).

During the optogenetic ramp, FS cells entrained RS cells into gamma-band oscillations until the stimulus became sufficiently strong that the rhythmicity was eliminated (Figure 4.6B-D). In this model, there no longer was a stimulus amplitude-frequency relationship, which matches the in vitro data significantly better.

The selective elimination of gap junctions from the model yielded results that were remarkably similar to those above. Again there was subtly increased high-frequency input visible in the spectrum modeling the knockout of Cx36 (Figure 4.6E). The spectrogram and power spectrum were quite similar to the model that included gap junctions (Figure 4.6D,F,G).

The rhythmic oscillations produced in the model hovered near 20 Hz. The stimulus intensities we calculated to produce 1200 pA of photocurrent in slices generated peak frequencies of roughly 42 Hz (Chapter 3 Figure 3G). Low stimulus intensities generated low-frequency oscillations in our slice experiments, although at maximum powers the frequency regularly increased to 50-60 Hz (Chapter 3). The low frequency of oscillations in our model was a direct result of the low FI curves of each of our modeled cells. At 200 pA above rheobase, the modeled RS cell spiked at roughly one third the rate of recorded RS cells (8 Hz and 30 Hz, respectively), the modeled FS cell spiked at 85% of the recorded rate (92 Hz and 110 Hz, respectively), and the LTS cell spiked at half of the rate (25 Hz and 50 Hz, respectively, Figure 4.1F). Taking these decreased firing rates into account, the model replicated well the optogenetic ramps from slices.

Next, we confirmed that the model required preferential optogenetic stimulation of excitatory cells. To test this, we drove the optogenetic ramp with a two-fold higher mean optogenetic stimulus in inhibitory cells than in excitatory cells. Excitatory cells were driven with a peak of 600 ± 800 pA of current, decreased by distance, while inhibitory cells received a peak of 1200 ± 800 pA of current. This replicated our results in slices; strong inhibitory drive eliminated rhythmic oscillations (Figure 4.7).

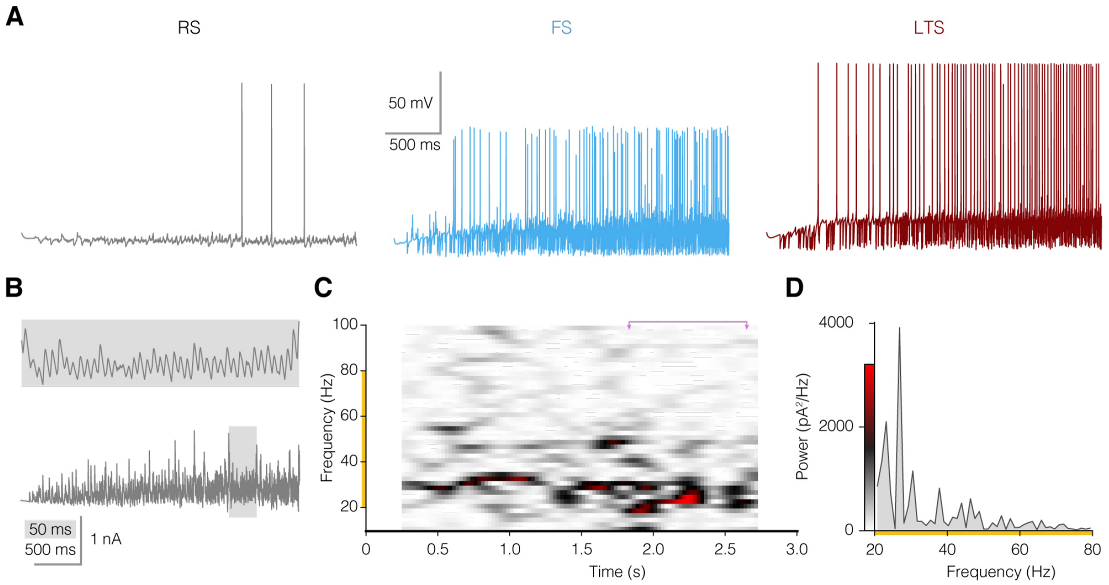

Figure 4.7: Simulation of optogenetic ramp with high connection strengths and strong inhibitory drive with and without gap junctions. Magenta arrows mark the region of strongest integrated gamma band power (20-80 Hz). (A) Example traces of an RS, FS, and LTS during the ramp with gap junctions. (B) Example trace of the central RS cell voltage-clamped at -40 mV with a ten-fold zoom inset. (C) Spectrogram of the trace from B. Powers are shown along Y-axis of D. (D) Power spectrum of the strongest 819 ms marked in magenta in C.

Although cells spiked as before (Figure 4.7A), they did not form into a primarily inhibitory gamma mechanism. IPSCs onto the RS cell no longer came in waves (Figure 4.7B) and the result was an arrhythmic noise (Figure 4.7C,D).

4.4.3 LTS cells do not play a role in high connection strength gamma oscillations

Recordings of gamma oscillations in hippocampus in vivo found decreases in gamma-band power in a Cx36KO only when the animal was active, and then primarily during one phase of theta oscillations Buhl et al. (2003). LTS and FS cells also form reciprocally inhibitory networks that could be synchronized by gap junctions. From this, we hypothesized that gap junctions may become more important either when LTS cells are silent, or when LTS cells are active at a competing frequency.

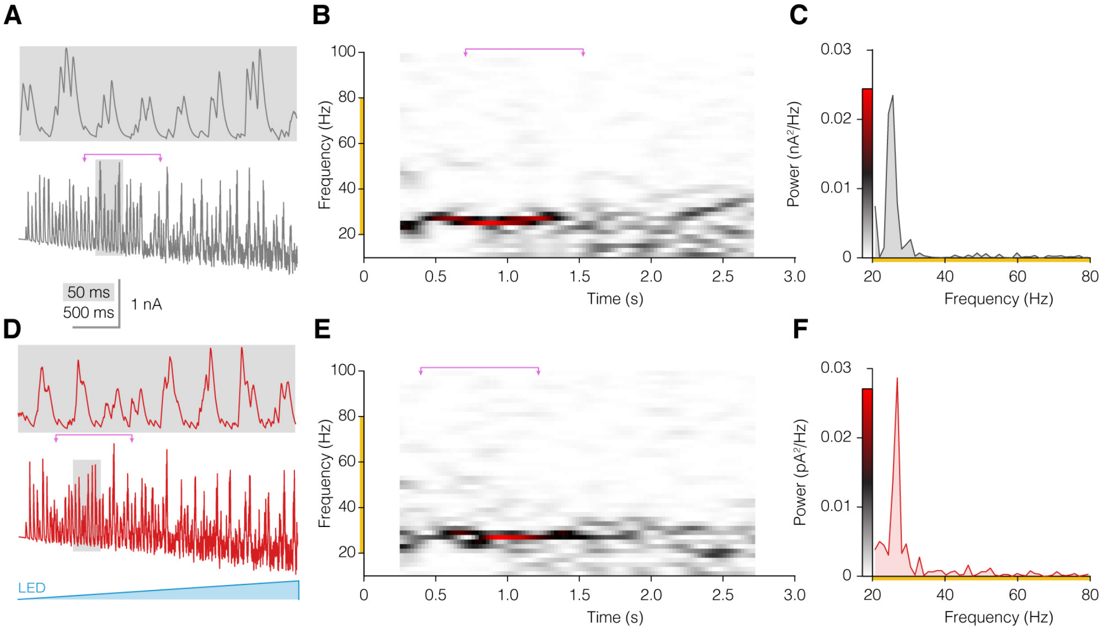

Figure 4.8: Simulation of optogenetic ramp with high connection strengths, without LTS cells, and with and without gap junctions. Magenta arrows mark the region of strongest integrated gamma band power (20-80 Hz). (A) Example trace of the central RS cell in an LTS-free network voltage-clamped at -40 mV with a ten-fold zoom inset. (B) Spectrogram of the trace from B. Powers are shown along Y-axis of C. (C) Power spectrum of the strongest 819 ms marked in magenta in A-B. (D) Example trace from the identical LTS-free network except that it lacks gap junctions. (E) Spectrogram of D. Powers are shown along Y-axis of F. (F) Power spectrum of magenta from E.

First, we selectively eliminated the LTS cell population from our high connection strength model. Once again, this network was identical to that shown above (Figure 4.6), except that it lacked LTS cells. Current clamp traces looked similar to those of Figure 4.4.

The elimination of LTS cells from the network did not alter the gamma oscillations (Figure 4.8). The peak powers, frequencies, and lengths of the gamma bouts were nearly indistinguishable from those measured in the network containing LTS cells. Therefore, the spiking of LTS cells plays a minimal role in the gamma oscillations of this network. This result is in stark contrast to the low connection strength network, which largely depended on LTS cells to generate the oscillations.

Finally, we drove all of the LTS cells with a simultaneous wave of 8 Hz, with a maximum of 150 pA of injected current and a minimum of -150 pA. This led to the generation of two simultaneous rhythms in the currents of the central excitatory cell (Figure 4.9).

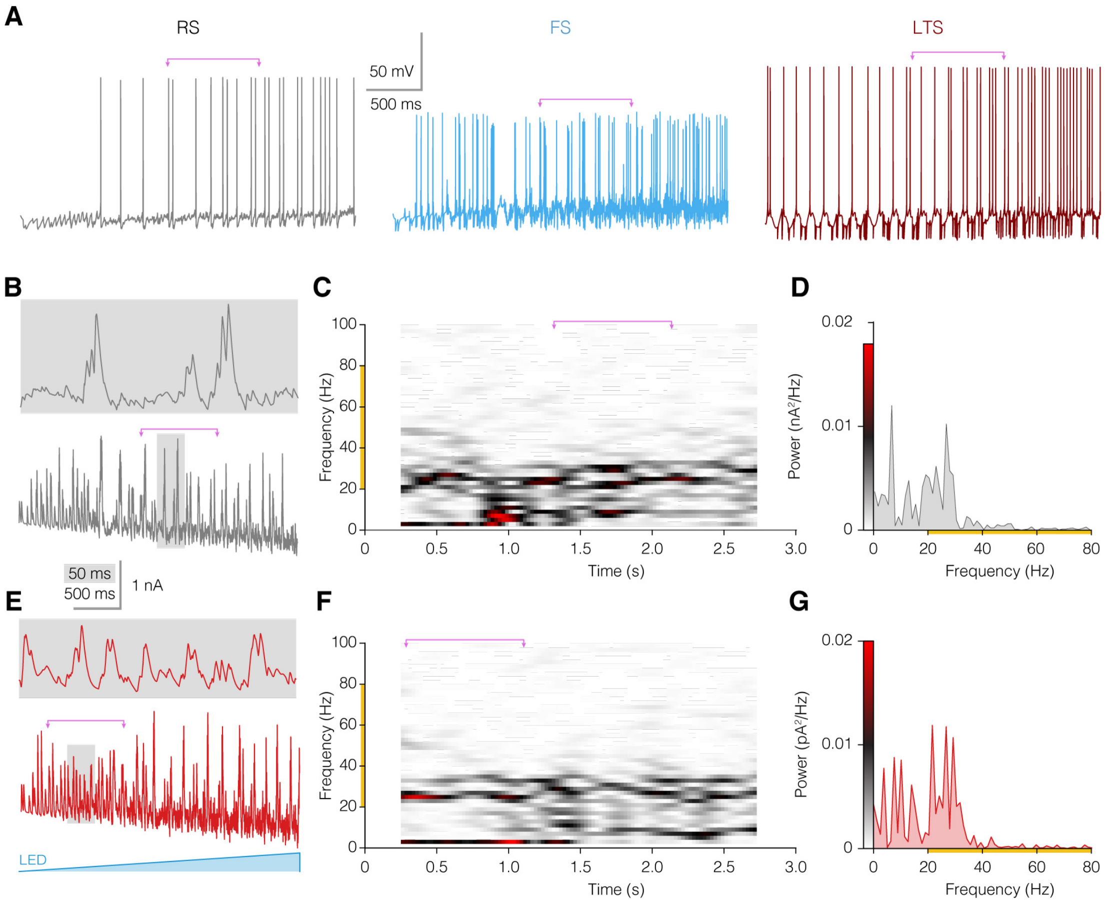

Figure 4.9: Simulation of optogenetic ramp with high connection strengths, with LTS cells being driven with theta oscillations, and with and without gap junctions. Magenta arrows mark the region of strongest integrated gamma band power (20-80 Hz). (A) Example traces of an RS, FS, and LTS during the ramp with gap junctions and theta oscillations. (B) Example trace of the central RS cell voltage-clamped at -40 mV with a ten-fold zoom inset. (C) Spectrogram of the trace from B. Powers are shown along Y-axis of D. (D) Power spectrum of the strongest 819 ms marked in magenta in B-C. (E) Example trace from the identical network except that it lacks gap junctions. (F) Spectrogram of E. Powers are shown along Y-axis of G. (G) Power spectrum of magenta from F.

The spiking patterns of RS cells appear similar to those of Model H without theta oscillations (Figure 4.9A, Figure 4.6A). FS cells had periods of hyperpolarization, driven by spiking from LTS cells, sufficient to prevent them from firing. LTS cells fired one or two action potentials at the peak of each theta wave. Although not immediately visible in the voltage clamped trace (Figure 4.9B), the LTS and FS cells were generating two separate rhythms (Figure 4.9C,D). One was at 8 Hz, visible after 1.5 s, and the other was between 22-30 Hz. Although the LTS cells were driven sinusoidally throughout the ramp, their rhythm only becomes visible with greater excitation from excitatory cells (Figure 4.9C).

The peak power was spread across a wider range of frequencies than for the simulations without theta, but the peak power decreased only by a factor of two.

Contrary to what we expected, these competing rhythms did not push the generation of gamma oscillations into a regime in which they required gap junctions. The simulation in which gap junctions had been removed generated remarkably similar results to that in which gap junctions were present (Figure 4.9E-G). Gamma oscillations were generated across the entire ramp both with and without gap junctions (Figure 4.9C,F) and the peak powers were similar (Figure 4.9D,G). This suggests that competing rhythms from LTS cells do not significantly affect the dependence on gap junctions of gamma oscillations generated by FS cells in the optogenetic ramp model of gamma.

4.5 Discussion

Inherent to modeling large networks of cells lies the difficulty that not all of the parameter space can be explored. The degrees of freedom of this model lie in the hundreds and a single simulation takes two hours. Furthermore, the problem has not been constrained experimentally; we do not know the complete complement of channels in a cell, let alone their localization. Therefore, we must tune our parameters to match the most important aspects of our recorded data. Remarkably, our model generated gamma oscillations when programmed with only experimentally realistic spiking shapes, spiking patterns, connection probabilities, and connection strengths. The model further aligned with our experiments in that dominant drive to inhibitory cells destabilized the gamma oscillations such that the synchronous input became arrhythmic.

Our conclusions that gamma-band oscillations are equal in models with and without gap junctions are based entirely upon the addition of the scaling parameter for IPSC amplitudes onto RS cells. As described above, we found a statistically significant decrease in the resistance of RS cells in the Cx36 knockout animal relative to wild-type (Chapter 3). If we assume that IPSP amplitudes onto RS cells are unchanged between the Cx36 knockout animal and wild-type, then there must be a homeostatic mechanism that increases IPSC amplitudes onto RS cells. With this assumption in place, our results confirm our measurements in slices (Chapter 3); gap junctions are not required for gamma oscillations. If instead, we apply measurements from visual cortex by Postma et al. (2011) to somatosensory cortex, then there is not a change in IPSC amplitude onto excitatory cells. This in turn would suggest that without gap junctions, the peak power of gamma oscillations would decrease by one third (Figure 4.4G, Figure 4.6G).

Our simulation has some important limitations. The most important is that the FI curves do not match those recorded in vitro (Figure 4.1). Directly as a result of these decreased FI curves, the peak frequency of our gamma-band oscillations is half of that measured in vitro. The second significant limitation is that slice measurements do not sufficiently constrain our estimates of distance-dependent connections or connection strengths. The latter is borne out by our generation of LTS-dependent gamma oscillations in Model L (Figure 4.4). Finally, the model is hampered by uncertainty about the presence of homeostatic regulation of IPSP amplitudes. This could be measured via pairs of cells in a slice or measurements could be made in a temporally selective conditional knockout of Cx36, which may limit compensation. However, our model is buoyed by suggesting that gap junctions play a role in 0-30% of the peak power of gamma oscillations, which is well-within the range of previous measurements.

To address these limitations, one could create a model in which all of the parameter space can be effectively explored. With a cluster of computers and a system for exploration such as Markov Chain Monte Carlo, one can effectively explore values of nine separate parameters Majewski and Johnston (2009). Such a model would lose the benefits of modeling dendritic filtering of synaptic events, but might still be able to effectively model our optogenetic gamma oscillations.

Our simulation generated rhythmic synaptic currents of up to 1 nA during the optogenetic ramp; in contrast, our slice recordings had peak currents only half as large (Chapter 3 Figures 1,3). This discrepancy was likely due to two differences between our in vitro measurements and in silico model. First, although the FI curves of each of the three simulated cell types was lower than those measured in slice (Figure 4.1), the current-frequency relationship of the FS cell was quite similar between cells recorded in slice and the model over 200-400 pA. In the slice, at low optogenetic intensities, FS cells may have spiked rhythmically but not with every oscillation. In the simulation, it is likely that FS cells spiked on a higher percentage of oscillations. Second, all of the cells in the simulation are identical. Although the RS cells all have different photocurrents, they have identical resistances, shapes, and amplitudes of PSPs. Therefore, a shared input to two simulated RS cells might induce simultaneous spiking. In contrast, a shared input to two RS cells in vitro might make only a single cell fire, or the different dendritic currents could lead to changes in the timing of the PSP by the time it arrives at the soma.

It is surprising that the first set of experimentally derived connection strengths that we tested generated LTS-dependent gamma oscillations in Model L (Figure 4.4) rather than FS-dependent oscillations in Model H (Figure 4.6). The connection strengths between models generating LTS-dependent gamma and the FS-dependent gamma differed by no more than a factor of four, but this was sufficient to entirely change the origin of oscillations. Activation of LTS cells in slices generates oscillations of 4-12 Hz, so the high frequencies found in our model are unexpected Long et al. (2005a). However, this may be due to a combination of stronger depolarization in our gamma optogenetic model and the fact that the oscillations generated in Model L were a PING mechanism, unlike the putative ING mechanism generated via ACPD activation Long et al. (2005a).

Many previous models focused solely on the effects of a single type of inhibitory cell (implicitly or explicitly FS cells) in gamma oscillations Buzsáki and Wang (2012); LeBeau et al. (2003); Traub et al. (1997); Wang and Rinzel (1992); Whittington et al. (2011). Our model has expanded upon previous models by explicitly comparing the importance of FS and LTS cells to gamma generation. At least in the optogenetic model of gamma oscillations, the decision to focus on only a single cell type is vindicated; only one inhibitory cell network seems to contribute to gamma oscillations at a time.

Our model makes some testable hypotheses. First, that LTS cells do not play a significant role in the gamma oscillations generated during an optogenetic ramp (Figure 4.8). This is important because in vivo measurements in hippocampus demonstrate a selective decrease in the amplitude of gamma oscillations during one phase of theta oscillations Buhl et al. (2003). This suggests a possible push-pull mechanism between the FS and LTS cell networks. To test this, designer receptors exclusively activated by designer drugs (DREADDS) could be expressed specifically in LTS cells during an optogenetic ramp Rogan and Roth (2011). In this way, one could test whether LTS cells are important in optogenetically-induced gamma.

The second hypothesis is that there is homeostatic regulation of IPSP amplitude. This seems to differ from measurements from the visual cortex Postma et al. (2011), but should be tested by measuring the connection amplitudes of pairs of cells in the Cx36 knockout and wild-type animals. If one could identify compensation for the lack of gap junctions, one might better understand their roles in neocortex.

It has been posited that purely reciprocal inhibition between FS cells can generate gamma oscillations Whittington et al. (2011). The third hypothesis from our model is that inhibition from LTS cells and low levels of excitation from RS cells likely prevent ING rhythms from forming in the neocortex (Figure 4.7). Testing the origins of gamma in vivo is difficult, but by measuring PSCs in pairs of RS cells in vivo, voltage clamped alternatingly at -40 and -80 mV, one could derive the relative timing of inhibition and excitation Okun and Lampl (2008). If ePSCs consistently precede iPSCs, it is likely to be a PING-based rhythm Tiesinga and Sejnowski (2009).

All measurements of gamma oscillations in Cx36 knockout and wild-type animals agree that the absence of gap junctions decreases the gamma power by at most 50%. In vivo in hippocampus, gamma oscillations are 90% of the amplitude in the knockout animal relative to wild-type Buhl et al. (2003). In vitro in hippocampus, gamma oscillations are 50% of the amplitude in the knockout animal relative to wild-type Hormuzdi et al. (2001). In our measurements in vitro, gap junctions do not play a role in gamma oscillations in neocortex. Finally, in the simulation, the absence of gap junctions yields peak gamma powers of 70-100% of the amplitudes with gap junctions.

Chapter Five

Conclusions and further experiments

This dissertation examined three aspects of neocortical fast-spiking cells. First, the commonly-stated overlap between parvalbumin (PV) and fast-spiking cells (FS) does not apply in ventral postrhinal cortex (vPOR). The majority of FS cells in this region are PV-negative, and these cells are also found in neighboring cortex along with canonical fast-spiking (cFS) cells (Chapter 2). Second, the absence of cFS cells from vPOR and the corresponding decrease in inhibitory cell density does not decrease total inhibition onto excitatory cells, due to decreased inhibition onto inhibitory cells in vPOR (Chapter 2). Third, gap junctions do not affect the strength or frequency of gap junctions in neocortex (Chapter 3), unless compensation in RS cells for the lack of gap junctions in inhibitory cells is masking the effect (Chapters 3, 4).

5.0.1 nFS cells have low-to-no PV but occasionally express SOM

FS cells are the predominant type of inhibitory cell across the neocortex Rudy et al. (2010); Xu et al. (2010). Over the years, it has become ingrained within the community that expression of the PV protein and the FS electrophysiological phenotype almost exclusively identify the same group of neurons Gelman and Marín (2010); Gentet et al. (2010); Helm et al. (2013); Lee et al. (2010); Pfeffer et al. (2013); Rudy et al. (2010); Uhlhaas and Singer (2010); Xu et al. (2010); Yang et al. (2012). It has been reported that a small percentage of cells in somatosensory cortex co-express PV and SOM mRNA, but that this does not reflect protein expression Lee et al. (2010). It has also been noted that the SOM-Cre animal labels some cells that express PV, but this was suggested to be due to transient developmental expression of SOM that later turned off Hu et al. (2013). An area free of canonical PV-cells, vPOR, has allowed us to identify a network of FS cells that express low-to-no PV.

Electrophysiological measurements of cells in vPOR demonstrated that there was a large population of non-canonical FS cells that went unlabeled by PV-IRES-Cre and appeared to have near-background levels of expression with antibodies to the PV protein (nFS). Careful immunohistochemistry of individually recorded and filled cells revealed that these FS cells expressed low levels of PV (18%), SOM (40%), or neither (42%). These cells were electrophysiologically similar to cFS cells, with some being identical. The remainder had properties between traditional FS and LTS cells. nFS cells were differentiated from cFS cells by their inputs; only cFS cells received strong inputs from retrosplenial area (RSA). Given that RSA is activated upon successful memory retrieval, but not during memory encoding, the RSA-POR cFS cell connection may play a role in gating the direction of information flow; it may be part of the "wall of inhibition" described by de Curtis and Paré (2004).

Our discovery of a previously uncharacterized type of FS cell leads to many questions, and thus inspires many future experiments. First, how can we selectively mark nFS cells? We propose two ways in which to do so, both using Flp-expressing mice. Flp-expressing mice are under active development, and Jackson Laboratories sells a PV-2A-Flp mouse. If this mouse expresses less strongly than the PV-2A-Cre mouse, then in combination with SOM-IRES-Cre and a viral Cre+Flp on reporter, it might label nFS cells across the neocortex. The spread of nFS cells into an area with cFS cells such as dPOR suggests that nFS cells may exist across cortex. Do they?

How are nFS cells further differentiated from cFS cells? Donato et al. (2013) used immunohistochemistry to determine that PV levels are actively modulated in the hippocampus. Decreased PV expression leads to lower excitatory-to-inhibitory ratios in the PV cells as measured by bassoon- to gephyrin-expressing synapses (excitatory to inhibitory synapses). Does vPOR have a higher ratio of gephyrin- to bassoon-expressing synapses onto its nFS cells? If so, does this hold true across cortex? Is total excitation, elicited via optogenetic or electrical stimulation under tetrodotoxin to block spiking and 4-aminopyridine to block potassium channels, enhancing excitability and calcium fluxes, greater onto nFS cells than cFS cells?

Do nFS cells come from a unique part of the medial ganglionic eminence? A WNT gradient is set up across the MGE and the level of WNT expression determines a cell's fate as either SOM- or PV-positive Chang (2014). Are nFS cells those at the center of the gradient, undirected and therefore undifferentiated?

RNAseq could provide unique insight into this population of cells. How much variation exists among nFS, and how similar are they to cFS cells? While RNA-seq analysis sometimes leads to the unnecessary subdivision of cell types into previously unknown categories Zeisel et al. (2015), in this case we have a genetically defined population that can be compared to other genetically defined populations.

In our quest to determine whether PV was actively modulated, we used both prediction of energetic binding and of phylogenetic similarity to determine probable microRNA targets in PV. One of the most probable miRNAs predicted by both systems was miRNA-298. Surprisingly, this has an equally strong binding site in the GAD67 transcript. Donato et al. (2013) showed that PV modulation in the hippocampus was linked tightly to GAD67 levels, so it is likely that the levels of both proteins are co-regulated. Using a miRNA sponge system directed towards miRNA-298, one could ask "does miRNA-298 actively modulate levels of PV in either the hippocampus or in nFS cells of the vPOR?"

5.0.2 Total inhibition onto RS cells in vPOR is equal to that in control cortex

Careful counts of inhibitory cell densities have confirmed that vPOR has about 20% fewer inhibitory cells than does dPOR. These measurements also demonstrated the variability with which knock-in animals mark the expression of the genes that they are designed to mark. VGAT-Cre had not been previously characterized in neocortex Vong et al. (2011) and likely expresses Cre in some non-GABAergic cells. A GAD65-Cre mouse line, which was already determined to have false-positive and false-negative rates of roughly 10% Taniguchi et al. (2011), was found to have significantly higher inhibitory densities than would be expected by any previous work. Finally, our floxed ChR2 reporter animal was found to have uneven expression across POR relative to tdTomato reporter expression and immunohistochemical reactivity.

We found that this lower density of inhibitory cells in vPOR can generate inhibition equal in strength to that generated by the higher density of inhibitory cells in dPOR due to decreased inhibition onto inhibitory cells.

This leads one to ask, what is the density of excitatory cells? Does excitation differ between vPOR and dPOR? To study this more fully, it would be optimal to record from cells in vivo, preferably via whole-cell recordings. With in vivo recordings, one could determine whether excitatory cells in vPOR receive functionally equal inhibition to those in dPOR during more natural forms of network activity.

5.0.3 Gamma oscillations do not require Cx36

Gamma oscillations require gap junctions for normal power in hippocampus in vitro Hormuzdi et al. (2001) and in vivo Buhl et al. (2003). Gap junctions also can synchronize the spiking of cells in slices Beierlein et al. (2000); Bennett and Zukin (2004); Deans et al. (2001); Gibson et al. (1999, 2005); Long et al. (2005a); Mancilla et al. (2007). The gap junction-coupled PV network is likely the origin of gamma oscillations Cardin et al. (2009); Traub et al. (1996b); Whittington et al. (2011). Therefore, we would predict that gap junctions in the neocortex aid in the generation or coordination of gamma oscillations. In an optogenetic model of gamma oscillations in slice, they do not appear to. A computational model also suggests that gap junctions do not affect gamma oscillations.

I have helped generate conditional knockout mouse lines in which the gap junction proteins Cx36 and Cx45 are selectively removed from SOM-Cre and PV-IRES-Cre cells. PV turns on around P12 del Río et al. (1994), so the PV conditional gap junction knockout has added temporal specificity. With this line, one could ask whether RS cells have the same change in membrane resistance. If not, do gamma oscillations require gap junctions?

Our optogenetic mechanism of gamma generation only probes oscillations generated through a coupled excitatory-inhibitory network, PING. There may be mechanisms in vivo that generate gamma differently. An exciting question then is, do in vivo recordings of gamma oscillations awake animals depend on gap junctions?

The experiments and results described in this dissertation are a reminder of how many basic questions about the types of inhibitory neurons and their mechanisms for communication remain. The human brain contains almost as many neurons as the Milky Way Galaxy contains stars, which might seem to be an insurmountable obstacle. However, in a single dissertation we have managed to better understand neocortical fast-spiking cells and separate them into two better-defined classes, we have found that the inhibitory network of vPOR matches the strength of inhibition of its neighbor, although it has a lower density of inhibitory cells, and we have helped understand gap junctions by narrowing their possible roles.

Bibliography

H. Adesnik and M. Scanziani. Lateral competition for cortical space by layer-specific horizontal circuits. *Nature*, 464(7292):1155--1160, Apr. 2010.

K. L. Agster and R. D. Burwell. Cortical efferents of the perirhinal, postrhinal, and entorhinal cortices of the rat. *Hippocampus*, 19(12):1159--1186, Dec. 2009.

K. L. Agster and R. D. Burwell. Hippocampal and subicular efferents and afferents of the perirhinal, postrhinal, and entorhinal cortices of the rat. *Behavioural brain research*, 254:50--64, Oct. 2013.

L. Alonso-Nanclares, J. Gonzalez-Soriano, J. R. Rodriguez, and J. DeFelipe. Gender differences in human cortical synaptic density. *Proceedings of the National Academy of Sciences*, 105(38): 14615--14619, Sept. 2008.

Y. Amitai, J. R. Gibson, M. Beierlein, S. L. Patrick, A. M. Ho, B. W. Connors, and D. Golomb. The spatial dimensions of electrically coupled networks of interneurons in the neocortex. *The Journal of neuroscience : the official journal of the Society for Neuroscience*, 22(10):4142--4152, May 2002.

K. L. Anderson, R. Rajagovindan, G. A. Ghacibeh, K. J. Meador, and M. Ding. Theta oscillations mediate interaction between prefrontal cortex and medial temporal lobe in human memory. *Cerebral Cortex*, 20(7):1604--1612, July 2010.

B. Asrican, G. J. Augustine, K. Berglund, S. Chen, N. Chow, K. Deisseroth, G. Feng, B. Gloss, R. Hira, C. Hoffmann, H. Kasai, M. Katarya, J. Kim, J. Kudolo, L. M. Lee, S. Q. Lo, J. Mancuso, M. Matsuzaki, R. Nakajima, L. Qiu, G. Tan, Y. Tang, J. T. Ting, S. Tsuda, L. Wen, X. Zhang, and S. Zhao. Next-generation transgenic mice for optogenetic analysis of neural circuits. *Frontiers in neural circuits*, 7:160, 2013.

M. Avermann, C. Tomm, C. Mateo, W. Gerstner, and C. C. H. Petersen. Microcircuits of excitatory and inhibitory neurons in layer 2/3 of mouse barrel cortex. *Journal of neurophysiology*, 107(11):3116--3134, June 2012.

A. Bahl, M. B. Stemmler, A. V. M. Herz, and A. Roth. Automated optimization of a reduced layer 5 pyramidal cell model based on experimental data. *Journal of Neuroscience Methods*, 210 (1):22--34, Sept. 2012.

E. A. Barnard, P. Skolnick, R. W. Olsen, H. Mohler, W. Sieghart, G. Biggio, C. Braestrup, A. N. Bateson, and S. Z. Langer. International Union of Pharmacology. XV. Subtypes of gamma-aminobutyric acidA receptors: classification on the basis of subunit structure and receptor function. *Pharmacological Reviews*, 50(2):291--313, June 1998.

M. Bartos, I. Vida, and P. Jonas. Synaptic mechanisms of synchronized gamma oscillations in inhibitory interneuron networks. *Nature Reviews Neuroscience*, 8(1):45--56, Jan. 2007.

A. A. Bazzini, M. T. Lee, and A. J. Giraldez. Ribosome profiling shows that miR-430 reduces translation before causing mRNA decay in zebrafish. *Science*, 336(6078):233--237, Apr. 2012.

S. A. Beaudin, T. Singh, K. L. Agster, and R. D. Burwell. Borders and Comparative Cytoarchitecture of the Perirhinal and Postrhinal Cortices in an F1 Hybrid Mouse. *Cerebral Cortex*, Feb. 2012.

M. Beaumont and G. Maccaferri. Is connexin36 critical for GABAergic hypersynchronization in the hippocampus? *The Journal of Physiology*, 589(Pt 7):1663--1680, Apr. 2011.

C. J. Behrens, R. u. Haq, A. Liotta, M. L. Anderson, and U. Heinemann. Nonspecific effects of the gap junction blocker mefloquine on fast hippocampal network oscillations in the adult rat in vitro. *NSC*, 192(C):11--19, Sept. 2011.

M. Beierlein, J. R. Gibson, and B. W. Connors. A network of electrically coupled interneurons drives synchronized inhibition in neocortex. *Nature Neuroscience*, 3(9):904--910, Sept. 2000.

M. Beierlein, J. R. Gibson, and B. W. Connors. Two dynamically distinct inhibitory networks in layer 4 of the neocortex. *Journal of neurophysiology*, 90(5):2987--3000, Nov. 2003.

M. V. L. Bennett and R. S. Zukin. Electrical coupling and neuronal synchronization in the Mammalian brain. *Neuron*, 41(4):495--511, Feb. 2004.

E. B. Bromfield, J. E. Cavazos, and J. I. Sirven. Basic Mechanisms Underlying Seizures and Epilepsy. 2006.

D. L. Buhl, K. D. Harris, S. G. Hormuzdi, H. Monyer, and G. Buzsáki. Selective impairment of hippocampal gamma oscillations in connexin-36 knock-out mouse in vivo. *The Journal of neuroscience : the official journal of the Society for Neuroscience*, 23(3):1013--1018, Feb. 2003.

R. D. Burwell. Borders and cytoarchitecture of the perirhinal and postrhinal cortices in the rat. *The Journal of comparative neurology*, 437(1):17--41, Aug. 2001.

R. D. Burwell and D. G. Amaral. Cortical afferents of the perirhinal, postrhinal, and entorhinal cortices of the rat. *The Journal of comparative neurology*, 398(2):179--205, Aug. 1998a.

R. D. Burwell and D. G. Amaral. Perirhinal and postrhinal cortices of the rat: interconnectivity and connections with the entorhinal cortex. *The Journal of comparative neurology*, 391(3):293--321, Feb. 1998b.

R. D. Burwell, M. P. Witter, and D. G. Amaral. Perirhinal and postrhinal cortices of the rat: a review of the neuroanatomical literature and comparison with findings from the monkey brain. *Hippocampus*, 5(5):390--408, 1995.

R. D. Burwell, D. J. Bucci, M. R. Sanborn, and M. J. Jutras. Perirhinal and postrhinal contributions to remote memory for context. *The Journal of neuroscience : the official journal of the Society for Neuroscience*, 24(49):11023--11028, Dec. 2004.

P. C. Bush and T. J. Sejnowski. Reduced compartmental models of neocortical pyramidal cells. *Journal of Neuroscience Methods*, 46(2):159--166, Feb. 1993.

T. J. Bussey, L. M. Saksida, and E. A. Murray. Impairments in visual discrimination after perirhinal cortex lesions: testing 'declarative' vs. 'perceptual-mnemonic' views of perirhinal cortex function. *The European journal of neuroscience*, 17(3):649--660, Feb. 2003.

G. Buzsáki and X.-J. Wang. Mechanisms of gamma oscillations. *Annual Review of Neuroscience*, 35(1):203--225, 2012.

G. Buzsáki, C. A. Anastassiou, and C. Koch. The origin of extracellular fields and currents--EEG, ECoG, LFP and spikes. *Nature Reviews Neuroscience*, 13(6):407--420, June 2012.

J. A. Cardin, M. Carlén, K. Meletis, U. Knoblich, F. Zhang, K. Deisseroth, L.-H. Tsai, and C. I. Moore. Driving fast-spiking cells induces gamma rhythm and controls sensory responses. *Nature*, 459(7247):663--667, June 2009.

R. P. Carne, S. Vogrin, L. Litewka, and M. J. Cook. Cerebral cortex: an MRI-based study of volume and variance with age and sex. *Journal of clinical neuroscience : official journal of the Neurosurgical Society of Australasia*, 13(1):60--72, Jan. 2006.

N. Carnevale and M. Hines. *The NEURON Book*. Cambridge University Press, Cambridge, UK, 2006.

J.-C. Cassel, A. P. de Vasconcelos, M. Loureiro, T. Cholvin, J. C. Dalrymple-Alford, and R. P. Vertes. Progress in Neurobiology. *Progress in Neurobiology*, 111:34--52, Dec. 2013.

R. Caton. The electric currents of the brain. *British Medical Journal*, 2(278), 1875.

R. Caton. Interim report on investigation of the electric currents of the brain. *British Medical Journal Supplement*, 1:62--65, 1877.

M. R. Celio. Parvalbumin in most gamma-aminobutyric acid-containing neurons of the rat cerebral cortex. *Science*, 231(4741):995--997, Feb. 1986.

M. R. Celio and C. W. Heizmann. Calcium-binding protein parvalbumin as a neuronal marker. *Nature*, 293:300--302, Sept. 1981.

M. M. Chang. *Secreted factors FGF and WNT in cortical neuron specification*. PhD thesis, New York University, ProQuest LLC, 789 East Eisenhower Parkway, P.O. Box 1346, Ann Arbor, MI 48106, 9 2014.

A. Chow, A. Erisir, C. Farb, M. S. Nadal, A. Ozaita, D. Lau, E. Welker, and B. Rudy. K(+) channel expression distinguishes subpopulations of parvalbumin- and somatostatin-containing neocortical interneurons. *The Journal of neuroscience : the official journal of the Society for Neuroscience*, 19(21):9332--9345, Nov. 1999.

D. F. Condorelli, N. Belluardo, A. Trovato-Salinaro, and G. Mudò. Expression of Cx36 in mammalian neurons. *Brain research Brain research reviews*, 32(1):72--85, Apr. 2000.

B. W. Connors. Tales of a dirty drug: carbenoxolone, gap junctions, and seizures. *Epilepsy currents / American Epilepsy Society*, 12(2):66--68, Mar. 2012.

B. W. Connors and M. A. Long. Electrical synapses in the mammalian brain. *Annual Review of Neuroscience*, 27(1):393--418, July 2004.

B. W. Connors, L. S. Benardo, and D. A. Prince. Coupling between neurons of the developing rat neocortex. *The Journal of neuroscience : the official journal of the Society for Neuroscience*, 3(4): 773--782, Apr. 1983.

W. L. Conte, H. Kamishina, J. V. Corwin, and R. L. Reep. Topography in the projections of lateral posterior thalamus with cingulate and medial agranular cortex in relation to circuitry for directed attention and neglect. *Brain research*, 1240:87--95, Nov. 2008.

R. Cossart. The maturation of cortical interneuron diversity: how multiple developmental journeys shape the emergence of proper network function. *Current opinion in neurobiology*, pages 1--9, Nov. 2010.

S. J. Cruikshank, M. Hopperstad, M. Younger, B. W. Connors, D. C. Spray, and M. Srinivas. Potent block of Cx36 and Cx50 gap junction channels by mefloquine. *Proceedings of the National Academy of Sciences*, 101(33):12364--12369, Aug. 2004.

S. J. Cruikshank, C. E. Landisman, J. G. Mancilla, and B. W. Connors. Connexon connexions in the thalamocortical system. *Progress in brain research*, 149:41--57, 2005.

S. J. Cruikshank, T. J. Lewis, and B. W. Connors. Synaptic basis for intense thalamocortical activation of feedforward inhibitory cells in neocortex. *Nature Neuroscience*, pages 1--8, Mar. 2007.

S. J. Cruikshank, O. J. Ahmed, T. R. Stevens, S. L. Patrick, A. N. Gonzalez, M. Elmaleh, and B. W. Connors. Thalamic control of layer 1 circuits in prefrontal cortex. *The Journal of neuroscience : the official journal of the Society for Neuroscience*, 32(49):17813--17823, Dec. 2012.

M. de Curtis and D. Paré. The rhinal cortices: a wall of inhibition between the neocortex and the hippocampus. *Progress in Neurobiology*, 74(2):101--110, Oct. 2004.

M. R. Deans, J. R. Gibson, C. Sellitto, B. W. Connors, and D. L. Paul. Synchronous activity of inhibitory networks in neocortex requires electrical synapses containing connexin36. *Neuron*, 31(3):477--485, Aug. 2001.

M. R. Deans, B. Völgyi, D. A. Goodenough, S. A. Bloomfield, and D. L. Paul. Connexin36 is essential for transmission of rod-mediated visual signals in the mammalian retina. *Neuron*, 36(4):703--712, Nov. 2002.

J. DeFelipe, S. H. Hendry, and E. G. Jones. Visualization of chandelier cell axons by parvalbumin immunoreactivity in monkey cerebral cortex. *Proceedings of the National Academy of Sciences*, 86(6):2093--2097, Mar. 1989.

J. A. del Río, L. de Lecea, I. Ferrer, and E. Soriano. The development of parvalbumin-immunoreactivity in the neocortex of the mouse. *Brain research Developmental brain research*, 81(2):247--259, Sept. 1994.

F. Donato, S. B. Rompani, and P. Caroni. Parvalbumin-expressing basket-cell network plasticity induced by experience regulates adult learning. *Nature*, 504(7479):272--276, Dec. 2013.

R. Eckhorn, R. Bauer, W. Jordan, M. Brosch, W. Kruse, M. Munk, and H. J. Reitboeck. Coherent oscillations: a mechanism of feature linking in the visual cortex? Multiple electrode and correlation analyses in the cat. *Biological cybernetics*, 60(2):121--130, 1988.

H. Eichenbaum. A cortical-hippocampal system for declarative memory. *Nature Reviews Neuroscience*, 1(1):41--50, Oct. 2000.

A. K. Engel and W. Singer. Temporal binding and the neural correlates of sensory awareness. *Trends in cognitive sciences*, 5(1):16--25, Jan. 2001.

W. H. Evans and P. E. M. Martin. Gap junctions: structure and function (Review). *Molecular Membrane Biology*, 19(2):121--136, 2002.

B. L. Finlay and R. B. Darlington. Linked regularities in the development and evolution of mammalian brains. *Science*, 268(5217):1578--1584, June 1995.

G. Fishell and B. Rudy. Mechanisms of inhibition within the telencephalon: "where the wild things are". *Annual Review of Neuroscience*, 34(1):535--567, 2011a.

G. Fishell and B. Rudy. Mechanisms of inhibition within the telencephalon: "where the wild things are". *Annual Review of Neuroscience*, 34(1):535--567, 2011b.

P. Fries. Neuronal gamma-band synchronization as a fundamental process in cortical computation. *Annual Review of Neuroscience*, 32:209--224, 2009.

P. Fries, J. H. Reynolds, A. E. Rorie, and R. Desimone. Modulation of oscillatory neuronal synchronization by selective visual attention. *Science*, 291(5508):1560--1563, Feb. 2001.

C. Frisch, M. A. De Souza-Silva, G. Söhl, M. Güldenagel, K. Willecke, J. P. Huston, and E. Dere. Stimulus complexity dependent memory impairment and changes in motor performance after deletion of the neuronal gap junction protein connexin36 in mice. *Behavioural brain research*, 157(1):177--185, Feb. 2005.

T. Fukuda. Structural organization of the gap junction network in the cerebral cortex. *The Neuroscientist : a review journal bringing neurobiology, neurology and psychiatry*, 13(3):199--207, June 2007.

S. C. Furtak, S.-M. Wei, K. L. Agster, and R. D. Burwell. Functional neuroanatomy of the parahippocampal region in the rat: the perirhinal and postrhinal cortices. *Hippocampus*, 17 (9):709--722, 2007.

L. Gabernet, S. P. Jadhav, D. E. Feldman, M. Carandini, and M. Scanziani. Somatosensory Integration Controlled by Dynamic Thalamocortical Feed-Forward Inhibition. *Neuron*, 48 (2):315--327, Oct. 2005.

M. Galarreta and S. Hestrin. A network of fast-spiking cells in the neocortex connected by electrical synapses. *Nature*, 402(6757):72--75, Nov. 1999.

M. Galarreta, F. Erdélyi, G. Szabó, and S. Hestrin. Cannabinoid sensitivity and synaptic properties of 2 GABAergic networks in the neocortex. *Cerebral Cortex*, 18(10):2296--2305, Oct. 2008.

B. Gasnier. The loading of neurotransmitters into synaptic vesicles. *Biochimie*, 82(4):327--337, Apr. 2000.

D. M. Gelman and O. Marín. Generation of interneuron diversity in the mouse cerebral cortex. *European Journal of Neuroscience*, 31(12):2136--2141, June 2010.

L. J. Gentet, M. Avermann, F. Matyas, J. F. Staiger, and C. C. H. Petersen. Membrane potential dynamics of GABAergic neurons in the barrel cortex of behaving mice. *Neuron*, 65(3): 422--435, Feb. 2010.

J. R. Gibson, M. Beierlein, and B. W. Connors. Two networks of electrically coupled inhibitory neurons in neocortex. *Nature*, 402(6757):75--79, Nov. 1999.

J. R. Gibson, M. Beierlein, and B. W. Connors. Functional properties of electrical synapses between inhibitory interneurons of neocortical layer 4. *Journal of neurophysiology*, 93(1):467--480, Jan. 2005.

L. L. Glickfeld, R. C. Reid, and M. L. Andermann. ScienceDirectA mouse model of higher visual cortical function. *Current opinion in neurobiology*, 24:28--33, Feb. 2014.

N. Gogolla, J. J. LeBlanc, K. B. Quast, T. C. Südhof, M. Fagiolini, and T. K. Hensch. Common circuit defect of excitatory-inhibitory balance in mouse models of autism. *Journal of Neurodevelopmental Disorders*, 1(2):172--181, July 2009.

D. Golomb, K. Donner, L. Shacham, D. Shlosberg, Y. Amitai, and D. Hansel. Mechanisms of firing patterns in fast-spiking cortical interneurons. *PLoS computational biology*, 3(8):e156, Aug. 2007.

Y. Gonchar and A. Burkhalter. Three distinct families of GABAergic neurons in rat visual cortex. *Cerebral cortex (New York, NY : 1991)*, 7(4):347--358, June 1997.

M. A. Goodale and A. D. Milner. Separate visual pathways for perception and action. *Trends in neurosciences*, 15(1):20--25, Jan. 1992.

C. M. Gray. Synchronous oscillations in neuronal systems: mechanisms and functions. *Journal of computational neuroscience*, 1994.

C. M. Gray and W. Singer. Stimulus-specific neuronal oscillations in orientation columns of cat visual cortex. *Proceedings of the National Academy of Sciences*, 86(5):1698--1702, Mar. 1989.

C. M. Gray, P. König, A. K. Engel, and W. Singer. Oscillatory responses in cat visual cortex exhibit inter-columnar synchronization which reflects global stimulus properties. *Nature*, 338(6213):334--337, Mar. 1989.

H. Gu, J. D. Marth, P. C. Orban, H. Mossmann, and K. Rajewsky. Deletion of a DNA polymerase beta gene segment in T cells using cell type-specific gene targeting. *Science*, 265 (5168):103--106, July 1994.

C. Günay, J. R. Edgerton, and D. Jaeger. Channel density distributions explain spiking variability in the globus pallidus: a combined physiology and computer simulation database approach. *The Journal of neuroscience : the official journal of the Society for Neuroscience*, 28(30): 7476--7491, July 2008.

O. Hamill, J. Huguenard, and D. Prince. Patch-clamp studies of voltage-gated currents in identified neurons of the rat cerebral cortex. *Cerebral Cortex*, 1(1):48--61, 1991.

E. Hartveit and M. L. Veruki. Electrical synapses between AII amacrine cells in the retina Function and modulation. *Brain research*, pages 1--13, July 2012.

I. Hayut, E. E. Fanselow, B. W. Connors, and D. Golomb. LTS and FS inhibitory interneurons, short-term synaptic plasticity, and cortical circuit dynamics. *PLoS computational biology*, 7(10): e1002248, Oct. 2011.

J. Helm, G. Akgul, and L. P. Wollmuth. Subgroups of parvalbumin-expressing interneurons in layers 2/3 of the visual cortex. *Journal of neurophysiology*, 109(6):1600--1613, Mar. 2013.

S. H. Hendry, E. G. Jones, J. DeFelipe, D. Schmechel, C. Brandon, and P. C. Emson. Neuropeptide-containing neurons of the cerebral cortex are also GABAergic. *Proceedings of the National Academy of Sciences*, 81(20):6526--6530, Oct. 1984.

S. Hestrin and M. Galarreta. Electrical synapses define networks of neocortical GABAergic neurons. *Trends in neurosciences*, 28(6):304--309, June 2005.

S. Hippenmeyer, E. Vrieseling, M. Sigrist, T. Portmann, C. Laengle, D. R. Ladle, and S. Arber. A developmental switch in the response of DRG neurons to ETS transcription factor signaling. *PLoS Biology*, 3(5):e159, May 2005.

S. G. Hormuzdi, I. Pais, F. E. N. LeBeau, S. K. Towers, A. Rozov, E. H. Buhl, M. A. Whittington, and H. Monyer. Impaired electrical signaling disrupts gamma frequency oscillations in connexin 36-deficient mice. *Neuron*, 31(3):487--495, Aug. 2001.

H. Hu, J. Z. Cavendish, and A. Agmon. Not all that glitters is gold: off-target recombination in the somatostatin-IRES-Cre mouse line labels a subset of fast-spiking interneurons. *Frontiers in neural circuits*, 7:195, 2013.

J. R. Huguenard, O. P. Hamill, and D. A. Prince. Developmental changes in Na+ conductances in rat neocortical neurons: appearance of a slowly inactivating component. *Journal of neurophysiology*, 59(3):778--795, Mar. 1988.

N. T. Ingolia. Ribosome profiling: new views of translation, from single codons to genome scale. *Nature reviews Genetics*, 15(3):205--213, Mar. 2014.

J. S. Isaacson and M. Scanziani. How inhibition shapes cortical activity. *Neuron*, 72(2):231--243, Oct. 2011.

D. Ji and M. A. Wilson. Coordinated memory replay in the visual cortex and hippocampus during sleep. *Nature Neuroscience*, 10(1):100--107, Jan. 2007.

K. Kaila, T. J. Price, J. A. Payne, M. Puskarjov, and J. Voipio. Cation-chloride cotransporters in neuronal development, plasticity and disease. *Nature Reviews Neuroscience*, 15(10):637--654, Oct. 2014.

B. M. Kampa and G. J. Stuart. Calcium spikes in basal dendrites of layer 5 pyramidal neurons during action potential bursts. *The Journal of neuroscience : the official journal of the Society for Neuroscience*, 26(28):7424--7432, July 2006.

F. Karube, Y. Kubota, and Y. Kawaguchi. Axon branching and synaptic bouton phenotypes in GABAergic nonpyramidal cell subtypes. *The Journal of neuroscience : the official journal of the Society for Neuroscience*, 24(12):2853--2865, Mar. 2004.

S. Katzner, I. Nauhaus, A. Benucci, V. Bonin, D. L. Ringach, and M. Carandini. Local origin of field potentials in visual cortex. *Neuron*, 61(1):35--41, Jan. 2009.

Y. Kawaguchi and Y. Kubota. GABAergic cell subtypes and their synaptic connections in rat frontal cortex. *Cerebral cortex (New York, NY : 1991)*, 7(6):476--486, Sept. 1997.

J. Kealy and S. Commins. The rat perirhinal cortex: A review of anatomy, physiology, plasticity, and function. *Progress in Neurobiology*, 93(4):522--548, Apr. 2011.

A. Kepecs and G. Fishell. Interneuron cell types are fit to function. *Nature*, 505(7483):318--326, Jan. 2014.

K. Kohara, M. Pignatelli, A. J. Rivest, H.-Y. Jung, T. Kitamura, J. Suh, D. Frank, K. Kajikawa, N. Mise, Y. Obata, I. R. Wickersham, and S. Tonegawa. Cell type-specific genetic and optogenetic tools reveal hippocampal CA2 circuits. *Nature Neuroscience*, 17(2):269--279, Feb. 2014.

H. Kondo and M. P. Witter. Topographic organization of orbitofrontal projections to the parahippocampal region in rats. *The Journal of comparative neurology*, 522(4):772--793, Mar. 2014.

N. M. Kumar and N. B. Gilula. The gap junction communication channel. *Cell*, 84(3):381--388, Feb. 1996.

H. J. Kwon, S. Ma, and Z. Huang. Radial glia regulate Cajal-Retzius cell positioning in the early embryonic cerebral cortex. *Developmental biology*, 351(1):25--34, Mar. 2011.

V. A. Lamme, H. Supèr, and H. Spekreijse. Feedforward, horizontal, and feedback processing in the visual cortex. *Current opinion in neurobiology*, 8(4):529--535, Aug. 1998.

C. E. Landisman and B. W. Connors. Long-term modulation of electrical synapses in the mammalian thalamus. *Science*, 310(5755):1809--1813, Dec. 2005.

M.-E. Laramée and D. Boire. Visual cortical areas of the mouse: comparison of parcellation and network structure with primates. *Frontiers in neural circuits*, 8:149, 2014.

F. E. N. LeBeau, R. D. Traub, H. Monyer, M. A. Whittington, and E. H. Buhl. The role of electrical signaling via gap junctions in the generation of fast network oscillations. *Brain research bulletin*, 62(1):3--13, Nov. 2003.

S. Lee, J. Hjerling-Leffler, E. Zagha, G. Fishell, and B. Rudy. The largest group of superficial neocortical GABAergic interneurons expresses ionotropic serotonin receptors. *The Journal of neuroscience : the official journal of the Society for Neuroscience*, 30(50):16796--16808, Dec. 2010.

S.-C. Lee, S. L. Patrick, K. A. Richardson, and B. W. Connors. Two functionally distinct networks of gap junction-coupled inhibitory neurons in the thalamic reticular nucleus. *The Journal of neuroscience : the official journal of the Society for Neuroscience*, 34(39):13170--13182, Sept. 2014.

S. Lefort, C. Tomm, J.-C. Floyd Sarria, and C. C. H. Petersen. The excitatory neuronal network of the C2 barrel column in mouse primary somatosensory cortex. *Neuron*, 61(2):301--316, Jan. 2009.

W. R. Loewenstein. Junctional intercellular communication: the cell-to-cell membrane channel. *Physiological Reviews*, 61(4):829--913, 1981.

M. A. Long, S. J. Cruikshank, M. J. Jutras, and B. W. Connors. Abrupt maturation of a spike-synchronizing mechanism in neocortex. *The Journal of neuroscience : the official journal of the Society for Neuroscience*, 25(32):7309--7316, Aug. 2005a.

M. A. Long, M. J. Jutras, B. W. Connors, and R. D. Burwell. Electrical synapses coordinate activity in the suprachiasmatic nucleus. *Nature Neuroscience*, 8(1):61--66, 2005b.

C.-b. Lu, Z.-h. Wang, Y.-h. Zhou, and M. Vreugdenhil. Temperature- and concentration-dependence of kainate-induced γ oscillation in rat hippocampal slices under submerged condition. *Acta pharmacologica Sinica*, 33(2):214--220, Feb. 2012.

J. H. Lui, D. V. Hansen, and A. R. Kriegstein. Development and Evolution of the Human Neocortex. *Cell*, 146(1):18--36, Aug. 2011.

A. Lutz, L. L. Greischar, N. B. Rawlings, M. Ricard, and R. J. Davidson. Long-term meditators self-induce high-amplitude gamma synchrony during mental practice. *Proceedings of the National Academy of Sciences*, 101(46):16369--16373, Nov. 2004.

Y. Ma, H. Hu, A. S. Berrebi, P. H. Mathers, and A. Agmon. Distinct subtypes of somatostatin-containing neocortical interneurons revealed in transgenic mice. *The Journal of neuroscience : the official journal of the Society for Neuroscience*, 26(19):5069--5082, May 2006.

L. Madisen, T. A. Zwingman, S. M. Sunkin, S. W. Oh, H. A. Zariwala, H. Gu, L. L. Ng, R. D. Palmiter, M. J. Hawrylycz, A. R. Jones, E. S. Lein, and H. Zeng. nn.2467. *Nature Neuroscience*, 13(1):133--140, Dec. 2009.

Z. F. Mainen and T. J. Sejnowski. Influence of dendritic structure on firing pattern in model neocortical neurons. *Nature*, 382(6589):363--366, July 1996.

S. R. Majewski and K. V. Johnston. Evidence for a triaxial Milky Way dark matter halo from the Sagittarius stellar tidal stream. *The Astrophysical Journal*, 2009.

J. G. Mancilla, T. J. Lewis, D. J. Pinto, J. Rinzel, and B. W. Connors. Synchronization of electrically coupled pairs of inhibitory interneurons in neocortex. *The Journal of neuroscience : the official journal of the Society for Neuroscience*, 27(8):2058--2073, Feb. 2007.

H. Markram, M. Toledo-Rodriguez, Y. Wang, A. Gupta, G. Silberberg, and C. Wu. Interneurons of the neocortical inhibitory system. *Nature Reviews Neuroscience*, 5(10):793--807, Oct. 2004.

C. Mas, N. Taske, S. Deutsch, M. Guipponi, P. Thomas, A. Covanis, M. Friis, M. J. Kjeldsen, G. P. Pizzolato, J.-G. Villemure, C. Buresi, M. Rees, A. Malafosse, M. Gardiner, S. E. Antonarakis, and P. Meda. Association of the connexin36 gene with juvenile myoclonic epilepsy. *Journal of medical genetics*, 41(7):e93, July 2004.

R. H. Masland. Neuronal cell types. *Current biology : CB*, 14(13):R497--500, July 2004.

D. A. McCormick, B. W. Connors, J. W. Lighthall, and D. A. Prince. Comparative electrophysiology of pyramidal and sparsely spiny stellate neurons of the neocortex. *Journal of neurophysiology*, 54(4):782--806, Oct. 1985.

D. A. McCormick, Y. Shu, and Y. Yu. Neurophysiology: Hodgkin and Huxley model--still standing? *Nature*, 445(7123):E1--2-- discussion E2--3, Jan. 2007.

C. B. McCracken and D. C. S. Roberts. A single evoked afterdischarge produces rapid time-dependent changes in connexin36 protein expression in adult rat dorsal hippocampus. *Neuroscience letters*, 405(1-2):84--88, Sept. 2006.

P. Meda. Cx36 involvement in insulin secretion: characteristics and mechanism. *Cell communication & adhesion*, 10(4-6):431--435, July 2003.

C. I. Moore, M. Carlén, U. Knoblich, and J. A. Cardin. Neocortical interneurons: from diversity, strength. *Cell*, 142(2):189--193, July 2010.

M. Morales, E. Battenberg, L. de Lecea, and F. E. Bloom. The type 3 serotonin receptor is expressed in a subpopulation of GABAergic neurons in the rat neocortex and hippocampus. *Brain research*, 731(1-2):199--202, Aug. 1996.

E. A. Murray and M. Mishkin. Object recognition and location memory in monkeys with excitotoxic lesions of the amygdala and hippocampus. *The Journal of neuroscience*, 18(16): 6568--6582, Aug. 1998.

E. A. Murray, T. J. Bussey, R. R. Hampton, and L. M. Saksida. The parahippocampal region and object identification. *Annals of the New York Academy of Sciences*, 911:166--174, June 2000.

J. J. Nassi and E. M. Callaway. Parallel processing strategies of the primate visual system. *Nature Reviews Neuroscience*, 10(5):360--372, May 2009.

G. T. Neske, S. L. Patrick, and B. W. Connors. Contributions of diverse excitatory and inhibitory neurons to recurrent network activity in cerebral cortex. *The Journal of neuroscience : the official journal of the Society for Neuroscience*, 35(3):1089--1105, Jan. 2015.

G. Norman and M. J. Eacott. Dissociable effects of lesions to the perirhinal cortex and the postrhinal cortex on memory for context and objects in rats. *Behavioral neuroscience*, 119(2): 557--566, Apr. 2005.

M. Okun and I. Lampl. Instantaneous correlation of excitation and inhibition during ongoing and sensory-evoked activities. *Nature Neuroscience*, 11(5):535--537, May 2008.

A. A. Oliva, M. Jiang, T. Lam, K. L. Smith, and J. W. Swann. Novel hippocampal interneuronal subtypes identified using transgenic mice that express green fluorescent protein in GABAergic interneurons. *The Journal of neuroscience : the official journal of the Society for Neuroscience*, 20(9):3354--3368, May 2000.

A. M. Packer and R. Yuste. Dense, unspecific connectivity of neocortical parvalbumin-positive interneurons: a canonical microcircuit for inhibition? *The Journal of neuroscience : the official journal of the Society for Neuroscience*, 31(37):13260--13271, Sept. 2011.

S.-B. Paik, T. Kumar, and D. A. Glaser. Spontaneous local gamma oscillation selectively enhances neural network responsiveness. *PLoS computational biology*, 5(3):e1000342, Mar. 2009.

J. G. Pelletier, J. Apergis, and D. Paré. Low-probability transmission of neocortical and entorhinal impulses through the perirhinal cortex. *Journal of neurophysiology*, 91(5):2079--2089, May 2004.

A. E. Pereda. Electrical synapses and their functional interactions with chemical synapses. *Nature Reviews Neuroscience*, 15(4):250--263, Apr. 2014.

C. K. Pfeffer, M. Xue, M. He, Z. J. Huang, and M. Scanziani. Inhibition of inhibition in visual cortex: the logic of connections between molecularly distinct interneurons. *Nature Neuroscience*, 16(8):1068--1076, June 2013.

A. Pitkänen and D. G. Amaral. Distribution of parvalbumin-immunoreactive cells and fibers in the monkey temporal lobe: The amygdaloid complex. *Journal of Comparative Neurology*, 1993.

M. I. Posner and S. E. Petersen. The attention system of the human brain. *Annual Review of Neuroscience*, 13:25--42, 1990.

F. Postma, C.-H. Liu, C. Dietsche, M. Khan, H.-K. Lee, D. Paul, and P. O. Kanold. Electrical synapses formed by connexin36 regulate inhibition- and experience-dependent plasticity. *Proceedings of the National Academy of Sciences*, 108(33):13770--13775, Aug. 2011.

H. H. J. Pothuizen, M. Davies, M. M. Albasser, J. P. Aggleton, and S. D. Vann. Granular and dysgranular retrosplenial cortices provide qualitatively different contributions to spatial working memory: evidence from immediate-early gene imaging in rats. *European Journal of Neuroscience*, 30(5):877--888, Sept. 2009.

P. Rakic. Evolution of the neocortex: a perspective from developmental biology. *Nature Reviews Neuroscience*, 10(10):724--735, Oct. 2009.

C. Ranganath and M. Ritchey. Two cortical systems for memory-guided behaviour. *Nature Reviews Neuroscience*, 13(10):713--726, Sept. 2012.

J. E. Rash, W. A. Staines, T. Yasumura, D. Patel, C. S. Furman, G. L. Stelmack, and J. I. Nagy. Immunogold evidence that neuronal gap junctions in adult rat brain and spinal cord contain connexin-36 but not connexin-32 or connexin-43. *Proceedings of the National Academy of Sciences*, 97(13):7573--7578, June 2000.

J. P. Revel and M. J. Karnovsky. Hexagonal array of subunits in intercellular junctions of the mouse heart and liver. *The Journal of cell biology*, 33(3):C7--C12, June 1967.

A. D. Reyes, R. Lujan, A. Rozov, N. Burnashev, P. Somogyi, and B. Sakmann. Target-cell-specific facilitation and depression in neocortical circuits. *Nature Neuroscience*, 1(4):279--285, Aug. 1998.

S. C. Rogan and B. L. Roth. Remote control of neuronal signaling. *Pharmacological Reviews*, 63 (2):291--315, June 2011.

B. Rudy, G. Fishell, S. Lee, and J. Hjerling-Leffler. Three groups of interneurons account for nearly 100GABAergic neurons. *Developmental neurobiology*, 71(1):45--61, Dec. 2010.

A. Schuz and G. Palm. Density of neurons and synapses in the cerebral cortex of the mouse. *The Journal of comparative neurology*, 286(4):442--455, Aug. 1989.

G. Silberberg and H. Markram. Disynaptic inhibition between neocortical pyramidal cells mediated by Martinotti cells. *Neuron*, 53(5):735--746, Mar. 2007.

A. Simon, S. Oláh, G. Molnár, J. Szabadics, and G. Tamás. Gap-junctional coupling between neurogliaform cells and various interneuron types in the neocortex. *The Journal of neuroscience : the official journal of the Society for Neuroscience*, 25(27):6278--6285, July 2005.

V. S. Sohal, F. Zhang, O. Yizhar, and K. Deisseroth. Parvalbumin neurons and gamma rhythms enhance cortical circuit performance. *Nature*, 459(7247):698--702, June 2009.

G. Söhl, S. Maxeiner, and K. Willecke. Expression and functions of neuronal gap junctions. *Nature Reviews Neuroscience*, 6(3):191--200, Mar. 2005.

P. Somogyi. A specific 'axo-axonal' interneuron in the visual cortex of the rat. *Brain research*, 136(2):345--350, Nov. 1977.

D. Sridharan, K. Boahen, and E. I. Knudsen. Space coding by gamma oscillations in the barn owl optic tectum. *Journal of neurophysiology*, 105(5):2005--2017, May 2011.

M. Srinivas, R. Rozental, T. Kojima, R. Dermietzel, M. Mehler, D. F. Condorelli, J. A. Kessler, and D. C. Spray. Functional properties of channels formed by the neuronal gap junction protein connexin36. *The Journal of neuroscience : the official journal of the Society for Neuroscience*, 19(22):9848--9855, Nov. 1999.

M. Srinivas, M. Hopperstad, and D. C. Spray. Quinine blocks specific gap junction channel subtypes. *Proceedings of the National Academy of Sciences*, 98(19):10942--10947, Sept. 2001.

W. A. Suzuki. Untangling memory from perception in the medial temporal lobe. *Trends in cognitive sciences*, 14(5):195--200, May 2010.

N. Tamamaki, Y. Yanagawa, R. Tomioka, J.-I. Miyazaki, K. Obata, and T. Kaneko. Green fluorescent protein expression and colocalization with calretinin, parvalbumin, and somatostatin in the GAD67-GFP knock-in mouse. *The Journal of comparative neurology*, 467(1):60--79, Dec. 2003.

G. Tamás, A. Lorincz, A. Simon, and J. Szabadics. Identified sources and targets of slow inhibition in the neocortex. *Science*, 299(5614):1902--1905, Mar. 2003.

H. Taniguchi, M. He, P. Wu, S. Kim, R. Paik, K. Sugino, D. Kvitsiani, D. Kvitsani, Y. Fu, J. Lu, Y. Lin, G. Miyoshi, Y. Shima, G. Fishell, S. B. Nelson, and Z. J. Huang. A resource of Cre driver lines for genetic targeting of GABAergic neurons in cerebral cortex. *Neuron*, 71(6): 995--1013, Sept. 2011.

H. Taniguchi, J. Lu, and Z. J. Huang. The spatial and temporal origin of chandelier cells in mouse neocortex. *Science*, 339(6115):70--74, Jan. 2013.

P. Tiesinga and T. J. Sejnowski. Cortical enlightenment: are attentional gamma oscillations driven by ING or PING? *Neuron*, 63(6):727--732, Sept. 2009.

P. H. Tiesinga and C. I. Buia. Spatial attention in area V4 is mediated by circuits in primary visual cortex. *Neural networks : the official journal of the International Neural Network Society*, 22 (8):1039--1054, Oct. 2009.

R. D. Traub, M. A. Whittington, S. B. Colling, G. Buzsáki, and J. G. Jefferys. Analysis of gamma rhythms in the rat hippocampus in vitro and in vivo. *The Journal of Physiology*, 493 (Pt 2): 471--484, June 1996a.

R. D. Traub, M. A. Whittington, I. M. Stanford, and J. G. Jefferys. A mechanism for generation of long-range synchronous fast oscillations in the cortex. *Nature*, 383(6601):621--624, Oct. 1996b.

R. D. Traub, J. G. Jefferys, and M. A. Whittington. Simulation of gamma rhythms in networks of interneurons and pyramidal cells. *Journal of computational neuroscience*, 4(2):141--150, Apr. 1997.

R. D. Traub, E. H. Buhl, T. Gloveli, and M. A. Whittington. Fast rhythmic bursting can be induced in layer 2/3 cortical neurons by enhancing persistent Na+ conductance or by blocking BK channels. *Journal of neurophysiology*, 89(2):909--921, Feb. 2003.

A. J. Trevelyan, D. Sussillo, B. O. Watson, and R. Yuste. Modular propagation of epileptiform activity: evidence for an inhibitory veto in neocortex. *The Journal of neuroscience : the official journal of the Society for Neuroscience*, 26(48):12447--12455, Nov. 2006.

P. J. Uhlhaas and W. Singer. Abnormal neural oscillations and synchrony in schizophrenia. *Nature Reviews Neuroscience*, 11(2):100--113, Feb. 2010.

R. S. Van Der Giessen, S. K. Koekkoek, S. van Dorp, J. R. De Gruijl, A. Cupido, S. Khosrovani, B. Dortland, K. Wellershaus, J. Degen, J. Deuchars, E. C. Fuchs, H. Monyer, K. Willecke, M. T. G. De Jeu, and C. I. De Zeeuw. Role of olivary electrical coupling in cerebellar motor learning. *Neuron*, 58(4):599--612, May 2008.

R. P. Vertes, W. B. Hoover, K. Szigeti-Buck, and C. Leranth. Nucleus reuniens of the midline thalamus: Link between the medial prefrontal cortex and the hippocampus. *Brain research bulletin*, 71(6):601--609, Mar. 2007.

D. Vierling-Claassen, J. A. Cardin, C. I. Moore, and S. R. Jones. Computational modeling of distinct neocortical oscillations driven by cell-type selective optogenetic drive: separable resonant circuits controlled by low-threshold spiking and fast-spiking interneurons. *Frontiers in human neuroscience*, 4:198, 2010.

K. L. Vilberg and M. D. Rugg. Memory retrieval and the parietal cortex: a review of evidence from a dual-process perspective. *Neuropsychologia*, 46(7):1787--1799, 2008.

L. Vong, C. Ye, Z. Yang, B. Choi, S. Chua Jr, and B. B. Lowell. Leptin Action on GABAergic Neurons Prevents Obesity and Reduces Inhibitory Tone to POMC Neurons. *Neuron*, 71 (1):142--154, July 2011.

N. R. Wall, I. R. Wickersham, A. Cetin, M. De La Parra, and E. M. Callaway. Monosynaptic circuit tracing in vivo through Cre-dependent targeting and complementation of modified rabies virus. *Proceedings of the National Academy of Sciences*, 107(50):21848--21853, Dec. 2010.

Q. Wang, E. Gao, and A. Burkhalter. Gateways of Ventral and Dorsal Streams in Mouse Visual Cortex. *The Journal of neuroscience : the official journal of the Society for Neuroscience*, 31(5): 1905--1918, Feb. 2011.

X. J. Wang and G. Buzsáki. Gamma oscillation by synaptic inhibition in a hippocampal interneuronal network model. *The Journal of neuroscience*, 16(20):6402--6413, Oct. 1996.

X. J. Wang and J. Rinzel. Alternating and synchronous rhythms in reciprocally inhibitory model neurons. *Neural computation*, 4(1):84--97, 1992.

K. Wellershaus, J. Degen, J. Deuchars, M. Theis, A. Charollais, D. Caille, B. Gauthier, U. Janssen-Bienhold, S. Sonntag, P. Herrera, P. Meda, and K. Willecke. A new conditional mouse mutant reveals specific expression and functions of connexin36 in neurons and pancreatic beta-cells. *Experimental cell research*, 314(5):997--1012, Mar. 2008.

M. A. Whittington, R. D. Traub, and J. G. Jefferys. Synchronized oscillations in interneuron networks driven by metabotropic glutamate receptor activation. *Nature*, 373(6515):612--615, Feb. 1995.

M. A. Whittington, M. O. Cunningham, F. E. N. LeBeau, C. Racca, and R. D. Traub. Multiple origins of the cortical γ rhythm. *Developmental neurobiology*, 71(1):92--106, 2011.

H. Wichterle, D. H. Turnbull, S. Nery, G. Fishell, and A. Alvarez-Buylla. In utero fate mapping reveals distinct migratory pathways and fates of neurons born in the mammalian basal forebrain. *Development (Cambridge, England)*, 128(19):3759--3771, Oct. 2001.

I. R. Wickersham, D. C. Lyon, R. J. O. Barnard, T. Mori, S. Finke, K.-K. Conzelmann, J. A. T. Young, and E. M. Callaway. Monosynaptic Restriction of Transsynaptic Tracing from Single, Genetically Targeted Neurons. *Neuron*, 53(5):639--647, Mar. 2007.

D. Xing, C.-I. Yeh, and R. M. Shapley. Spatial spread of the local field potential and its laminar variation in visual cortex. *The Journal of neuroscience : the official journal of the Society for Neuroscience*, 29(37):11540--11549, Sept. 2009.

X. Xu, K. D. Roby, and E. M. Callaway. Immunochemical characterization of inhibitory mouse cortical neurons: three chemically distinct classes of inhibitory cells. *The Journal of comparative neurology*, 518(3):389--404, Feb. 2010.

S. R. y Cajal. *Manual de anatoma patolgica general: seguida de un resumen de microscopia aplicado a la histologa y bacteriologa patolgicas*. 1 edition, 1890.

T. Yamashita, A. Pala, L. Pedrido, Y. Kremer, E. Welker, and C. C. H. Petersen. Membrane potential dynamics of neocortical projection neurons driving target-specific signals. *Neuron*, 80(6):1477--1490, Dec. 2013.

J.-M. Yang, J. Zhang, Y.-Q. Yu, S. Duan, and X.-M. Li. Postnatal Development of 2 Microcircuits Involving Fast-Spiking Interneurons in the Mouse Prefrontal Cortex. *Cerebral cortex (New York, NY : 1991)*, Oct. 2012.

X. W. Yang, P. Model, and N. Heintz. Homologous recombination based modification in Escherichia coli and germline transmission in transgenic mice of a bacterial artificial chromosome. *Nature Biotechnology*, 15(9):859--865, Sept. 1997.

O. Yizhar, L. E. Fenno, M. Prigge, F. Schneider, T. J. Davidson, D. J. O'Shea, V. S. Sohal, I. Goshen, J. Finkelstein, J. T. Paz, K. Stehfest, R. Fudim, C. Ramakrishnan, J. R. Huguenard, P. Hegemann, and K. Deisseroth. Neocortical excitation/inhibition balance in information processing and social dysfunction. *Nature*, 477(7363):171--178, Sept. 2011.

Y. Yu, Y. Shu, and D. A. McCormick. Cortical action potential backpropagation explains spike threshold variability and rapid-onset kinetics. *The Journal of neuroscience : the official journal of the Society for Neuroscience*, 28(29):7260--7272, July 2008.

A. Zeisel, A. B. Muñoz-Manchado, S. Codeluppi, P. Lönnerberg, G. La Manno, A. Juréus, S. Marques, H. Munguba, L. He, C. Betsholtz, C. Rolny, G. Castelo-Branco, J. Wang, J. Hjerling-Leffler, and S. Linnarsson. Brain structure. Cell types in the mouse cortex and hippocampus revealed by single-cell RNA-seq. *Science*, 347(6226):1138--1142, Mar. 2015.

S. Zhao, J. T. Ting, H. E. Atallah, L. Qiu, J. Tan, B. Gloss, G. J. Augustine, K. Deisseroth, M. Luo, A. M. Graybiel, and G. Feng. Cell type–specific channelrhodopsin-2 transgenic mice for optogenetic dissection of neural circuitry function. *Nature methods*, 8(9):745--752, Aug. 2011.

A. Zlomuzica, D. Viggiano, J. Degen, S. Binder, L. A. Ruocco, A. G. Sadile, K. Willecke, J. P. Huston, and E. Dere. Behavioral alterations and changes in Ca/calmodulin kinase II levels in the striatum of connexin36 deficient mice. *Behavioural brain research*, 226(1):293--300, 2012.